

2

AFWL-TR-82-101

AFWL-TR-
82-101

ADA 124013

NOVA-2S CORRELATION WITH KC-135A FUSELAGE SHOCK TUBE TEST RESULTS

Lawrence J. Mente
William N. Lee

Kaman AviDyne
83 Second Avenue
Burlington, MA 01803

November 1982

Final Report

Copy available to DTIC does not
permit fully legible reproduction

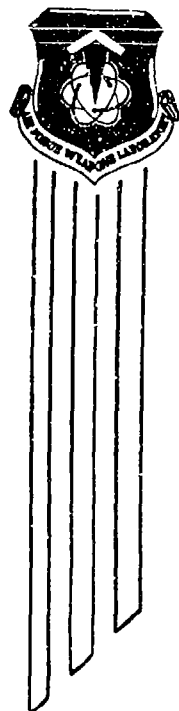
Approved for public release; distribution unlimited.

AIR FORCE WEAPONS LABORATORY
Air Force Systems Command
Kirtland Air Force Base, NM 87117

DTIC
ELECTE
FEB 01 1983
S D E

83 02 01 015

DTIC FILE COPY



This final report was prepared by the Kaman Avidyne, Burlington, Massachusetts, under Contract F29601-81-C-0031, Job Order 88090348 with the Air Force Weapons Laboratory, Kirtland Air Force Base, New Mexico. Mr. Gerald M. Campbell (NTYV) was the Laboratory Project Officer-in-Charge.

When Government drawings, specifications, or other data are used for any purpose other than in connection with a definitely Government-related procurement, the United States Government incurs no responsibility or any obligation whatsoever. The fact that the Government may have formulated or in any way supplied the said drawings, specifications, or other data, is not to be regarded by implication, or otherwise in any manner construed, as licensing the holder, or any other person or corporation; or conveying any rights or permission to manufacture, use, or sell any patented invention that may in any way be related thereto.

This report has been authored by a contractor of the United States Government. Accordingly, the United States Government retains a nonexclusive, royalty-free license to publish or reproduce the material contained herein, or allow others to do so, for the United States Government purposes.

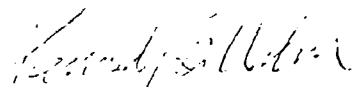
The Public Affairs Office has reviewed this report, and it is releasable to the National Technical Information Service, where it will be available to the general public, including foreign nationals.

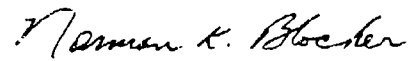
If your address has changed, if you wish to be removed from our mailing list, or if your organization no longer employs the addressee, please notify AFWL/NTYV, Kirtland AFB, NM 87117 to help us maintain a current mailing list.

This technical report has been reviewed and is approved for publication.


GERALD M. CAMPBELL
Project Officer

FOR THE COMMANDER


KENNEDY B. WILSON
Lt Colonel, USAF
Chief, Environment and Effects Branch


NORMAN K. BLOCKER
Colonel, USAF
Chief, Applied Physics Division

DO NOT RETURN COPIES OF THIS REPORT UNLESS CONTRACTUAL OBLIGATIONS OR NOTICE ON A SPECIFIC DOCUMENT REQUIRES THAT IT BE RETURNED.

UNCLASSIFIED

SECURITY CLASSIFICATION OF THIS PAGE (When Data Entered)

REPORT DOCUMENTATION PAGE		READ INSTRUCTIONS BEFORE COMPLETING FORM
1. REPORT NUMBER AFWL-TR-82-101	2. GOVT ACCESSION NO. AD-4124 013	3. RECIPIENT'S CATALOG NUMBER
4. TITLE (and Subtitle) NOVA-2S CORRELATION WITH KC-135A FUSELAGE SHOCK TUBE TEST RESULTS		5. TYPE OF REPORT & PERIOD COVERED Final Report
		6. PERFORMING ORG. REPORT NUMBER KA TR-202
7. AUTHOR(s) Lawrence J. Mente William N. Lee		8. CONTRACT OR GRANT NUMBER(s) F29601-81-C-0031
9. PERFORMING ORGANIZATION NAME AND ADDRESS Kaman Avidyne 83 Second Avenue Burlington, MA 01803		10. PROGRAM ELEMENT, PROJECT, TASK AREA & WORK UNIT NUMBERS 62601F/88090348
11. CONTROLLING OFFICE NAME AND ADDRESS Air Force Weapons Laboratory (NTYV) Kirtland Air Force Base, NM 87117		12. REPORT DATE November 1982
		13. NUMBER OF PAGES 136
14. MONITORING AGENCY NAME & ADDRESS (if different from Controlling Office)		15. SECURITY CLASS. (of this report) Unclassified
		15a. DECLASSIFICATION DOWNGRADING SCHEDULE
16. DISTRIBUTION STATEMENT (of this Report) Approved for public release; distribution unlimited.		
17. DISTRIBUTION STATEMENT (of the abstract entered in Block 20, if different from Report)		
18. SUPPLEMENTARY NOTES		
19. KEY WORDS (Continue on reverse side if necessary and identify by block number) NOVA-2S Computer Code Test Correlation Blast Overpressure Stiffened Panels Fuselage Response Local Skin Buckling		
20. ABSTRACT (Continue on reverse side if necessary and identify by block number) Correlation of the experimental results from KC-135A fuselage tests in the Sandia shock tube with analytical results generated through the NOVA-2LTS structural response code were performed in this effort. It was found that skin buckling between stringers was a very important factor in the overall response of the frames. NOVA-2LTS had to be modified to handle skin buckling in an approximate manner without generating a prohibitive large solution model.		

DD FORM 1473

1 JAN 73

EDITION OF 1 NOV 65 IS OBSOLETE

UNCLASSIFIED

SECURITY CLASSIFICATION OF THIS PAGE (When Data Entered)

UNCLASSIFIED

SECURITY CLASSIFICATION OF THIS PAGE(When Data Entered)

20. ABSTRACT (Continued)

Comparisons are made between the experimental results and NOVA-2LTS analytical strain results for the unpressurized and pressurized KC-135A fuselage. Overall the strain response results for the central frame correlated well considering the uncertainties involved in defining structurally an actual large stiffened aircraft section. NOVA-2LTS could not model the local plastic buckling of the frames for the final inelastic response test shot and therefore, future modifications of NOVA-2LTS are required to handle this compressive failure mechanism. In general, it has been found from fuselage response correlations that the local skin buckling, boundary conditions, structural geometry and spatial loading distribution can be important factors in analyzing large stiffened aircraft sections.

UNCLASSIFIED

SECURITY CLASSIFICATION OF THIS PAGE(When Data Entered)

PREFACE

This work was performed by Kaman AvIDyne for the Air Force Weapons Laboratory (AFWL) under contract number F29601-81- C-0031. Mr. Gerald M. Campbell of AFWL served as technical monitor. The project leader for Kaman AvIDyne was Mr. Lawrence J. Mente of the Structural Mechanics Section. The authors wish to thank Mrs. Margaret K. Bonnice and Mr. Thomas R. Stagliano for their technical assistance furnished during this project.

Accession For		
NTIS GRA&I		<input checked="checked" type="checkbox"/>
DTIC TAB		<input type="checkbox"/>
Unannounced		<input type="checkbox"/>
Justification		
By		
Distribution/		
Availability Codes		
Dist	Avail and/or	Special
A		23



CONTENTS

<u>Section</u>		<u>Page</u>
I	INTRODUCTION	9
II	DESCRIPTION OF THE KC-135A TEST PROGRAM AND RESULTS	12
	1. General Test Procedures	12
	2. Test Specimen Description	13
	3. Test Instrumentation and Response Results	19
	4. General Response Behavior of Fuselage Test Section	19
III	ANALYTICAL NOVA-2LTS MODELS FOR THE KC-135 FUSELAGE SECTION	24
	1. The NOVA-2LTS Structural Model for the KC-135A Fuselage Test Section	24
	2. Skin Buckling Criterion Method	26
	3. Structural Response Sensitivity to Various Parameters	30
	4. Description of Final Structural Models	33
IV	CORRELATION OF NOVA-2LTS RESULTS WITH THE TEST DATA	61
V	EVALUATION OF THE NOVA-2S COMPUTER CODE	87
VI	CONCLUSIONS AND RECOMMENDATIONS	93
	REFERENCES	97
	APPENDIX	99

I L L U S T R A T I O N S

<u>Figure</u>		<u>Page</u>
1	End View of KC-135A Fuselage Section	14
2	Detailed View of KC-135A Fuselage Section	15
3	Schematic of KC-135A Fuselage Test Section Construction	17
4	Instrumentation Locations for Central Frame	20
5	Maximum Strain Versus Incident Overpressure for 90° Loading Orientation on the Unpressurized Fuselage Section	62
6	Maximum Compressive Strain Versus Circumferential Position at the 90° Loading Orientation for Shot 6	64
7	Maximum Compressive Strain Versus Circumferential Position at the 90° Loading Orientation for Shot 17	65
8	Maximum Compressive Strain Versus Circumferential Position at the 90° Loading Orientation for Shot 5	66
9	Comparison of Peak Strain Time Histories at the 90° Loading Orientation for Shot 6	67
10	Comparison of Peak Strain Time Histories at the 90° Loading Orientation for Shot 17	68
11	Comparison of Peak Strain Time Histories at the 90° Loading Orientation for Shot 5	69
12	Maximum Compressive Strain Versus Circumferential Position at the 45° Loading Orientation for Shot 21	73
13	Comparison of Peak Strain Time Histories at the 45° Loading Orientation for Shot 21	74
14	Maximum Compressive Strain Versus Circumferential Position at the 90° Loading Orientation for Shot 22	76
15	Comparison of Strain Time Histories at the 90° Loading Orientation for Shot 22	78
16	Comparison of Strain Time Histories at the 90° Loading Orientation for Shot 16	81
17	Comparison of Strain Time Histories at the 45° Loading Orientation for Shot 20	82

ILLUSTRATIONS - CONCLUDED

<u>Figure</u>		<u>Page</u>
18	Maximum Inward Radial Displacement Versus Incident Overpressure for all Selected Shots	83
19	Inward Radial Displacement Circumferential Distribution for Shots 17 and 21	84
20	Radial Displacement Time Histories for Shots 5 (Elastic Response) and 22 (Inelastic Response)	86

TABLES

<u>Table</u>		<u>Page</u>
	Conversion factors for U.S. customary to metric (SI) units of measurement	7/8
1	Selected Blast Shots for Correlation	12
2	Frame and Stringer Cross Section Dimensions	18
3	Pressure and Strain Gage Locations	21
4	Stiffener Cross Section Models	27
5	KC-135A Fuselage Structural Response Sensitivity	31
6	NOVA-2LTS Data Deck Listing of the KC-135A Fuselage for Shot 5	34
7	Nova-2LTS Data Deck Listing of the KC-135A Fuselage for Shot 22	47
8	Strain Comparisons for Pressurized KC-135A Fuselage Test Section in Shots 16 and 20	79

Conversion factors for U.S. customary
to metric (SI) units of measurement.

To Convert From	To	Multiply By
angstrom	meters (m)	$1.000\ 000 \times 10^{-10}$
atmosphere (normal)	kilo pascal (kPa)	$1.013\ 25 \times 10^5$
bar	kilo pascal (kPa)	$1.000\ 000 \times 10^5$
barn	meter ² (m ²)	$1.000\ 000 \times 10^{-28}$
British thermal unit (thermochemical)	joule (J)	$1.054\ 350 \times 10^3$
calorie (thermochemical)	joule (J)	4.184 000
cal (thermochemical)/cm ²	mega joule/m ² (MJ/m ²)	$4.184\ 000 \times 10^{-2}$
curie	giga becquerel (GBq)**	$3.700\ 000 \times 10^4$
degree (angle)	radian /rad)	$1.745\ 329 \times 10^{-1}$
degree Fahrenheit	degree kelvin (K)	$T_K = (T_F + 459.67)/1.8$
electron volt	joule (J)	$1.602\ 19 \times 10^{-19}$
erg	joule (J)	$1.000\ 000 \times 10^{-7}$
erg/second	watt (W)	$1.000\ 000 \times 10^{-7}$
foot	meter (m)	$3.048\ 000 \times 10^{-1}$
foot-pound-force	joule (J)	1.355 818
gallon (U.S. liquid)	meter ³ (m ³)	$3.785\ 412 \times 10^{-3}$
inch	meter (m)	$2.540\ 000 \times 10^{-2}$
jerk	joule (J)	$1.000\ 000 \times 10^9$
joule/kilogram (J/kg) (radiation dose absorbed)	Gray (Gy)**	1.000 000
kilotons	terajoules	4.183
kip (1000 lbf)	newton (N)	$4.448\ 222 \times 10^3$
kip/inch ² (k/in ²)	kilo pascal (kPa)	$6.894\ 757 \times 10^5$
ktap	newton-second/m ² (N-s/m ²)	$1.000\ 000 \times 10^2$
micron	meter (m)	$1.000\ 000 \times 10^{-6}$
mil	meter (m)	$2.540\ 000 \times 10^{-5}$
mile (international)	meter (m)	$1.609\ 344 \times 10^3$
ounce	kilogram (kg)	$2.834\ 952 \times 10^{-2}$
pound-force (lbf avoirdupois)	newton (N)	4.448 222
pound-force inch	newton-meter (N-m)	$1.129\ 848 \times 10^{-1}$
pound-force/inch	newton/meter (N/m)	$1.751\ 268 \times 10^2$
pound-force/foot ²	kilo pascal (kPa)	$4.788\ 026 \times 10^2$
pound-force/inch ² (lb/in ²)	kilo pascal (kPa)	6.894 757
pound-mass (lbm avoirdupois)	kilogram (kg)	$4.535\ 924 \times 10^{-1}$
pound-mass-foot ² (moment of inertia)	kilogram-meter ² (kg-m ²)	$4.214\ 011 \times 10^{-2}$
pound-mass/foot ³	kilogram/meter ³ (kg/m ³)	$1.601\ 846 \times 10^1$
rad (radiation dose absorbed)	Gray (Gy)**	$1.000\ 000 \times 10^{-2}$
roentgen	coulomb/kilogram (C/kg)	$2.579\ 760 \times 10^{-4}$
shake	second (s)	$1.000\ 000 \times 10^{-8}$
slug	kilogram (kg)	$1.459\ 390 \times 10^1$
torr (mm Hg, 0° C)	kilo pascal (kPa)	$1.333\ 22 \times 10^{-1}$

*The becquerel (Bq) is the SI unit of radioactivity; 1 Bq = 1 event/s.

**The Gray (Gy) is the SI unit of absorbed radiation.

A more complete listing of conversions may be found in "Metric Practice Guide E 380-79," American Society for Testing and Materials.

SECTION I

INTRODUCTION

The response of aircraft structures to the blast overpressure generated by a nuclear explosion is an important consideration of the nuclear survivability for aircraft during several phases of its mission. The computer code NOVA (Nuclear Overpressure Vulnerability Analysis) given in References 1 and 2 was developed by Kaman Avidyne for the Air Force Weapons Laboratory (AFWL) originally to predict the dynamic response of individual aircraft structural elements, such as stringers, frames and unstiffened panels, to the transient overpressure loads associated with a nuclear burst. The NOVA-2S version (Reference 3) extended the panel response subroutine DEPROP (Dynamic Elastic Plastic Response of Panels) to handle flat or circular curved stiffened panels in both the elastic and inelastic response regimes. Thus, NOVA-2S could analyze stringers and frames in combination with the panel skin and, thereby, represent major components of an aircraft, such as fuselage sections and stiffened panels between spars and ribs of the wing, vertical tail and horizontal stabilizer. While the NOVA-2S computer code is used for nuclear overpressure loading, the special version NOVA-2LTS is available for general pressure loadings and, in particular, for use with measured pressure test data stored on digitized tapes.

The stiffened panel components of an aircraft can have arbitrarily curved cylindrical geometry and nonideal boundary conditions. To provide better approximate techniques for analyzing these complex stiffened panel structures, NOVA-2S was modified in KA TM-118* and Reference 4 to include free and elastic rotationally constrained

*Stagliano, T.R., Mente, L.J. and Lee, W.N., "Memorandum on the Support Work for the STRESNO Phase 11 Test Program", Kaman Avidyne, KA TM-118, March 1979.

boundary conditions, discrete linear elastic springs and forces, and a method of analysis for an arbitrarily curved cylindrical panel by specifying initial radial deviations from a nominal circular shape. Thus, any combination of clamped, pinned, free and elastic rotationally constrained boundary conditions are permitted coupled with either fixed or free inplane conditions. The translational springs and inplane forces can be used in conjunction with the normal and inplane free boundary conditions to represent elastic restrained boundaries with or without boundary loading. These new options within NOVA-2S will allow the analyst more latitude in representing the actual boundaries of aircraft panels.

The NOVA-2 response results have been compared with experimental data from unstiffened and stiffened panels that have well defined geometry and boundary conditions. These comparisons are presented in Reference 5 and show very good correlation between analytical and experimental results from various panels loaded by pressure pulses. These results gave a good indication that the theoretical framework of the panel analysis in NOVA-2S for unstiffened and stiffened panels in both the linear and nonlinear response regimes was sound when the geometry and boundary conditions are well defined.

The objective of this effort is to determine whether the NOVA-2S computer code is applicable for analyzing actual aircraft stiffened panels consisting of skin-stringer-frame combinations. Shock tube tests were performed by the Boeing Wichita Company in 1978 on a section of the KC-135A aircraft's fuselage for AFWL and on the aft fuselage and bomb bay doors sections of the B-52 aircraft for Defense Nuclear Agency (DNA). A NOVA-2S correlation with the B-52 tests results is given in Reference 4 in which good strain response comparisons were obtained for the B-52 aft fuselage. These B-52 correlation results will be contrasted with the current correlation with the KC-135A data since the common two types of fuselage construction are represented; namely, the KC-135A fuselage is a stringer-fuselage system and the B-52 fuselage is a longeron-fuselage system. The stringer system of the KC-135A fuselage is characterized by numerous stringers attached to the skin and supported by floating frames (not attached directly to skin) while the

longeron system of the B-52 consists of four longerons supported by frames directly attached to the skin. The frame spacing in the KC-135A fuselage is double that of the B-52 fuselage which is a normal difference between the two fuselage systems. Both these fuselage sections provide a severe test of NOVA-2S capability to predict the response of actual large aircraft components to blast overpressure loading.

The shock tube test program for the KC-135A fuselage section was used to evaluate overpressure damage to this structure with and without internal pressurization. Extensive pressure and strain experimental data were obtained and documented in Reference 6 for several overpressure levels at two blast orientations. The measured pressure data from these tests were stored on digitized tapes which are used directly in this effort with the NOVA-2LTS code version.

Section II of this report presents a description of the KC-135A tests and the overall test results. The NOVA-2LTS analytical models for the KC-135A fuselage section for the various loading cases considered are presented in Section III. In addition, new modifications of the NOVA-2S computer code required to represent the actual structural behavior are presented in Section III and the Appendix. The comparison of the analytical response results with the experimental results are given in Section IV for the seven selected cases under investigation. Section V presents an evaluation of the NOVA-2S (and NOVA-2LTS) computer code for predicting the structural response and damage occurring in the KC-135A fuselage section. The conclusions and recommendations for this effort are given in Section VI.

SECTION II

DESCRIPTION OF THE KC-135A TEST PROGRAM AND RESULTS

1. GENERAL TEST PROCEDURES

The KC-135A test program was conducted by the Boeing Wichita Company and documented in Reference 6. The overpressure blast tests were performed at the THUNDERPIPE Shock Tube at Sandia Corporation in Albuquerque, New Mexico. A 7-ft section of the KC-135A fuselage from BS 980 to BS 1100 was sealed with end bulkheads and was placed in the 19-ft shock tube and subjected to generated blast waves. The upper lobe compartment of the fuselage test section was instrumented with pressure and strain gages and these measurements were recorded for all test conditions covered. Since the lower lobe of the fuselage has intermediate bulkheads to strengthen this compartment, the upper lobe compartment was considered the structural component to be tested and analyzed. There were 22 shots in the test series at the Sandia shock tube at two blast orientation angles, namely, 90 and 45°. The 90° orientation corresponds to the blast wave intersecting the upper lobe compartment at the center of the crown (overhead burst simulation) while the 45° orientation simulates a burst between overhead and side-on. Eight unpressurized test shots were performed at the 90° orientation from overpressure levels from 0.3 to 3.5 lb/in², and two unpressurized shots were performed at the 45° orientation. Twelve pressurized test shots were performed at the two orientations at various combinations of internal pressure and incident blast overpressure. The upper lobe compartment of the KC-135A test section was pressurized for these test shots. From these 22 shots seven were selected for the KC-135A correlation with NOVA-2LTS and are given in Table 1. There are four test events at the 90° orientation and no internal pressure, one test event at 90° orientation with internal pressure, and two test events at 45° orientation with and without internal pressure.

TABLE 1
SELECTED BLAST SHOTS FOR CORRELATION

Shot No.	Event No.	Blast Orientation (deg)	Incident Overpressure (lb/in ²)	Internal Pressure (lb/in ²)
6	78-112	90	1.52	0.0
17	78-130	90	1.95	0.0
5	78-105	90	2.50	0.0
22	78-140	90	3.50	0.0
21	78-139	45	2.10	0.0
16	78-129	90	2.08	2.5
20	78-138	45	1.85	2.7

2. TEST SPECIMEN DESCRIPTION

The KC-135A fuselage is a stringer system type, that is, a large number of evenly spaced longitudinal stringers are attached to the skin and supported by circumferential frames attached to the inner flanges of the stringers as shown in the end view photograph in Figure 1 and in a more detailed view in Figure 2. The test section was six bays long from BS 860 to BS 1100. End bulkheads were attached to the skin and stringers of the fuselage section by a series of angle clips around the circumference of the section. This fuselage section consists of upper and lower lobe compartments separated by a floor system between WL 202

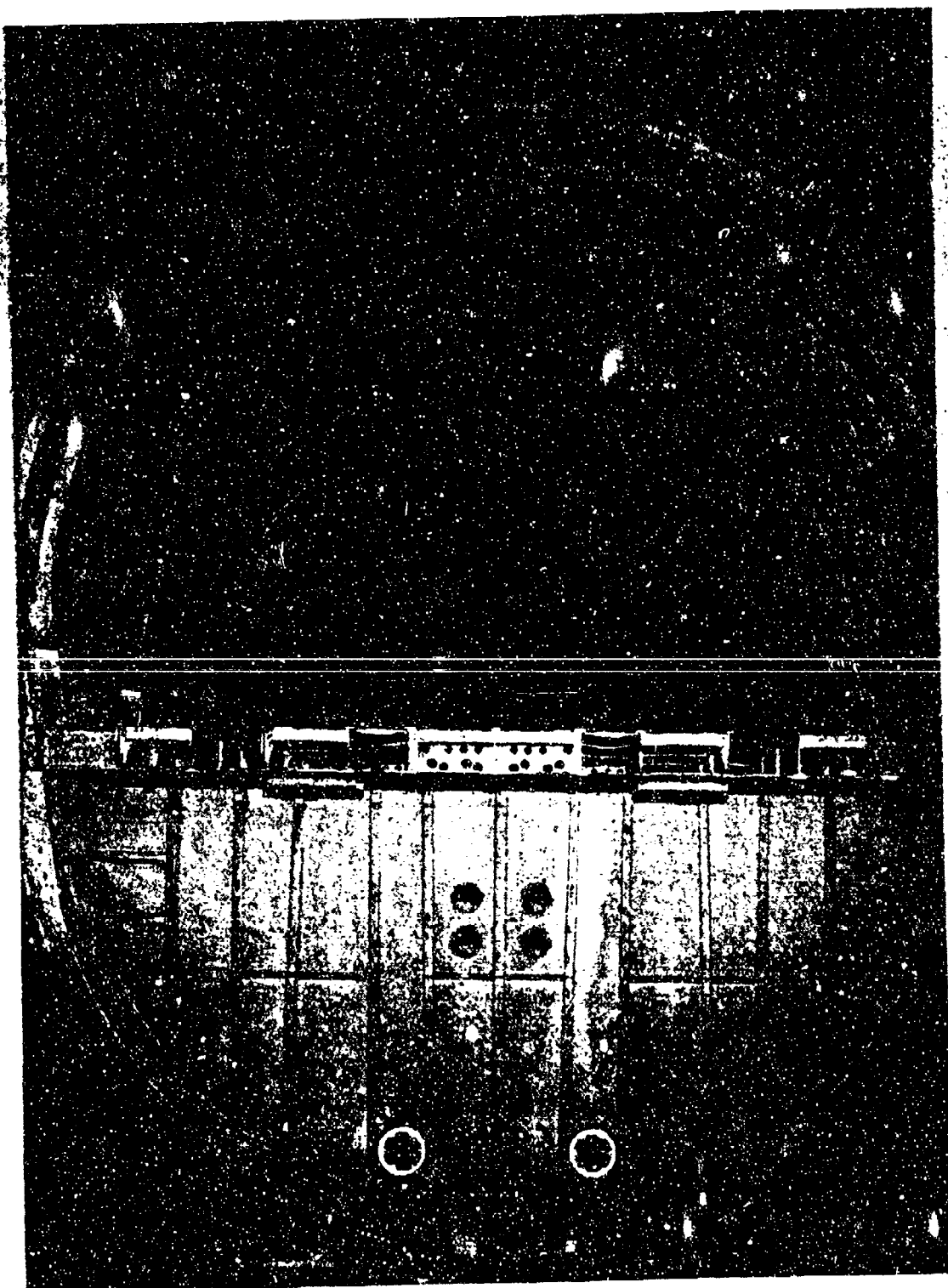


Figure 1. End View of KC-135A Fuselage Section

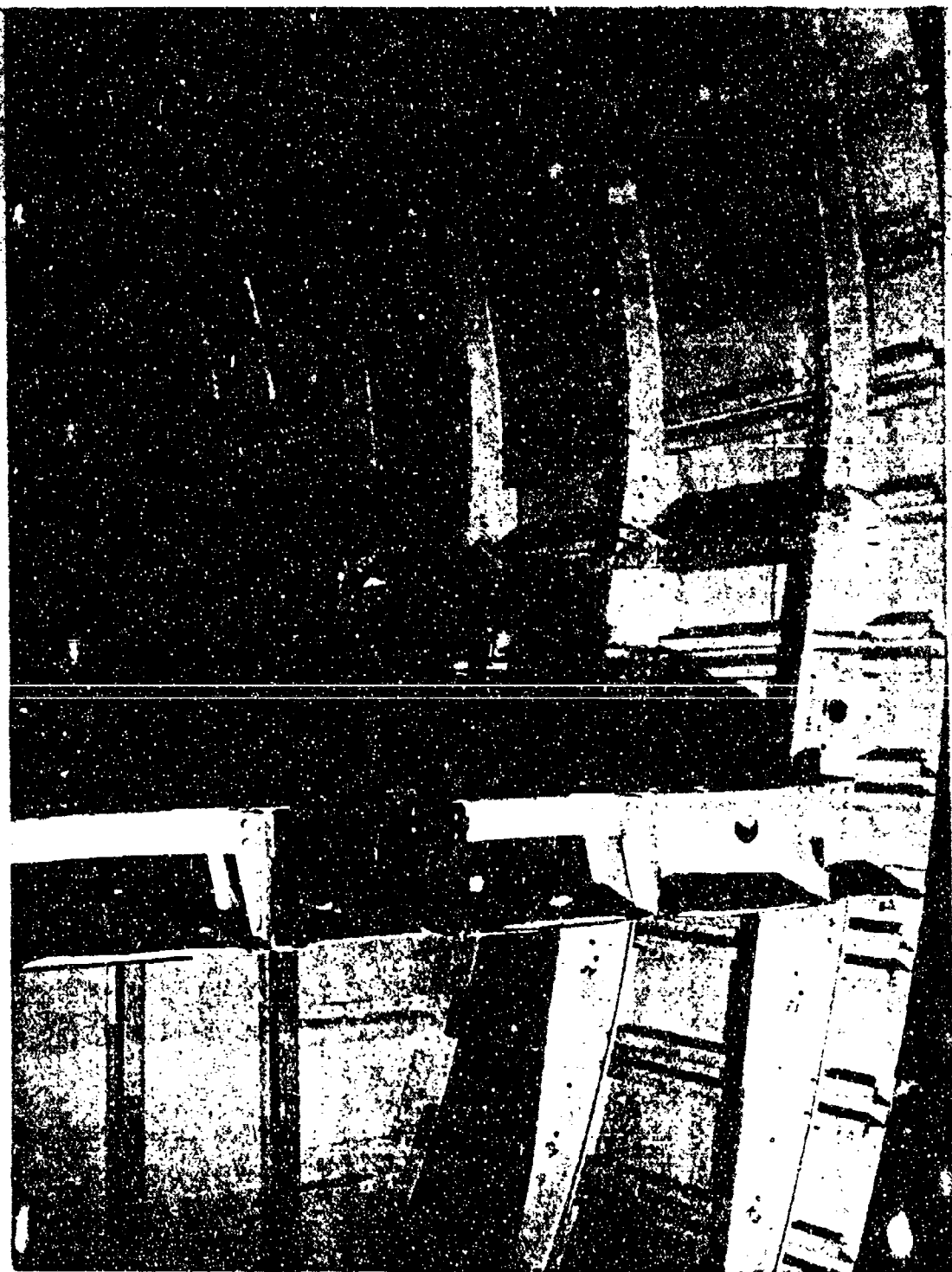


Figure 2. Detailed View of KC-135A Fuselage Section

and WL 210 as illustrated in Figure 3. The upper lobe compartment can be pressurized and was for some of the tests. The upper lobe compartment of this truncated fuselage section is the component that was instrumented to measure the dynamic response from a simulated blast overpressure. It should be noted that this fuselage section was part of an airplane that underwent full-scale fatigue tests prior to this 22 shot test series. Hence, the structure of the test specimen had been worked and certainly represents joint conditions common to those in airplanes that have logged significant flight time.

Figure 3 shows two views of the KC-135A fuselage test section. Figure 3b illustrates the side profile view of the upper lobe compartment while a cross section view at BS 1040 is given in Figure 3a. In the six bay test section, five Z-section frames of 7075-T6 aluminum are spaced 20 in apart at the body station designated in Figure 3b. These frames are attached by two fasteners (see Fig. 2) to each of the 31 hat stringers of 7075-T6 aluminum which are evenly spaced around the circumference of the upper lobe. There are three types of hat stringers and the number in parenthesis at each location indicates which type exists at BS 1040. It should be noted that, in general, a stringer is not homogeneous over the entire length of the fuselage section. There are splices at which the cross section changes from one type to another. The cross section dimensions of the Z section frame and the hat section stringer are given in Table 2. The type of skin fastened to the stringers varied over the upper lobe compartment as shown in Figure 3b, where the skin is divided into three areas indicated by the dashed lines. In the crown area above stringer S-7 the skin is 0.064-in 7075-T6 aluminum. Side skin of 2024-T3 aluminum below stringer S-7 and between BS 980 and 1020 is 0.064-in thick while between BS 1020 and 1080 the skin is 0.051-in thick. Above WL 230 the fuselage cross section is circular with a radius to the outer skin surface of 72 inches. Below WL 230, the cross section deviates slightly from a circular shape and the frames are deeper in this region. Above WL 230 the cross sections of the frames are constant. It is noted that the frame and stringer cross sections are formed and, therefore, have rounded corners.

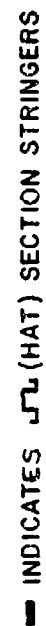
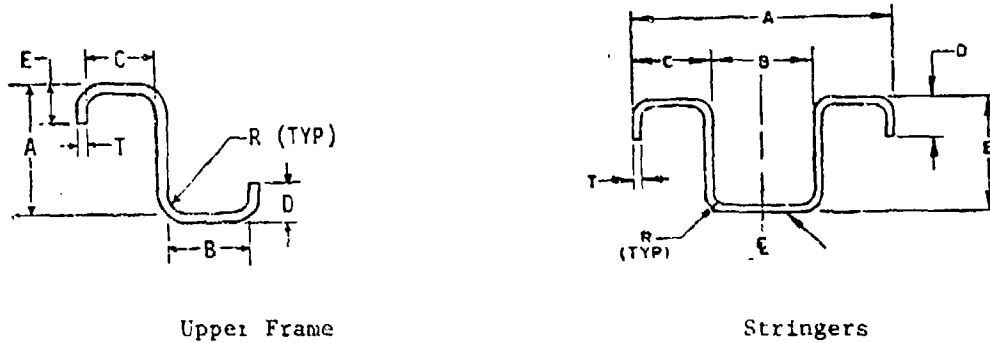


Figure 3. Schematic of AC-13A PaveLage Test Section Construction

TABLE 2
FRAME AND STRINGER CROSS SECTION DIMENSIONS



Dimension	Frame	Stringers		
		Type 1	Type 2	Type 3
A	2.44	2.24	2.76	2.76
B	0.9	0.76	1.0	1.0
C	0.9	0.74	0.88	0.88
D	0.33	0.25	0.3	0.2
E	0.33	1.25	1.25	1.25
T	0.064	0.051	0.056	0.064
R	0.25	0.13	0.16	0.16

All dimensions are in inches

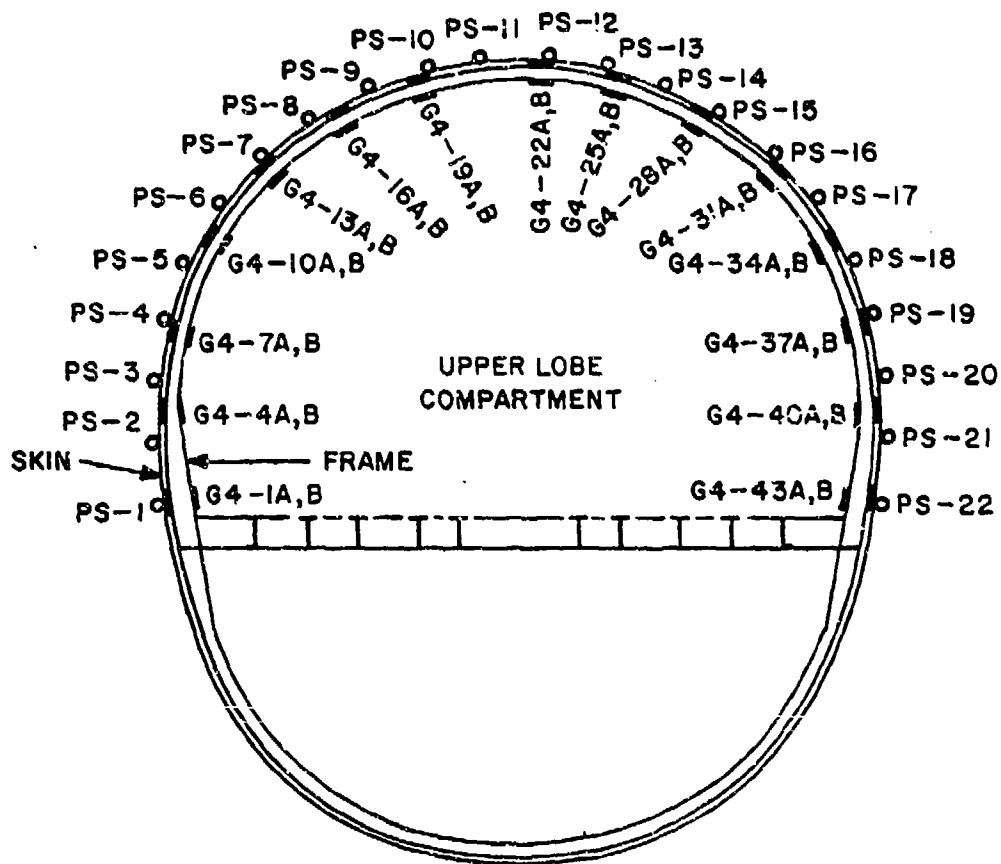
3. TEST INSTRUMENTATION AND RESPONSE RESULTS

The test instrumentation consists of pressure transducers and strain gages placed on the upper lobe portion of the KC-135A fuselage test section. At BS 1038, 22 pressure transducers were mounted to the fuselage at approximately 10° intervals. Uniaxial strain gages were placed on the inner and outer flanges of all the frames of the test specimen with major emphasis on the central frame at BS 1040. Shear rosette gages were also mounted on the web of the frame at BS 1040. The locations of all this instrumentation are given in Reference 6. In this correlation effort, emphasis was placed on the response of the flanges on the central frame at BS 1040. Thus, Figure 4 shows the approximate locations of pressure transducers and the strain gages on the inner and outer flanges of the central frame. The inner flange gage designated by A is located on the inboard surface and the outer flange gage designated by B is located on the outboard surface. The rosette gages are not shown since they were not used in the correlation. The more exact positions of the pressure and strain gages are given in Table 3.

The pressure data for each shot was put on a separate magnetic tape that could be used directly by the NOVA-2 LTS computer code to define the loading over the upper lobe fuselage section. These loading tapes were used to create data files which were accessed through the AFWL computer by designating the event number of the shot. The measured strain time histories on the flanges of the frame at BS 1040 are presented in plot form in Reference 6. The pressure time histories at each position are also given in Reference 6. These pressure plots were used to determine if any gage produced bad data, so that the corresponding tape channel could be ignored in the pressure model. It was found that only very few pressure channels had to be eliminated from all the data sets used in the correlation effort.

4. GENERAL RESPONSE BEHAVIOR OF FUSELAGE TEST SECTION

The test shots given in Table 1 were selected for correlation because they represent the various loading conditions covered in the test series presented in Reference 6. In the test series the test



- PRESSURE TRANSDUCERS (BS 1038)
- STRAIN GAGES ON FRAME (BS 1040)
- A INDICATES INNER FLANGE
- B INDICATES OUTER FLANGE

Figure 4. Instrumentation Locations for Central Frame

TABLE 3
PRESSURE AND STRAIN GAGE LOCATIONS

Pressure Gages BS 1038		Strain Gages BS 1040	
Gage No.	θ -Position (deg)	Gage No.	θ -Position (deg)
PS-1	2.64	G4-1	3.8
PS-2	13.28	G4-4	21.0
PS-3	22.43	G4-7	37.1
PS-4	32.58	G4-10	50.9
PS-5	42.33	G4-13	65.1
PS-6	53.07	G4-16	78.8
PS-7	63.02	G4-19	91.4
PS-8	73.16	G4-22	110.8
PS-9	82.91	G4-25	126.2
PS-10	92.02	G4-28	138.4
PS-11	102.86	G4-31	151.2
PS-12	113.0	G4-34	165.9
PS-13	123.91	G4-37	179.3
PS-14	132.95	G4-40	195.7
PS-15	142.6	G4-43	213.3
PS-16	152.85		
PS-17	162.74		
PS-18	173.48		
PS-19	182.89		
PS-20	193.43		
PS-21	202.68		
PS-22	213.13		

specimen was exposed to blast overpressure loadings from directly above the crown and 45° to the side as shown in Figure 3a. The longitudinal axis of the test specimen was always parallel to the blast front. For both orientations, four levels of static internal pressure (0.0, 2.6, 5.9, 8.7) were investigated to determine the effect of internal pressurization. Except for the last shot (22), the measured strains in the frame at BS 1040 remained in the elastic range.

For the blast orientation of 90° and no internal pressure, incident overpressure levels of 1.52 lb/in² (shot 6), 1.95 lb/in² (shot 17) and 2.5 lb/in² (shot 5) produced maximum measured compressive strains of 3200, 5000 and 6600 μ in/in, respectively, at 18.25° to the right of the center crown line. For the final shot, 22, at 3.5 lb/in², the maximum inelastic compressive strain is estimated between 40000 and 50000 μ in/in at 16.55° to the left of the center crown line before the gage failed. Since the peak response is significantly off center in all these tests and has switched sides during the final test, there are probably anomalies in both the symmetry of the pressure loading and the structure. If there are local weak points in the structure due to fabrication procedures or the prior loading history of the fuselage, these anomalies cannot be analytically modeled. For the blast orientation of 45° to the right of the center crown line and no internal pressure, an incident overpressure level of 2.1 lb/in² (shot 21) produced a maximum compression strain of 4200 μ in/in at 30.45° to the right of the center crown line. This peak response position is 14.55° to the left of the loading line. It should be noted that for a slightly higher incident pressure (2.1 versus 1.95 lb/in²), the 45° orientation produced a lower peak strain level (-4200 versus -5000 μ in/in) than the 90° orientation loading. When internal pressurization was used in the upper lobe compartment, the strain levels were significantly reduced for the same incident blast overpressure. For example, with an internal pressure of 2.5 lb/in² and an incident overpressure of 2.08 lb/in² (shot 16), the peak strains were reduced to -1080 and +1270 μ in/in from the -5000 μ in/in in shot 17 (Δp = 1.95 lb/in²) with no internal

pressure. The strain response time histories for the pressurization cases exhibited higher frequency oscillations. Further increases in the internal pressure to 8.75 lb/in^2 from 2.5 lb/in^2 only reduces the peak strains by about 25% for the 2.0 lb/in^2 blast overpressure level.

In the final shot, 22, ($\Delta p = 3.5 \text{ lb/in}^2$) significant permanent damage occurred to the frames in the crown region of the upper lobe fuselage section. A detail assessment of this permanent damage is given in Reference 6. Briefly, in the crown region there was yielding in the outer flange of the central frame. At several local positions in this crown region severe yielding of the frame occurred which led to rupture of the frame section. This severe damage was precipitated by local plastic buckling of the outer flange of the frame and subsequent plastic buckling of the web of the frame.

SECTION III

ANALYTICAL NOVA-2LTS MODELS FOR THE KC-135 FUSELAGE SECTION

Initially, a structural model of the KC-135A fuselage test section was generated assuming that the pressure loading was symmetric for the 90° orientation case. This model took advantage of double symmetry and, therefore, contained 16 longitudinal hat section stiffeners and three circumferential Z section frame stiffeners. This first trial model used 34 modes and an integration net of 19 by 17, so that Central Processing Unit (CPU) time on the CRAY computer was quite reasonable. From response solutions for shot 5 using this model it was found that local buckling of the skin between stringers had to be taken into account in some manner that would not require a prohibitive number of modes and integration points for an accurate solution. Furthermore, it was found that the pressure loading for the 90° orientation was not symmetric about the crown line and, therefore, a full model in the circumferential direction would be required in all cases for an accurate solution. However, the symmetric model was used to determine response sensitivity to various parameters such as spatial loading distribution, boundary conditions, buckling criteria and skin thickness. Thus, in this section the general structural model, the skin buckling method, the response sensitivity and the final model description are presented.

1. THE NOVA-2LTS STRUCTURAL MODEL FOR THE KC-135A FUSELAGE TEST SECTION

The analytical NOVA-2LTS structural model for the upper lobe compartment of the KC-135A fuselage test section is based on the test specimen description given in Section II-2. For the analytical model the geometry, boundary conditions, skin thickness, stiffener cross sections and material properties must be specified. For the actual structure described in Section II-2, it was apparent that some compromises would be necessary in the modeling for NOVA-2LTS. It is recalled that the crown section of the upper lobe compartment is circular above WL 230 and slightly deviates from circular between WL 230 and 210. Since the major strains occurred in the crown region of the

fuselage, the modeling below WL 230 could be compromised. Hence, the whole upper lobe compartment was assumed to be circular with a radius of 72 in to the outer surface of the skin. The subtended angle of this stiffened fuselage panel was taken as 215.9° and the length of the six bay fuselage test section is 120 in. In the NOVA-2LTS program the γ coordinate refers to the longitudinal direction and the β coordinate refers to the circumferential direction. In the γ -direction the boundaries are assumed to be simply supported along the circumferential edges that are attached to the end bulkhead by angle clips. In the β -direction the boundaries are assumed to be clamped where the frames intersect the floor of the compartment. Even though these assumed boundary conditions are probably not exact and could be modified by allowing elastic torsional constraint at the edges, the boundaries are far enough removed from the crown region so as not to have a significant effect on the major strain response. In NOVA-2LTS only one skin thickness can be specified over the entire panel while from Figure 2 it can be seen that the thickness varies over the panel. So again based on the fact that the major strains occurred in the crown region, it is assumed that the skin of this upper lobe compartment panel is 0.064-in 7075-T6 aluminum. The reference surface of the panel is set in NOVA-2LTS at the midsurface of the skin, so that the radius to this reference surface is 71.968 in.

The six bay test specimen panel was stiffened by five internal frames and 31 stringers. The frames were spaced 20 in apart and the stringers were evenly spaced around the circumference. In the final structural model symmetry was assumed only in the γ direction, so that the model required just three frames to be specified. The hat section stringers are attached directly to the skin and the flanges of the hat sections are attached to the Z section frames. Thus, there is a 1.25-in gap between the frames and the lower surface of the skin. The stringers are assumed to have constant cross sections over the length of panel based upon the cross sections at BS 1040. The type of cross section

varies around the circumference as indicated in Figure 2 and Table 2. The frames are all the same for the structural model. Their cross sections are constant above WL 230 and variable below WL 230. Both the stringers and frames are formed sections which contain rounded corners. In defining the cross sections of these stiffeners for the structural model the rounded corners are approximately taken into account. Table 4 gives the cross section input dimensions for the three types of hat section stringers and the variable Z section frame used in the structural mode. For the variable section of the frames the cross sections follow those given in Reference 6.

The stiffeners and the skin of the structural model are 7075-T6 aluminum. The material properties used in the model are as follows:

Modulus of Elasticity	$10.3 \times 10^6 \text{ lb/in}^2$
Shear Modulus	$4.0 \times 10^6 \text{ lb/in}^2$
Poisson's Ratio	0.3
Mass Density	$0.259 \times 10^{-3} \text{ lb-s}^2/\text{in}^4$
Yield Stress (elastic model)	72000 lb/in^2
Yield Stress (elastic-plastic model)	76400 lb/in^2
Strain Hardening slope	$1.85 \times 10^5 \text{ lb/in}^2$

2. SKIN BUCKLING CRITERION METHOD

From the preliminary model of the KC-135 fuselage section for shot 5 it was found that if the skin between stringers was not allowed to buckle, very large compression stresses were generated in the skin. These 0.064-in skin panels between stringers are separated from the frames and are about 8.5 in wide in the circumferential direction and 120 in long. They will buckle elastically in the circumferential direction at a low stress level. Therefore, their stiffness contribution in the preliminary model was much too high and this caused a very low response level of the fuselage section as compared to the experimental data. Since the buckling of these skin panels are very important, a method of incorporating this effect into the structural model was established.

TABLE 4
STIFFENER CROSS SECTION MODELS

Stringers

Stringer Type	Segments							
	1		2		3		4	
	h_1 (in)	b_1 (in)	h_1 (in)	b_1 (in)	h_1 (in)	b_1 (in)	h_1 (in)	b_1 (in)
1	0.051	0.76	1.0	0.102	1.199	0.183	1.25	1.33
2	0.056	0.985	0.95	0.112	1.194	0.201	1.25	1.58
3	0.064	0.985	0.95	0.128	1.186	0.201	1.25	1.58

Frames

($h_0 = 1.25$ in)

Position (deg)	Segments									
	1		2		3		4		5	
	h_1 (in)	b_1 (in)	h_1 (in)	b_1 (in)	h_1 (in)	b_1 (in)	h_1 (in)	b_1 (in)	h_1 (in)	b_1 (in)
0.0	1.322	0.872	2.28	0.144	4.08	0.072	5.88	0.072	5.952	0.87
6.74687	1.322	0.872	2.28	0.144	3.84	0.072	5.40	0.072	5.472	0.87
13.4937	1.322	0.872	2.28	0.144	3.415	0.072	4.55	0.072	4.622	0.87
20.2406	1.322	0.875	2.28	0.144	2.965	0.072	3.682	0.075	3.754	0.87
26.9875	1.314	0.8866	1.58	0.1104	3.424	0.064	3.69	0.1104	3.754	0.8866
107.95	1.314	0.8866	1.58	0.1104	3.424	0.064	3.69	0.1103	3.754	0.8866

A skin buckling criterion method has been developed and programmed into NOVA-2S and NOVA-2LTS. This method provides a practical approximate solution to a complicated local skin buckling response that occurs in the fuselage section. The buckling of the thin skin panels between stringers or/and frames of a fuselage section results from induced compressive membrane stresses caused by the engulfing blast pressure loading. To represent the local skin buckling modal patterns directly into a NOVA-2S structural model of an entire fuselage section would require a prohibitive number of integration points and modes. A smaller time increment for solution would also be required which would result in additional computer time. It should be noted that similar problems would also exist for nonlinear finite element structural models in that many small elements would be required to represent the local buckling.

For structures in which the response of the frames and stringers are of prime importance, the skin buckling criterion method offers an attractive alternative. In this method a critical buckling stress for the skin panels is selected and when the circumferential compressive membrane stress in the panel reaches this value, the membrane stress is reduced in some prescribed manner. This process is performed at each integration point on the skin for each time step of the solution. If the stress in the panel becomes lower than the buckling stress, the skin becomes fully active again. This method requires the definition of two parameters, namely, the critical buckling stress and the stress decay constant. The selection of these two parameters were guided by static buckling design procedures. Thus, the critical buckling stress can be computed from various static buckling formulas for flat and curved panels. It should be noted that panel buckling is influenced by geometric imperfections (usually unknown), snap-through action (shallow curved panels), dynamic effects and local panel boundary conditions. The design procedure for fuselage sections (see Reference 7) indicates that the effective area of the skin panels between stringers is reduced after buckling by the ratio of the critical buckling stress (σ_{cr}) to the applied stress (σ_a). Therefore, the stress reduction ratio evaluated for this method in NOVA-2S is $(\sigma_{cr}/\sigma_a)^n$, where n is defined as the

the stress decay constant. For the 8.5-in x 120-in panels between stringers of the KC-135A fuselage section, the static critical buckling stress was estimated from the following buckling formula for a clamped flat panel compressively loaded along the long edges:

$$s_{cr} = \frac{\pi k E}{12(1-\nu^2)} \left(\frac{h}{a}\right)^2 \sim 2100 \text{ lb/in}^2$$

where

k_c = buckling coefficient = 4

E = Modulus of Elasticity = $10.3 \times 10^6 \text{ lb/in}^2$

ν = Poisson's Ratio = 0.3

h = skin thickness = 0.064 in

a = short length = 8.5 in

In the final NOVA-2LTS models, the stress decay factor (η) was set at unity for the best correlation. The selection of $\eta = 1$ is consistent with static design procedures and the η used for the correlation with the B-52 aft fuselage section data in Reference 4. Thus, η was permanently set in the program at unity and it was not introduced as an input quantity.

To accomodate the skin buckling criterion method additions in the DEPROP subroutine of the NOVA-2S and NOVA-2LTS versions, the following modifications were made in the DEPROP input.

Group 10, p. 116 of Reference 3, has been modified as follows:

Group 10 (3112) NL, NSHEAR, NBUCK

Number of layers. (NL)

(NL must be 1 for KTYPE = 1 or 2; and 3 for KTYPE = 3 or 4.)

Core shear deformation option (KTYPE = 3 or 4) (NSHEAR)

0, no shear deformation

1, shear deformation included

Skin buckling criterion option (NBUCK)

0, no skin buckling

1, skin allowed to buckle

If NSHEAR = 0 (Group 10) skip to Group 17K, unless NBUCK = 0

The following data group is included in Group 17.

Skip Group 17K if NBUCK = 0

Group 17K: (F12.1) BUCKS

Critical Compressive Buckling Stress, lb/in^2 (BUCKS)
(should be a negative number)

The changes in the NOVA-2S and NOVA-2LTS program listings to extend DEPROP to include the aforementioned addition are presented in the Appendix. It should be noted that the core shear deformation option for honeycomb panels indicated in Group 10 is an in-house addition to DEPROP that is not yet complete. Therefore, users should just set NSHEAR to zero.

Since the frames of the KC-135A fuselage are not directly attached to the skin, the skin buckling criterion was applied to all integration points. However, in the case of the B-52 aft fuselage in Reference 4 where the frames are directly attached to the skin, integration points along the frames were excluded from the skin buckling option in order to allow for local fully effective skin. At present there are separate options for each fuselage model which have been handled by internal changes in the program. In the future, the fully or partially effective skin options should become part of input groupings for specified lines of integration points.

3. STRUCTURAL RESPONSE SENSITIVITY TO VARIOUS PARAMETERS

In the preliminary phase of this effort many KC-135 fuselage runs were made with the symmetry model at relatively low CPU time to investigate the response sensitivity to various parameters, especially those parameters associated with the skin buckling criterion method. A summary of all these runs are given in Table 5 which was organized to indicate the response sensitivity to the spatial loading distribution, stress decay constant, critical buckling stress, boundary conditions and skin thickness. All the computer results shown in Table 5 are for

TABLE 5
KC-135A FUSELAGE STRUCTURAL RESPONSE SENSITIVITY

(Shot 5, $\Delta p = 2.5 \text{ lb/in}^2$)

Load Model	Boundary Conditions Code	Stress Decay Constant	Buckling Stress (psi)	Skin Thickness (in)	Maximum Strain ($\mu\text{in/in}$)
Loading Distribution					
RS Sym.	21	0.33	-2000	0.064	-6900
LS Sym.	21	0.33	-2000	0.064	-5950
Full	21	0.33	-2000	0.064	-5430
Stress Decay Constant					
RS Sym.	21	0.0	-2000	0.064	-5500
RS Sym.	21	0.2	-2000	0.064	-6500
RS Sym.	21	0.33	-2000	0.064	-6900
RS Sym.	21	0.5	-2000	0.064	-7150
RS Sym.	21	1.0	-2000	0.064	-7400
Critical Buckling System					
Sym.	21	1.0	-2000	0.064	-7400
ym.	21	1.0	-2500	0.064	-7500
RS Sym.	21	1.0	-3000	0.064	-7900
RS Sym.	21	1.0	-3500	0.064	-7300
RS Sy	21	1.0	-4000	0.064	-7800
RS Sy	21	1.0	∞	0.064	-1500
Boundary Condition					
RS Sym.	11	0.0	-2000	0.064	-6000
RS Sym.	21	0.0	-2000	0.064	-5500
RS Sym.	22	0.0	-2000	0.064	-5250
Skin Thickness					
RS Sym.	21	1.0	-2000	0.064	-5500
RS Sym.	21	1.0	-2000	0.0575	-5800

shot 5 at an incident overpressure of 2.5 lb/in^2 and no internal pressure. The load model, boundary conditions code, stress decay constant, buckling stress and skin thickness are the parameters that were varied in the preliminary analysis. Table 5 shows the result of varying one parameter at a time based on the comparison of the maximum strain occurring in the flanges of the central frame. The load models considered are the symmetry structural case using the right side (RS) and left side (LS) loads and the full structural and load case. In the boundary condition code the first digit indicates the condition in the γ -direction and the second digit the condition in the β -direction. A number one (1) designates clamped-clamped and a number two (2) designates pinned-pinned.

The differences in the spatial loading distributions represented by the three load models for the 90° orientation in Table 5 are not significant from cursory comparison of pressure time histories, yet the change in maximum strain response can be as much as 27% by simplifying the full loading case by assuming symmetry. If the stress decay constants were varied from the linear reduction of stress ($\eta = 1$) case to the constant stress ($\eta = 0$) case, the maximum strain decreased by about 26%. It was also found that if the skin membrane stress was allowed to vanish after buckling ($\eta = \infty$), the maximum strain increased by about 30% based on the $\eta = 1$ case. When the critical buckling stress was varied from -2000 to -4000 lb/in^2 , the maximum difference in strain response produced only an 6.8% change. Thus, the maximum strain response is not very sensitive to the critical buckling stress at this low stress level regime. However, when skin buckling is ignored ($\sigma_{cr} = \infty$), the maximum strain response reduced by about 80%. For the boundary condition sensitivity evaluation the code 21 is considered the base case, that is, pinned in the γ -direction and clamped in the β direction. If the boundaries are clamped in both direction, the maximum strain response increased by about 9%. If the boundaries are pinned in both directions, the maximum strain response decreased by about 4.5%. Since the location of the maximum strain in the crown region is far removed from the boundaries,

this strain response was not very sensitive to the boundary condition. Since the skin thickness varies over the upper fuselage compartment, response sensitivity to skin thickness was considered. A structural model using an average skin thickness of 0.0575 in increased the maximum strain response by about 5.5% over the model based on the crown region skin thickness of 0.064 in.

Based partially on these results, the final NOVA-2LTS models for the KC-135A fuselage test section used the full loading model (ie, no symmetry about center of crown), a stress decay constant of unity, the critical buckling stress of -2000 lb/in^2 , the 21 boundary condition code and the 0.064-in skin thickness.

4. DESCRIPTION OF FINAL STRUCTURAL MODELS

The final structural NOVA-2LTS models for the KC-135A fuselage test section were constructed based on the information generated in Sections III-1 through III-3. In summary, the structural model uses symmetry only in the γ direction, so that the model has three Z-section frame stiffeners in the β direction and 31 hat section stringers stiffeners in the γ direction. A uniform 0.064-in skin was assumed to be attached to the stringers and the frames are attached to the inner flanges of the stringers with a 1.25-in gap between the frames and the skin. All materials are assumed to be 7075-T6 aluminum. The fuselage test section is 120 in long in the γ direction and is assumed to be circular in the β direction with a radius of 71.968 in to the midsurface of the skin and a subtended angle of 215.9° . The γ boundaries (circular edges) are assumed to be simply supported and the β boundaries (straight edges) are assumed to be clamped. The inplane boundary conditions are assumed to be fixed in both coordinate directions. The loading model used the appropriate data tape and assumed that the loading distribution in the γ direction was uniform.

There are two basic NOVA-2LTS models that are representative of the seven shots investigated in this effort. These two models are given in Tables 6 and 7 and are based on an elastic response model (shot 5) and an elastic-plastic model (shot 22), respectively. The data deck listing for shot 5 given in Table 6 represents the model used for

NOVA-2LTS DATA DECK LISTING OF THE KC-135A FUSELAGE FOR SHOP 5

34

Table 6 (Continued)

9	5	GP 7-19
9	7	GP 7-20
9	8	GP 7-21
9	9	GP 7-22
9	10	GP 7-23
9	11	GP 7-24
9	12	GP 7-25
9	13	GP 7-26
9	14	GP 7-27
9	15	GP 7-28
9	16	GP 7-29
9	17	GP 7-30
9	18	GP 7-31
9	19	GP 7-32
9	20	GP 7-33
11	4	GP 7-34
11	5	GP 7-35
11	6	GP 7-36
11	7	GP 7-37
11	8	GP 7-38
11	9	GP 7-39
11	10	GP 7-40
11	11	GP 7-41
11	12	GP 7-42
11	13	GP 7-43
11	14	GP 7-44
11	15	GP 7-45
11	16	GP 7-46
11	17	GP 7-47
11	18	GP 7-48
11	19	GP 7-49
11	20	GP 7-50
13	4	GP 7-51
13	5	GP 7-52
13	6	GP 7-53
13	7	GP 7-54
13	8	GP 7-55
13	9	GP 7-56
13	10	GP 7-57

Table 6 (Continued)

13	11	GP 7-58
13	12	GP 7-59
13	13	GP 7-60
13	14	GP 7-61
13	15	GP 7-62
13	16	GP 7-63
13	17	GP 7-64
13	18	GP 7-65
13	19	GP 7-66
13	20	GP 7-67
31		GP 8
19	1	GP 9-1
19	3	GP 9-2
19	5	GP 9-3
19	7	GP 9-4
19	9	GP 9-5
19	11	GP 9-6
19	13	GP 9-7
19	15	GP 9-8
19	17	GP 9-9
19	19	GP 9-10
19	21	GP 9-11
19	23	GP 9-12
19	25	GP 9-13
19	27	GP 9-14
19	29	GP 9-15
19	31	GP 9-16
19	33	GP 9-17
19	35	GP 9-18
19	37	GP 9-19
19	39	GP 9-20
19	41	GP 9-21
19	43	GP 9-22

Table 6 (Continued)

[illegible]

Table 6 (Continued)

0.00025	4	0				GP 21-3
0.056						GP 22-3
0.95						GP 23-1
1.194						GP 23-2
1.25						GP 23-3
-1.0						GP 23-4
		10.3E6	4.0E6 0.000259	72000.	72000.	GP 19-4
	4	0				GP 21-4
0.00025						GP 22-4
0.055						GP 23-1
0.95						GP 23-2
1.194						GP 23-3
1.25						GP 23-4
-1.0						GP 19-5
		10.3E6	4.0E6 0.000259	72000.	72000.	GP 21-5
	4	0				GP 22-5
0.00025						GP 23-1
0.055						GP 23-2
0.95						GP 23-3
1.194						GP 23-4
1.25						GP 19-6
-1.0						GP 21-6
		10.3E6	4.0E6 0.000259	72000.	72000.	GP 22-6
	4	0				GP 23-1
0.00039						GP 23-2
0.064						GP 23-3
0.95						GP 23-4
1.185						GP 19-7
1.25						GP 21-7
-1.0						GP 22-7
		10.3E6	4.0E6 0.000259	72000.	72000.	GP 23-1
	4	0				GP 23-2
0.00039						GP 23-3
0.064						GP 23-4
0.95						GP 19-8
1.185						
1.25						
-1.0						
		10.3E6	4.0E6 0.000259	72000.	72000.	
	4	0				

Table 6 (Continued)

0.00039	4	0.0	0			GP 21-8
0.064		0.985				GP 22-8
0.95		0.128				GP 23-1
1.185		0.201				GP 23-2
1.25		1.58				GP 23-3
-1.0			10.3E5	4.0E6 0.000259	72030.	GP 23-4
			0			GP 19-9
0.00017	4	0.0				GP 21-9
0.051		0.76				GP 22-9
1.0		0.102				GP 23-1
1.199		0.183				GP 23-2
1.25		1.33				GP 23-3
-1.0			10.3E5	4.0E6 0.000259	72000.	GP 23-4
			0			GP 19-10
0.00017	4	0.0				GP 21-10
0.051		0.76				GP 22-10
1.0		0.102				GP 23-1
1.199		0.183				GP 23-2
1.25		1.33				GP 23-3
-1.0			10.3E5	4.0E6 0.000259	72000.	GP 23-4
			0			GP 19-11
0.00017	4	0.0				GP 21-11
0.051		0.76				GP 22-11
1.0		0.102				GP 23-1
1.199		0.183				GP 23-2
1.25		1.33				GP 23-3
-1.0			10.3E5	4.0E6 0.000259	72030.	GP 23-4
			0			GP 19-12
0.00039	4	0.0				GP 21-12
0.064		0.985				GP 22-12
0.95		0.128				GP 23-1
1.185		0.201				GP 23-2
1.25		1.58				GP 23-3
-1.0			10.3E5	4.0E6 0.000259	72030.	GP 23-4
			0			GP 19-13
0.00017	4	0.0				GP 21-13
0.051		0.76				GP 22-13
			10.3E5	4.0E6 0.000259	72000.	GP 23-1

Table 6 (Continued)

1.0	0.102				GP 23-2
1.199	0.183				GP 23-3
1.25	1.33				GP 23-4
-1.0		10.3E6	4.0E6 0.000259	72000.	GP 19-14
					GP 21-14
0.00017	0.0				GP 22-14
0.051	0.76				GP 23-1
1.0	0.102				GP 23-2
1.199	0.183				GP 23-3
1.25	1.33				GP 23-4
-1.0		10.3E6	4.0E6 0.000259	72000.	GP 19-15
					GP 21-15
0.00039	0.0				GP 22-15
0.064	0.985				GP 23-1
0.95	0.128				GP 23-2
1.186	0.201				GP 23-3
1.25	1.58				GP 23-4
-1.0		10.3E6	4.0E6 0.000259	72000.	GP 19-16
					GP 21-16
0.00039	0.0				GP 22-16
0.064	0.985				GP 23-1
0.95	0.128				GP 23-2
1.186	0.201				GP 23-3
1.25	1.58				GP 23-4
-1.0		10.3E6	4.0E6 0.000259	72000.	GP 19-17
					GP 21-17
0.00039	0.0				GP 22-17
0.064	0.985				GP 23-1
0.95	0.128				GP 23-2
1.186	0.201				GP 23-3
1.25	1.58				GP 23-4
-1.0		10.3E6	4.0E6 0.000259	72000.	GP 19-18
					GP 21-18
0.00017	0.0				GP 22-18
0.051	0.76				GP 23-1
1.0	0.102				GP 23-2
1.199	0.183				GP 23-3
1.25	1.33				GP 23-4

Table 6 (Continued)

-1.0	4	10.3E5	4.0E6	0.000259	72000.	72000.	GP 19-19
0.00017							GP 21-19
0.051	0.0						GP 22-19
1.0	0.76						GP 23-1
1.199	0.102						GP 23-2
1.25	0.183						GP 23-3
-1.0	1.33						GP 23-4
		10.3E5	4.0E6	0.000259	72000.	72000.	GP 19-20
0.00039	4						GP 21-20
0.064	0.0						GP 22-20
0.95	0.985						GP 23-1
1.185	0.128						GP 23-2
1.25	0.201						GP 23-3
-1.0	1.58						GP 23-4
		10.3E5	4.0E6	0.000259	72000.	72000.	GP 19-21
0.00017	4						GP 21-21
0.051	0.0						GP 22-21
1.0	0.76						GP 23-1
1.199	0.102						GP 23-2
1.25	0.183						GP 23-3
-1.0	1.33						GP 23-4
		10.3E5	4.0E6	0.000259	72000.	72000.	GP 19-22
0.00017	4						GP 21-22
0.051	0.0						GP 22-22
1.0	0.76						GP 23-1
1.199	0.102						GP 23-2
1.25	0.183						GP 23-3
-1.0	1.33						GP 23-4
		10.3E5	4.0E6	0.000259	72000.	72000.	GP 19-23
0.00017	4						GP 21-23
0.051	0.0						GP 22-23
1.0	0.76						GP 23-1
1.199	0.102						GP 23-2
1.25	0.183						GP 23-3
-1.0	1.33						GP 23-4
		10.3E5	4.0E6	0.000259	72000.	72000.	GP 19-24
0.00017	4						GP 21-24
0.051	0.0						GP 22-24
1.0	0.76						GP 23-1
1.199	0.102						GP 23-2
1.25	0.183						GP 23-3
-1.0	1.33						GP 23-4
		10.3E5	4.0E6	0.000259	72000.	72000.	GP 19-24

Table 6 (Continued)

0.00039	4	0.0	0				GP 21-24
0.064		0.985					GP 22-24
0.95		0.128					GP 23-1
1.185		0.201					GP 23-2
1.25		1.58					GP 23-3
-1.0			10.3E5	4.0E6	0.000259	72000.	GP 23-4
			0				GP 19-25
0.00039	4	0.0					GP 21-25
0.064		0.985					GP 22-25
0.95		0.128					GP 23-1
1.185		0.201					GP 23-2
1.25		1.58					GP 23-3
-1.0			10.3E6	4.0E6	0.000259	72000.	GP 23-4
			0				GP 19-26
0.00039	4	0.0					GP 21-26
0.064		0.985					GP 22-26
0.95		0.128					GP 23-1
1.185		0.201					GP 23-2
1.25		1.58					GP 23-3
-1.0			10.3E5	4.0E6	0.000259	72000.	GP 23-4
			0				GP 19-27
0.00025	4	0.0					GP 21-27
0.056		0.985					GP 22-27
0.95		0.112					GP 23-1
1.194		0.201					GP 23-2
1.25		1.58					GP 23-3
-1.0			10.3E5	4.0E6	0.000259	72000.	GP 23-4
			0				GP 19-28
0.00025	4	0.0					GP 21-28
0.056		0.985					GP 22-28
0.95		0.112					GP 23-1
1.194		0.201					GP 23-2
1.25		1.58					GP 23-3
-1.0			10.3E5	4.0E6	0.000259	72000.	GP 23-4
			0				GP 19-29
0.00025	4	0.0					GP 21-29
0.056		0.985					GP 22-29
			10.3E5	4.0E6	0.000259	72000.	GP 23-1
			0				

Table 6 (Continued)

[illegible]

Table 6 (Continued)

4.55	0.072			GP 29-4
4.622	0.87			GP 29-5
0.00053	1.25	20.240625		GP 28-4
1.322	0.872			GP 29-1
2.28	0.144			GP 29-2
2.965	0.072			GP 29-3
3.682	0.072			GP 29-4
3.754	0.87			GP 29-5
0.00041	1.25	26.9875		GP 28-5
1.314	0.8866			GP 29-1
1.58	0.1104			GP 29-2
3.424	0.064			GP 29-3
3.69	0.1104			GP 29-4
3.754	0.8866			GP 29-5
0.00041	1.25	107.95		GP 28-6
1.314	0.8866			GP 29-1
1.58	0.1104			GP 29-2
3.424	0.064			GP 29-3
3.69	0.1104			GP 29-4
3.754	0.8866			GP 29-5
0.00041	1.25	188.9125		GP 28-7
1.314	0.8866			GP 29-1
1.58	0.1104			GP 29-2
3.424	0.064			GP 29-3
3.69	0.1104			GP 29-4
3.754	0.8866			GP 29-5
0.00053	1.25	195.5594		GP 28-8
1.322	0.872			GP 29-1
2.28	0.144			GP 29-2
2.965	0.072			GP 29-3
3.682	0.072			GP 29-4
3.754	0.87			GP 29-5
0.00074	1.25	202.406		GP 28-9
1.322	0.872			GP 29-1
2.28	0.144			GP 29-2
3.415	0.072			GP 29-3
4.55	0.072			GP 29-4
4.622	0.87			GP 29-5
0.00034	1.25	209.153		GP 28-10
1.322	0.872			GP 29-1

GP 29-2
GP 29-3
GP 29-4
GP 29-5
GP 28-11
GP 29-1
GP 29-2
GP 29-3
GP 29-4
GP 29-5
GP 30-1
GP 30-2
GP 30-3
GP 30-4
GP 30-5
GP 30-6
GP 30-7
GP 30-8
GP 30-9
GP 30-10
GP 30-11
GP 30-12
GP 30-13
GP 30-14
GP 30-15
GP 30-16
GP 30-17
GP 30-18
GP 30-19
GP 30-20
GP 30-21
GP 30-22
GP 30-23
GP 30-24
GP 31
G 6

[illegible]

1.0E-5 10.0E-3 20.0

47

Table 6 (Concluded)

[illegible]

TABLE 7

NOVA-2LTS DATA DECK LISTING OF THE KC-135A FUSELAGE FOR SHOT 22

0.5	KC-135 FUSELAGE		FULL MODEL - SHOT 22		GRAY	CRAY	G 1
	1	100	2	0			
	1	1	20	19	65	1	G 2
	1	3	5	5	7	9	G 3
	13						G 4
	1	2	3	3	4	5	GP 1
	7	8	9	9	10	11	11GP 2-1
	13	14	15	15	15	17	GP 2-2
	19	20					5GP 3-1
	0	1	11				12GP 3-2
	1	21	2				19GP 3-3
	67		31				GP 3-4
	5	14					GP 4
	5	15					GP 5
	5	16					GP 6
	5	17					GP 7-1
	5	18					GP 7-2
	5	19					GP 7-3
	5	20					GP 7-4
	7	10					GP 7-5
	7	11					GP 7-6
	7	12					GP 7-7
	7	13					GP 7-8
	7	14					GP 7-9
	7	15					GP 7-10
	7	16					GP 7-11
	7	17					GP 7-12
	7	18					GP 7-13
	7	19					GP 7-14
	7	20					GP 7-15
	9	5					GP 7-16
	9	7					GP 7-17
	9	8					GP 7-18
	9	9					GP 7-19
							GP 7-20
							GP 7-21
							GP 7-22

Table 7 (Continued)

9	10	GP 7-23
9	11	GP 7-24
9	12	GP 7-25
9	13	GP 7-26
9	14	GP 7-27
9	15	GP 7-28
9	16	GP 7-29
9	17	GP 7-30
9	18	GP 7-31
9	19	GP 7-32
9	20	GP 7-33
11	4	GP 7-34
11	5	GP 7-35
11	6	GP 7-36
11	7	GP 7-37
11	8	GP 7-38
11	9	GP 7-39
11	10	GP 7-40
11	11	GP 7-41
11	12	GP 7-42
11	13	GP 7-43
11	14	GP 7-44
11	15	GP 7-45
11	16	GP 7-46
11	17	GP 7-47
11	18	GP 7-48
11	19	GP 7-49
11	20	GP 7-50
13	4	GP 7-51
13	5	GP 7-52
13	6	GP 7-53
13	7	GP 7-54
13	8	GP 7-55
13	9	GP 7-56
13	10	GP 7-57
13	11	GP 7-58
13	12	GP 7-59
13	13	GP 7-50
13	14	GP 7-61

Table 7 (Continued)

13	15	GP 7-62
13	15	GP 7-63
13	17	GP 7-64
13	19	GP 7-65
13	19	GP 7-66
13	20	GP 7-67
33		GP 8
19	1	GP 9-1
19	3	GP 9-2
19	5	GP 9-3
19	7	GP 9-4
19	9	GP 9-5
19	11	GP 9-6
19	13	GP 9-7
19	15	GP 9-8
19	17	GP 9-9
19	19	GP 9-10
19	21	GP 9-11
19	23	GP 9-12
19	25	GP 9-13
19	27	GP 9-14
19	29	GP 9-15
19	31	GP 9-16
19	33	GP 9-17
19	35	GP 9-18
19	37	GP 9-19
19	39	GP 9-20
19	41	GP 9-21
19	43	GP 9-22
19	45	GP 9-23
19	47	GP 9-24
19	49	GP 9-25
19	51	GP 9-26
19	53	GP 9-27
19	55	GP 9-28
19	57	GP 9-29
19	59	GP 9-30
19	51	GP 9-31
19	63	GP 9-32
19	65	GP 9-33

Table 7 (Continued)

120.	1	0	1	GP 10
0.064	215.9	71.962		GP 11
0.3	.000259	10.3E6		GP 16
-2000.	0	1.0E5 0.0	0.1	GP 17
	3	5	0	3GP 17A
	15	17	7	GP 17K
	27	29	19	13GP 18-1
	39	41	31	25GP 18-2
	51	53	43	37GP 18-3
	63		55	49GP 18-4
				51GP 18-5
				GP 18-6
-1.0	10.3E5	4.0E6 0.000259	72000.	GP 19-1
0.00025	4	3		GP 21-1
0.055	0.0			GP 22-1
0.95	0.985			GP 23-1
1.194	0.112			GP 23-2
1.25	0.201			GP 23-3
-1.0	1.58			GP 23-4
	10.3E5	4.0E6 0.000259	72000.	GP 19-2
0.00025	4	3		GP 21-2
0.055	0.0			GP 22-2
0.95	0.965			GP 23-1
1.194	0.112			GP 23-2
1.25	0.201			GP 23-3
-1.0	1.58			GP 23-4
	10.3E5	4.0E6 0.000259	72000.	GP 19-3
0.00025	4	3		GP 21-3
0.055	0.0			GP 22-3
0.95	0.985			GP 23-1
1.194	0.112			GP 23-2
1.25	0.201			GP 23-3
-1.0	1.58			GP 23-4
	10.3E5	4.0E6 0.000259	72000.	GP 19-4
0.00025	4	3		GP 21-4
0.056	0.0			GP 22-4
0.95	0.985			GP 23-1
1.194	0.112			GP 23-2
1.25	0.201			GP 23-3
-1.0	1.58			GP 23-4
	10.3E5	4.0E6 0.000259	72000.	GP 19-5

Table 7 (Continued)

0.00025	4	0.0	0		GP 21-5
0.055		0.985			GP 22-5
0.95		0.112			GP 23-1
1.194		0.201			GP 23-2
1.25		1.58			GP 23-3
-1.0			10.3E5	4.0E6 0.000259 72000.	GP 23-4
			0		GP 19-6
0.00039	4	0.0			GP 21-6
0.064		0.985			GP 22-6
0.95		0.128			GP 23-1
1.185		0.201			GP 23-2
1.25		1.58			GP 23-3
-1.0			10.3E5	4.0E6 0.000259 72000.	GP 23-4
			0		GP 19-7
0.00039	4	0.0			GP 21-7
0.064		0.985			GP 22-7
0.95		0.128			GP 23-1
1.185		0.201			GP 23-2
1.25		1.58			GP 23-3
-1.0			10.3E5	4.0E6 0.000259 72000.	GP 23-4
			0		GP 19-8
0.00039	4	0.0			GP 21-8
0.064		0.985			GP 22-8
0.95		0.128			GP 23-1
1.185		0.201			GP 23-2
1.25		1.58			GP 23-3
-1.0			10.3E5	4.0E6 0.000259 72000.	GP 23-4
			0		GP 19-9
0.00017	4	0.0			GP 21-9
0.051		0.76			GP 22-9
1.0		0.102			GP 23-1
1.193		0.183			GP 23-2
1.25		1.33			GP 23-3
-1.0			10.3E5	4.0E6 0.000259 72000.	GP 23-4
			0		GP 19-10

Table 7 (Continued)

0.00017	4	0.0	3				GP 21-10
0.051		0.76					GP 22-10
1.0		0.102					GP 23-1
1.193		0.183					GP 23-2
1.25		1.33					GP 23-3
-1.0			10.3E5	4.0E6	0.000259	72000.	GP 23-4
			3				GP 19-11
0.00017	4	0.0					GP 21-11
0.051		0.76					GP 22-11
1.0		0.102					GP 23-1
1.193		0.183					GP 23-2
1.25		1.33					GP 23-3
-1.0			10.3E6	4.0E6	0.000259	72000.	GP 23-4
			3				GP 19-12
0.00033	4	0.0					GP 21-12
0.064		0.985					GP 22-12
0.95		0.128					GP 23-1
1.185		0.201					GP 23-2
1.25		1.58					GP 23-3
-1.0			10.3E5	4.0E6	0.000259	72000.	GP 23-4
			3				GP 19-13
0.00017	4	0.0					GP 21-13
0.051		0.76					GP 22-13
1.0		0.102					GP 23-1
1.193		0.183					GP 23-2
1.25		1.33					GP 23-3
-1.0			10.3E6	4.0E6	0.000259	72000.	GP 23-4
			3				GP 19-14
0.00017	4	0.0					GP 21-14
0.051		0.76					GP 22-14
1.0		0.102					GP 23-1
1.193		0.183					GP 23-2
1.25		1.33					GP 23-3
-1.0			10.3E6	4.0E6	0.000259	72000.	GP 23-4
			3				GP 19-15
0.00033	4	0.0					GP 21-15
0.064		0.985					GP 22-15
0.95		0.128					GP 23-1
1.185		0.201					GP 23-2
1.25		1.58					GP 23-3
-1.0			10.3E5	4.0E6	0.000259	72000.	GP 23-4
			3				GP 19-16

Table 7 (Continued)

0.00339	4	0			GP 21-16
0.064					GP 22-16
0.95					GP 23-1
1.186					GP 23-2
1.25					GP 23-3
-1.0					GP 23-4
		10.3E5	4.0E6 0.000259	72000.	GP 19-17
	4	0			GP 21-17
0.00039					GP 22-17
0.064					GP 23-1
0.95					GP 23-2
1.185					GP 23-3
1.25					GP 23-4
-1.0					GP 19-18
		10.3E6	4.0E6 0.000259	72000.	GP 21-18
	4	0			GP 22-18
0.00017					GP 23-1
0.051					GP 23-2
1.0					GP 23-3
1.199					GP 23-4
1.25					GP 19-19
-1.0					GP 21-19
		10.3E6	4.0E6 0.000259	72000.	GP 22-19
	4	0			GP 23-1
0.00017					GP 23-2
0.051					GP 23-3
1.0					GP 23-4
1.199					GP 19-20
1.25					GP 21-20
-1.0					GP 22-20
		10.3E5	4.0E6 0.000259	72000.	GP 23-1
	4	0			GP 23-2
0.00039					GP 23-3
0.054					GP 23-4
0.95					GP 19-20
1.185					GP 21-20
1.25					GP 22-20
-1.0					GP 23-1
		10.3E5	4.0E6 0.000259	72000.	GP 23-2
	4	0			GP 23-3
0.00017					GP 23-4
0.051					GP 19-21
1.0					GP 21-21
1.199					GP 22-21
1.25					GP 23-1
-1.0					GP 23-2
					GP 23-3
					GP 23-4

Table 7 (Continued)

-1.0	10.3E6	4.0E6	0.000259	72000.	72000.	72000.	GP 19-22
0.00017	0.0						GP 21-22
0.051	0.76						GP 22-22
1.0	0.102						GP 23-1
1.199	0.183						GP 23-2
1.25	1.33						GP 23-3
-1.0	10.3E6	4.0E6	0.000259	72000.	72000.	72000.	GP 23-4
	0						GP 19-23
							GP 21-23
0.00017	0.0						GP 19-22
0.051	0.76						GP 21-22
1.0	0.102						GP 22-22
1.199	0.183						GP 23-1
1.25	1.33						GP 23-2
-1.0	10.3E6	4.0E6	0.000259	72000.	72000.	72000.	GP 23-3
	0						GP 23-4
							GP 19-26
							GP 21-25
							GP 22-25
							GP 23-1
							GP 23-2
							GP 23-3
							GP 23-4
							GP 19-26
							GP 21-25
							GP 22-25
							GP 23-1
							GP 23-2
							GP 23-3
							GP 23-4
							GP 19-27

Table 7 (Continued)

2.28	0.144			GP 29-2
4.08	0.072			GP 29-3
5.88	0.072			GP 29-4
5.952	0.87			GP 29-5
0.00034	1.25	6.746875		GP 28-2
1.322	0.872			GP 29-1
2.28	0.144			GP 29-2
3.84	0.072			GP 29-3
5.4	0.072			GP 29-4
5.472	0.87			GP 29-5
0.00074	1.25	13.49375		GP 28-3
1.322	0.872			GP 29-1
2.28	0.144			GP 29-2
3.413	0.072			GP 29-3
4.55	0.072			GP 29-4
4.622	0.87			GP 29-5
0.00053	1.25	20.240625		GP 28-4
1.322	0.872			GP 29-1
2.28	0.144			GP 29-2
2.965	0.072			GP 29-3
3.682	0.072			GP 29-4
3.754	0.87			GP 29-5
0.00041	1.25	26.9875		GP 28-5
1.314	0.8866			GP 29-1
1.58	0.1104			GP 29-2
3.424	0.064			GP 29-3
3.69	0.1104			GP 29-4
3.754	0.8866			GP 29-5
0.00041	1.25	107.95		GP 28-6
1.314	0.8866			GP 29-1
1.58	0.1104			GP 29-2
3.424	0.064			GP 29-3
3.59	0.1104			GP 29-4
3.754	0.8866			GP 29-5
0.00041	1.25	188.9125		GP 28-7
1.314	0.8866			GP 29-1

Table 7 (Continued)

1.58	0.1104				GP 29-2
3.424	0.064				GP 29-3
3.69	0.1104				GP 29-4
3.754	0.8866				GP 29-5
0.00053	1.25	195.6594			GP 28-8
1.322	0.872				GP 29-1
2.28	0.144				GP 29-2
2.965	0.072				GP 29-3
3.682	0.072				GP 29-4
3.754	0.87				GP 29-5
0.00074	1.25	202.406			GP 28-9
1.322	0.872				GP 29-1
2.28	0.144				GP 29-2
3.415	0.072				GP 29-3
4.55	0.072				GP 29-4
4.622	0.87				GP 29-5
0.00084	1.25	209.153			GP 28-10
1.322	0.872				GP 29-1
2.28	0.144				GP 29-2
3.84	0.072				GP 29-3
5.4	0.072				GP 29-4
5.472	0.87				GP 29-5
0.0009	1.25	215.9			GP 28-11
1.322	0.872				GP 29-1
2.28	0.144				GP 29-2
4.08	0.072				GP 29-3
5.88	0.072				GP 29-4
5.952	0.87				GP 29-5
0.0	0.0	0.0	0.0	0.0	GP 30-1
0.0	0.0	0.0	0.0	0.0	GP 30-2
0.0	0.0	0.0	0.0	0.0	GP 30-3
0.0	0.0	0.0	0.0	0.0	GP 30-4
0.0	0.0	0.0	0.0	0.0	GP 30-5
0.0	0.0	0.0	0.0	0.0	GP 30-6
0.0	0.0	0.0	0.0	0.0	GP 30-7

54

elastic solutions of the 90° and 45° orientation loading cases. This basic model was used for shots 6, 17, 5, 21, 16, and 20, except for minor changes in the pressurization cases. This model employed 7 symmetric γ modes and 20 β modes and used 73 modal combinations for the solution. The model used an 19 by 65 spatial integration net. The time increment selected for solution was 10 ms. The loading input changes for the various shot events. The start times for shots 6, 17, 5, 21, 16 and 20 are 0.3725, 0.3451, 0.3, 0.33675, 0.3394, and 0.3458 s, respectively. In shot 17 channel 13 (123.9°) had to be eliminated as bad data and in shot 5 channel 3 (22.4°) was also eliminated as shown in Table 6. All the pressure data for the remaining shots were fully usable.

For the unpressurized shots 6, 17, 5, and 21 the critical buckling stress was set at -2000 lb/in^2 . For the pressurized shots 16 and 20, it was assumed that the internal pressure would prevent the skin from buckling. Therefore, NBUCK in Group 10 was set to zero and Group 17K (BUCKS) was eliminated. In order to include the internal pressure in shots 16 and 20, KDS was set at 3 in Group 3 in both cases and Group 5 was added in which PS was set at -2.5 and -2.7 lb/in^2 , respectively.

The data deck listing for shot 22 given in Table 7 represents the KC-135A fuselage elastic-plastic structural model. In this model the modes, integration net and time increment are the same as the previous model for shot 5. Since the critical buckling stress was set at -2000 lb/in^2 for elastic buckling of the skin, a large yield stress value was inputted to keep the pseudo skin response elastic so that the overriding buckling criterion would not be confused by inelastic skin response quantities in the program. Therefore, only one skin layer was necessary in the model. Since the stringers remain elastic during the response, only a perfectly plastic material model was inputted with the yield stress at 72000 lb/in^2 . For the frames which went inelastic, a more accurate bilinear representation was used by matching an actual stress-strain curve for 7075-T6 aluminum. This curve fitting resulted in a yield stress of 76400 lb/in^2 and a strain hardening slope of $1.85 \times 10^5 \text{ lb/in}^2$ for the frame material. The start time for shot 22 was 0.2949 s and all pressure channels were usable.

The NOVA-2S (NOVA-2LTS) program was redimensioned for the CRAY-1 computer at AFWL to accomodate the models given in Tables 6 and 7. These dimension changes are indicated in the common block listing given in the Appendix.

The preliminary runs for shot 5 using double symmetry, 42 modes and a 19 x 33 integration net used CPU time on the CRAY-1 computer at a rate of 70 s/ms of response. Some runs were made at about 40 s/ms of response by reducing the integration net to 19 x 17. The final runs using 73 modes, a 19 by 65 integration net and symmetry in only one direction used CPU time at a rate of 234 s/ms of response for shot 5 and 292 s/ms of response for shot 22. The final models used for correlation are probably conservative relative to general accuracy. By reducing the number of modes to about 60 and β integration points to 33, a good model for frame response could be run at a rate of about 100 CPU s/ms of response. It should be noted that peak response occurred within 6 ms of response.

SECTION IV

CORRELATION OF NOVA-2LTS RESULTS WITH THE TEST DATA

The experimental strain results of the central frame from the seven selected test shots are compared with the corresponding results from NOVA-2LTS. In reviewing all the data it became apparent that there were anomalies in the actual fuselage structure which could not be defined for analytical modeling. Since strain response is very sensitive to irregularities in a circular curved structure, position by position comparisons did not make sense. Hence, for each test shot the overall distribution of strain maximums around the circumference of the upper lobe compartment of the KC-135A fuselage test section are presented from experimental and analytical results. In addition, the strain time histories associated with the largest of the experimental and analytical strain maximums are compared for the outer and inner flanges of the central frame. These experimental and analytical strain time histories do not necessarily occur at the same circumferential position. The elastic response cases at the 90° loading orientation (shots 6, 17, 5) are presented first and then the 45° loading orientation case is presented. Next the elastic-plastic response case of shot 22 is considered. Finally, the correlation results of the pressurized cases (shots 16 and 20) are presented.

For the 90° loading orientation and no internal pressure, shots 6, 17, and 5 produced elastic response of the central frame of the KC-135A upper lobe fuselage section. In these three shots the fuselage test section was subjected to engulfing blast waves at incident overpressure levels of 1.52, 1.95, and 2.5 lb/in², respectively. Figure 5 shows the maximum experimental outer flange strain of the center frame at three key positions in the crown region of the fuselage versus the incident overpressure. These three measured strains from gages SG 19B, SG 22B, and SG 25B indicate that the largest measured strain (SG 25) occurred about 18 degrees to the right of crown center line. As the incident overpressure increases the spread among these three measurements also increases. The strain value for the measurement

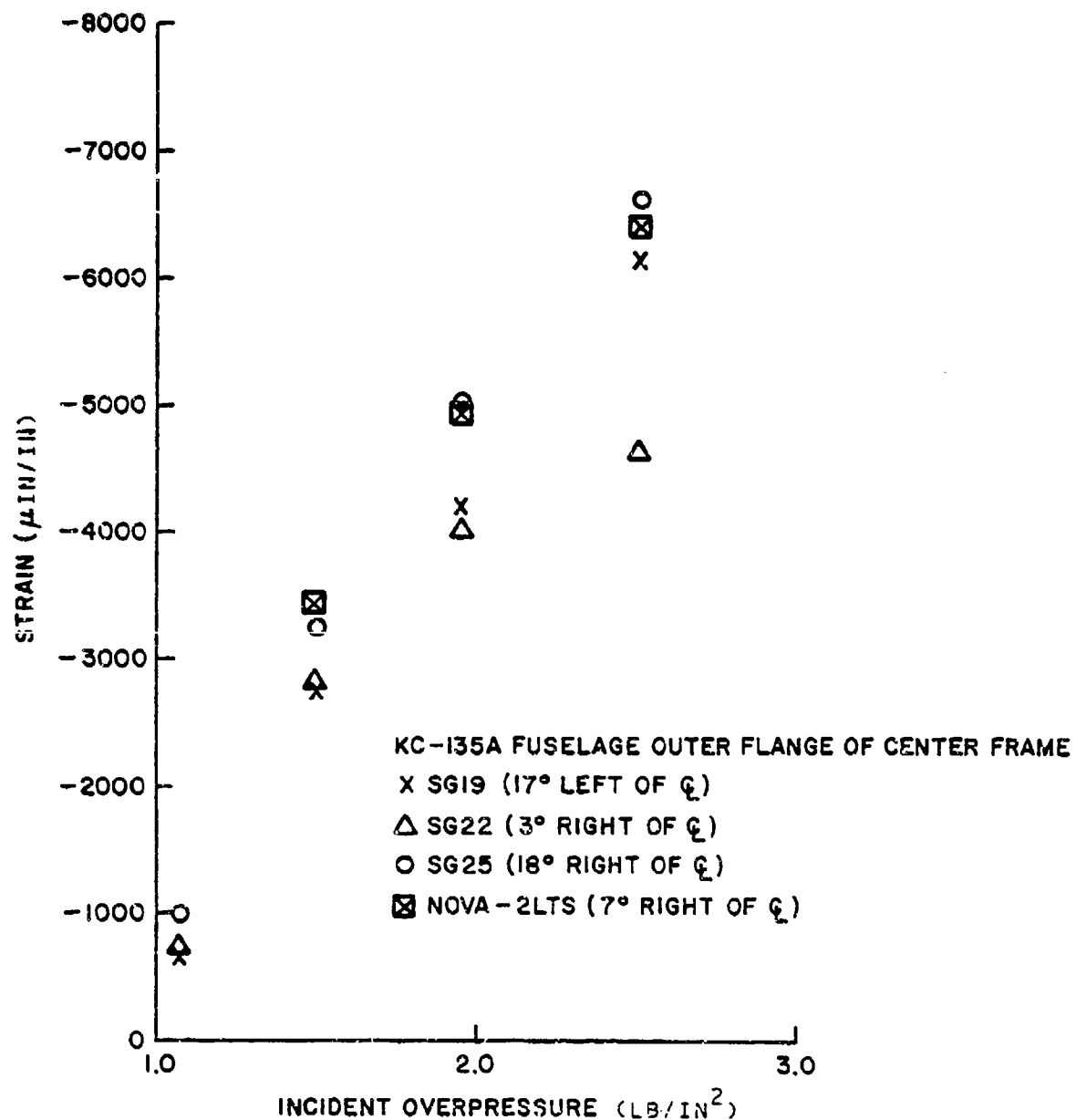


Figure 5. Maximum Strain Versus Incident Overpressure for 90° Loading Orientation on the Unpressurized Fuselage Section

SG 22B, three degrees right of the center becomes significantly lower than the other two measurements. This drop in the center strain measurement is not consistent with the expected strain distribution for a circular fuselage section or the analytically determined distribution. This observation was the first indication that there may be structural anomalies in the crown region of the fuselage. Furthermore, it will be shown later that for the final shot 22, in which the material behavior was inelastic in the crown region, the largest strains occurred on the left side of the crown at gage positions GS 13B, GS 16B and GS 22B. Thus, it appears that the experimental strain response in the crown region did not follow a consistent deformation pattern as the level of loading was increased. The maximum strains obtained from the NOVA-2LTS analytical model are also plotted in Figure 5 for incident overpressures of 1.52, 1.95, and 2.5 lb/in². These maximum strains occurred at about seven degrees to the right of the crown center line and compare well with the corresponding maximum experimental values of gage SG 25B (18 degrees to the right of center). Although the maximum experimental and analytical strains compare very well there are differences in the strain distribution patterns in the central frame. It should be noted that shot 5 ($\Delta p = 2.5 \text{ lb/in}^2$) represents a deformation condition that is near the threshold of yielding for the frames of the KC-135A fuselage.

A more in depth understanding of the strain pattern occurring experimentally and analytically in the central frame is obtained by examining the results generated in Figures 6 through 11 for shots 6, 17, and 5. In Figures 6, 7, and 8, the circumferential distribution of strain maximums for both the outer and inner flanges of the central frame are given, respectively, for shots 6, 17, and 5. In these plots, the solid and dashed lines represent the strain distribution from NOVA-2LTS analytical response calculations for the outer and inner flanges, respectively. The circular and triangular symbols represent the strain distribution from the various strain gage measurements for the outer and inner flanges, respectively. The results from these comparisons are consistent for shots 6, 17, and 5 and the following observations are made:

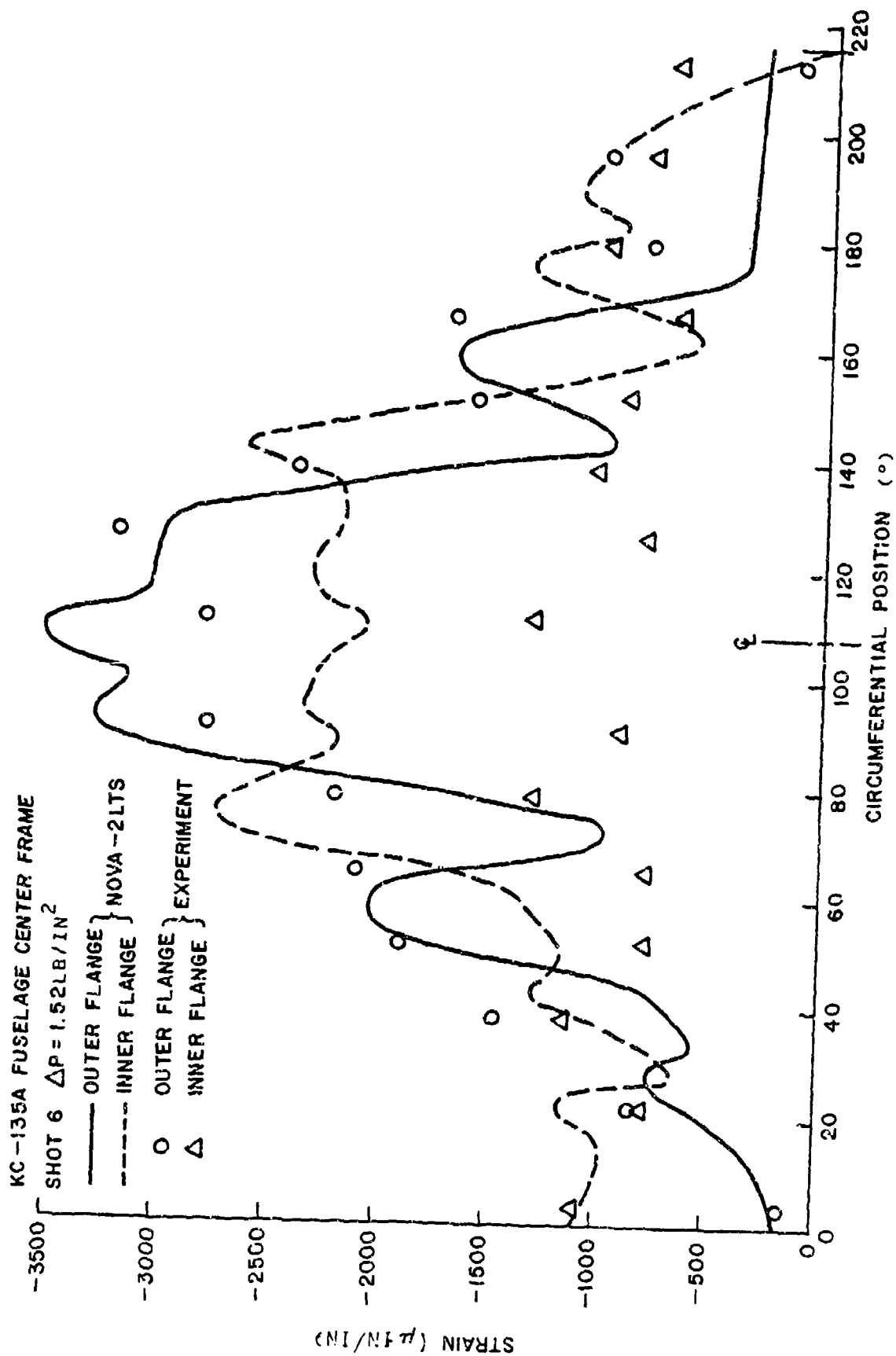


Figure 6. Maximum Compressive Strain Versus Circumferential Position at the 90° Loading Orientation for Shot 6

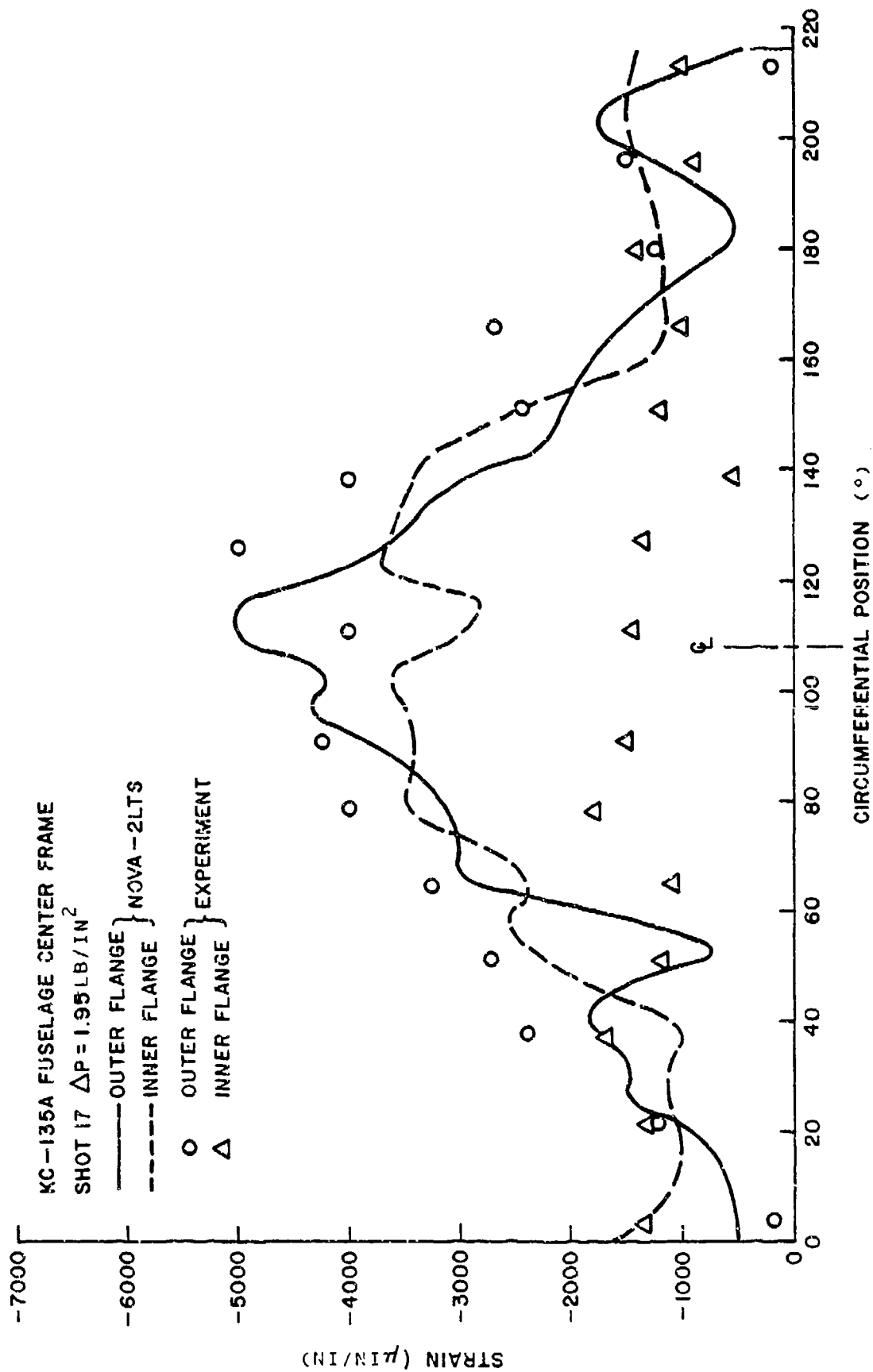


Figure 7. Maximum Compressive Strain Versus Circumferential Position at the 90° Loading Orientation for Shot 17.

KC-135A FUSELAGE CENTER FRAME

SHOT 5 $\Delta P = 2.5 \text{ LB/IN}^2$

— OUTER FLANGE } NOVA-2LTS
 - - - - - INNER FLANGE }

○ OUTER FLANGE } EXPERIMENT
 △ INNER FLANGE }

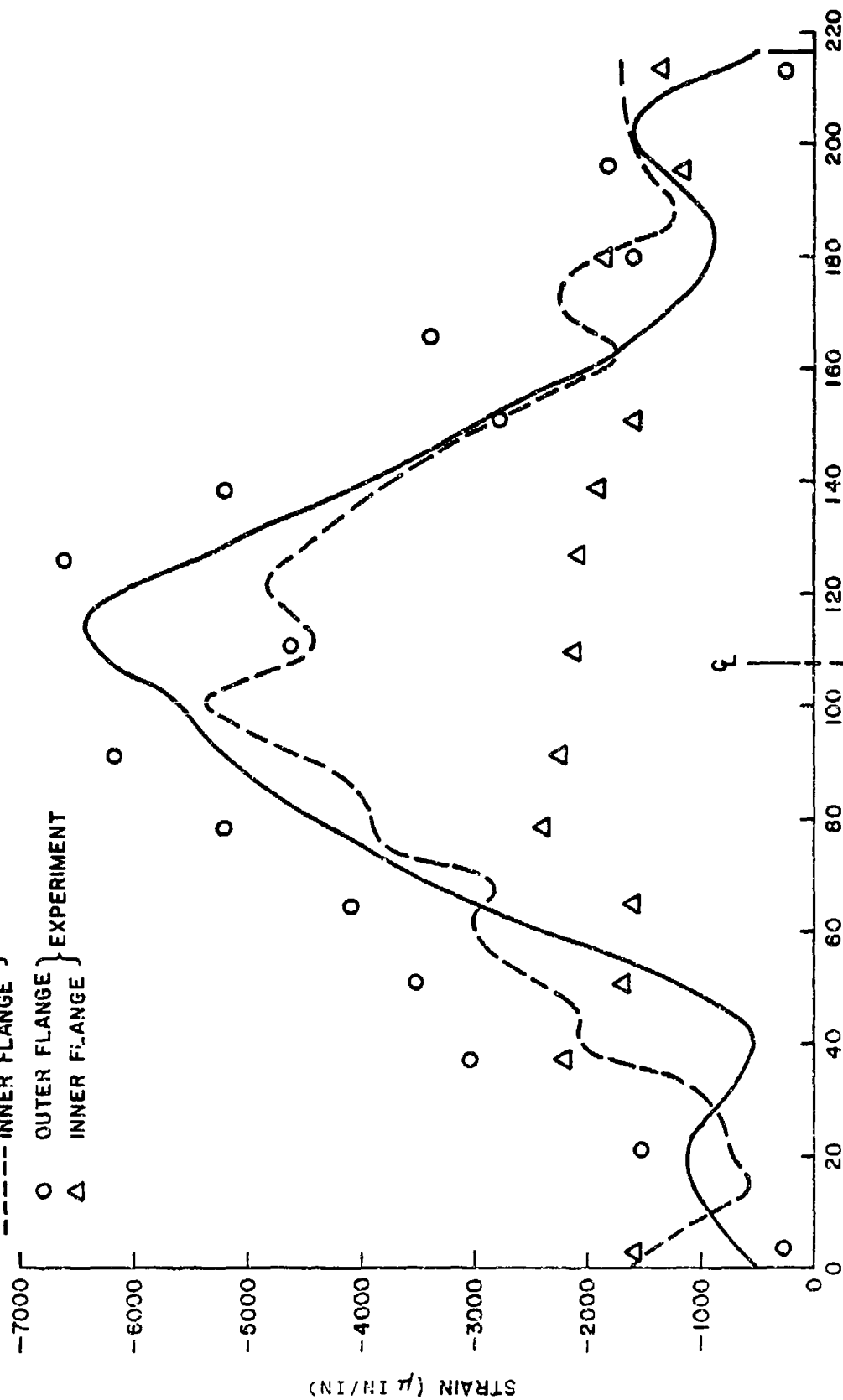


Figure 8. Maximum Compressive Strain Versus Circumferential Position at the 90° Loading Orientation for Shot 5

- (1) The largest compressive strains occur on the outer flange and in the crown region of the frame and the analytical and experimental values compare well even though they occur at different positions about 12 to 16° apart.
- (2) In the crown region the maximum strains distribution predicted by NOVA-2LTS on the inner flange are much higher (about double) than the experimental values. However, it should be noted that the inner flange strains would not be a governing factor in the damage criteria used in NOVA-2S.
- (3) The irregularities in the analytical strain distributions about the center line of the crown are caused by asymmetry of the loading, while the experimental distribution irregularities may also be attributed in part to structural anomalies as well as the loading asymmetry.
- (4) In the crown region, the analytical results show stronger membrane action across the frames cross section than the experimental results.

In Figures 9 through 11, experimental and analytical strain time histories are compared for the outer and inner flanges of the central frame. The analytical and experimental time histories are given for positions at which the largest of the strain maximums for each shot occurred in the previous figures. Experimentally, the peak strain occurred at $\theta = 126.2^\circ$ (SG 25) for all three shots. In the NOVA-2LTS results, the peak strain occurred at $\theta = 114.7^\circ$ for shots 5 and 17 and at $\theta = 107.95^\circ$ for shot 6. The general shape of the time history curves compare well, although the phasing of curves differed by about 2 ms. The maximum compressive strains occurred on the outer flange and they compare well in magnitude for all three elastic cases at the 90° loading orientation. Again these figures demonstrate that the NOVA-2LTS analytical results show stronger membrane response across the frame cross section. Possible explanations for the differences in the strain distribution across the cross section and the phasing are considered.

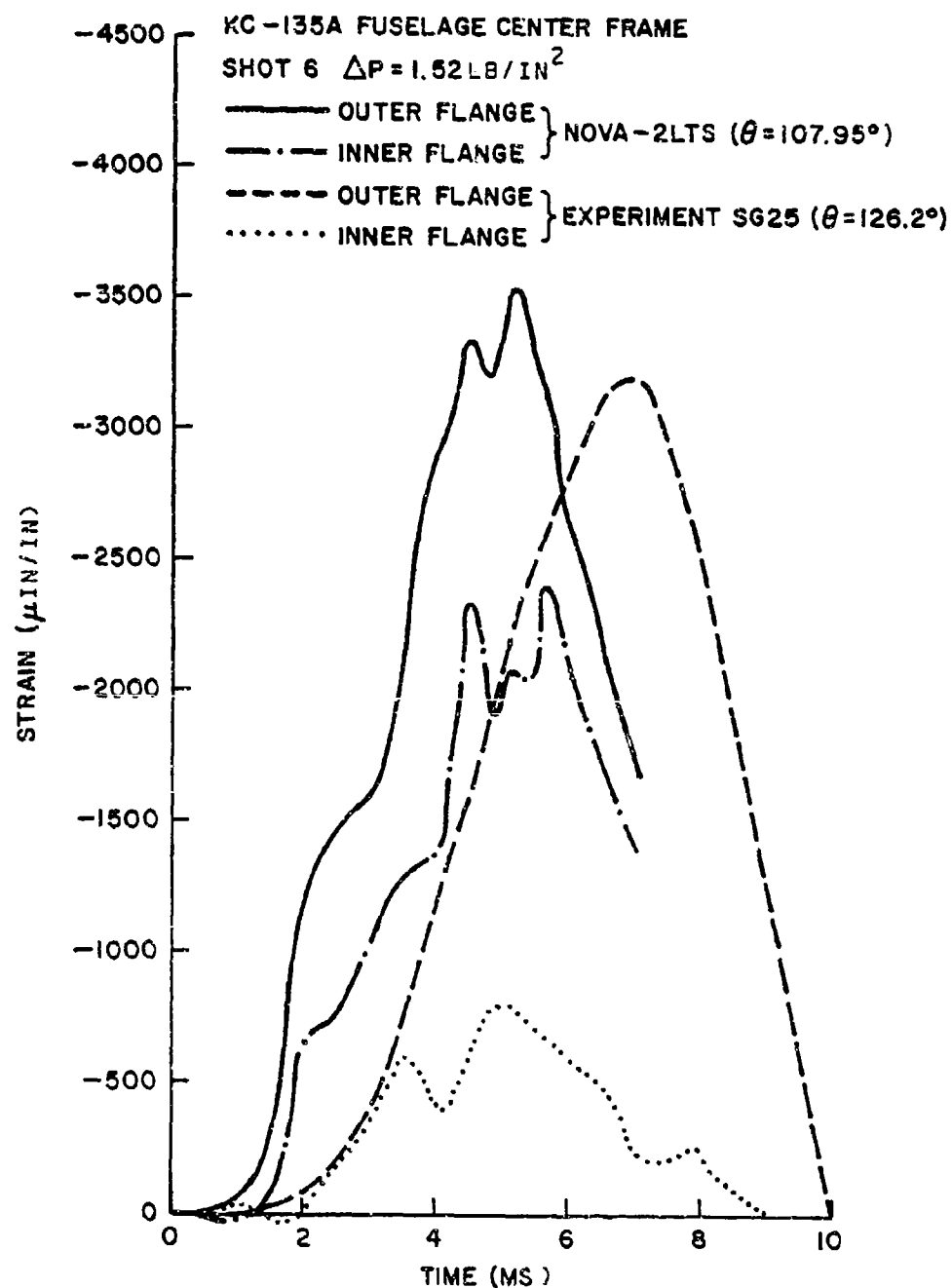


Figure 9. Comparison of Peak Strain Time Histories at the 90° Loading Orientation for Shot 6

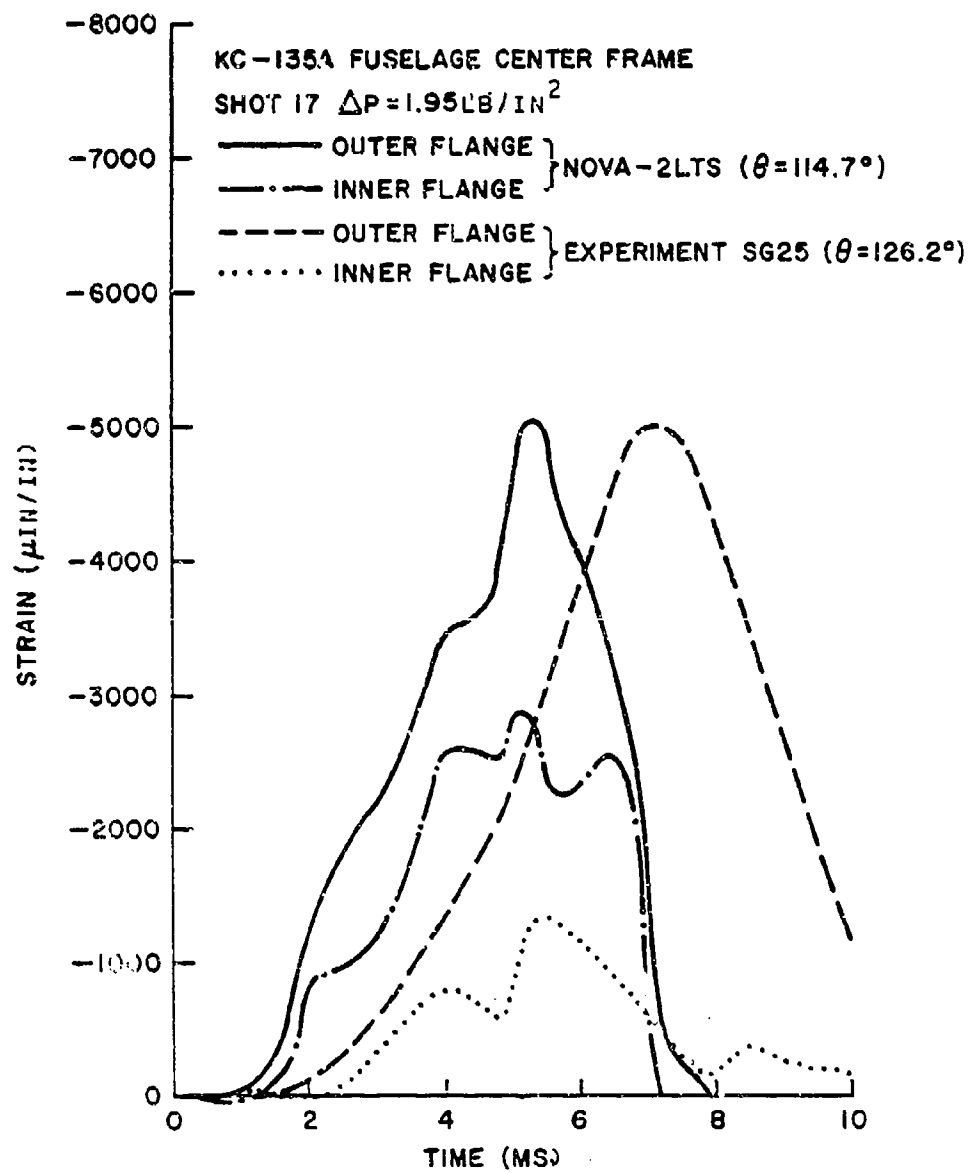


Figure 10. Comparison of Peak Strain Time Histories at the 90° Loading Orientation for Shot 17

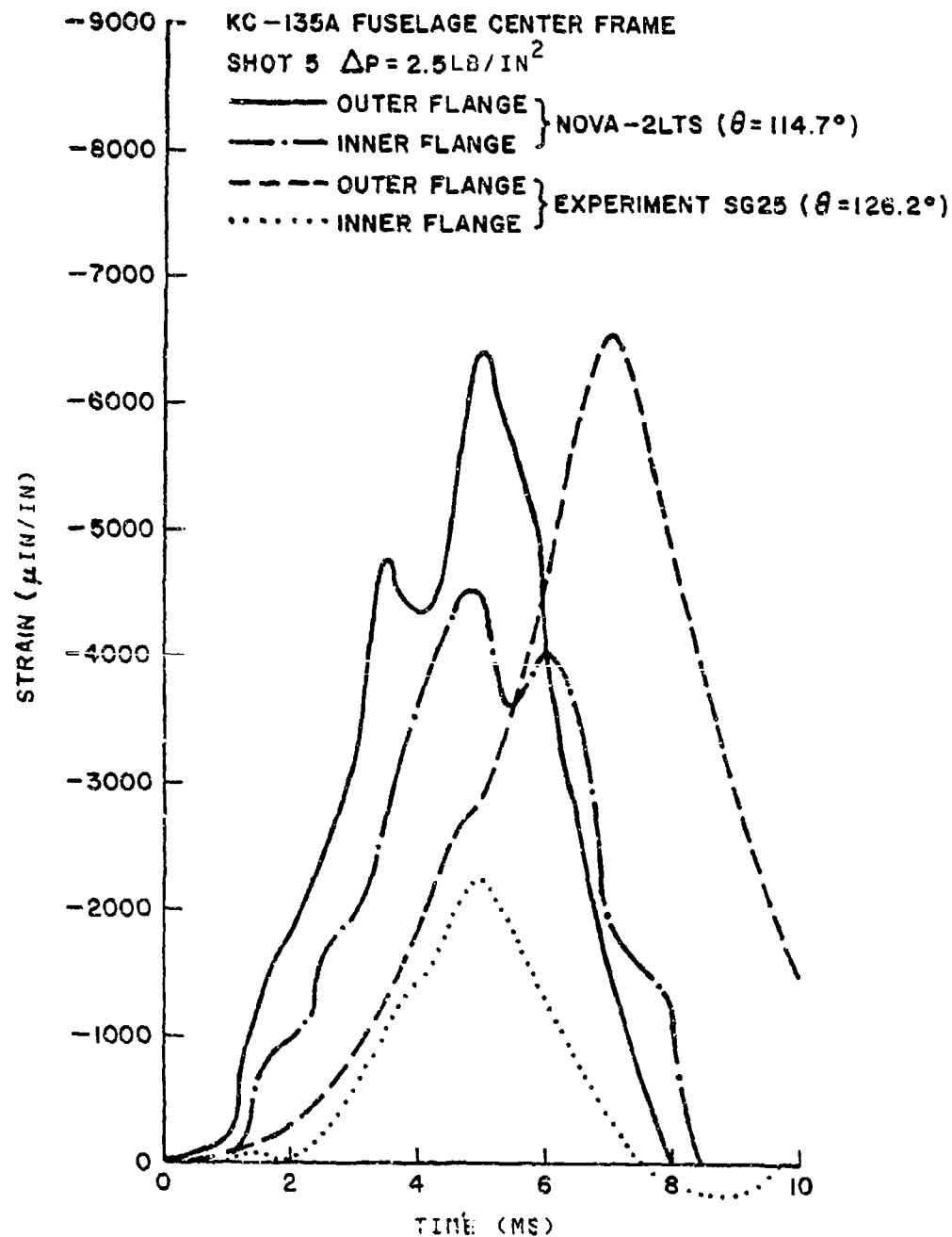


Figure 11. Comparison of Peak Strain Time Histories at the 90° Loading Orientation for Shot 5

The most plausible explanation appears to be out-of-roundness of the fuselage section in the crown region. Deviations from the assumed circular shape would produce more bending action around the circumference and also lower the frequency of response, since membrane response is of higher frequency content than bending. It is well known that the responses of circular shell structures are sensitive to out-of-roundness (initial radial imperfections), unfortunately, the true shape of the fuselage prior to each test shot is not known. If out-of-roundness information existed for this KC-135A fuselage test section, such data could have been incorporated into the NOVA-2LTS structural model through the initial imperfection option in the code. The inability of the NOVA-2LTS theoretical formulation to properly predict the strain distribution across the frame's cross section given the correct definition of the actual structure was discounted because of the good results of previous correlation efforts in References 4 and 5. In particular, the correlation of the B-52 aft fuselage results showed that the frames exhibited very strong bending action in the region of maximum strain which was predicted very well by NOVA-2LTS when the actual geometry of the B-52 fuselage panel section was modeled through the initial imperfection option.

In the KC-135A fuselage the frames are not directly attached to the skin as in the case of the B-52 aft fuselage. The NOVA-2LTS formulation is based on the assumption that plane sections remain plane during deformation of the whole cross section which includes the skin and frames. If the attachments between the stringers and the frames became very flexible (sloppy) during the response this assumption could be violated. However, since the skin between stringers buckles at a low stress level, the effect of such joint flexibility on the strain and stress distributions across the floating frames should not be an important factor. In any event, such undetermined joint flexibility would be difficult to model accurately with any structural response code. It should also be mentioned that errors in the experimental data are not uncommon, in particular, phasing and polarity errors generated

during the data acquisition and/or reduction procedures. When the correlation of results are performed soon after the tests, systematic differences between analytical and experimental responses can be challenged and the experimental data rechecked.

Figures 12 and 13 illustrate the comparison of experimental and analytical results for shot 21 which was for the 45° loading orientation at the incident overpressure of 2.1 lb/in². Figure 12 shows the distribution of strain maximums which is different than those shown before for the 90° loading orientation. The region of the largest strains has shifted to the right towards the direction of the loading at $\theta = 153^\circ$ for both the experimental and analytical results. On the outer flange of the center frame the largest of the strain maximums occurred at $\theta = 142^\circ$ and 155° from the NOVA-2LTS calculations, while the largest experimental strain occurred at $\theta = 138^\circ$. This experimental position favors the side where the maximum experimental strain occurred for the 90° loading case at $\theta = 126^\circ$. This trend again indicates the possibility of a structural anomaly on the right side of the crown region. The largest experimental and NOVA-2LTS strains differ by about 10% on the outer flange. On the inner flange in the region of maximum deformation the analytical values are significantly higher than the experimental values in the same manner as the 90° loading cases, thereby, indicating more bending action in the experimental results. Overall the distribution comparison for the 45° loading case is more consistent than the 90° loading case. It should be noted that with the loading direction nearer the floor support, the analytical strains at the right clamped edge are higher. Since the experimental strains at this boundary position are about the same as in the 90° loading case (shot 17), the floor joint with the fuselage is probably somewhat flexible. Figure 13 compares the experimental and analytical strain time histories of the largest peak strains. The phasing differences are less for the 45° loading case than the 90° loading case. The experimental strain distribution across the frame's cross section exhibits more bending action than the analytical results.

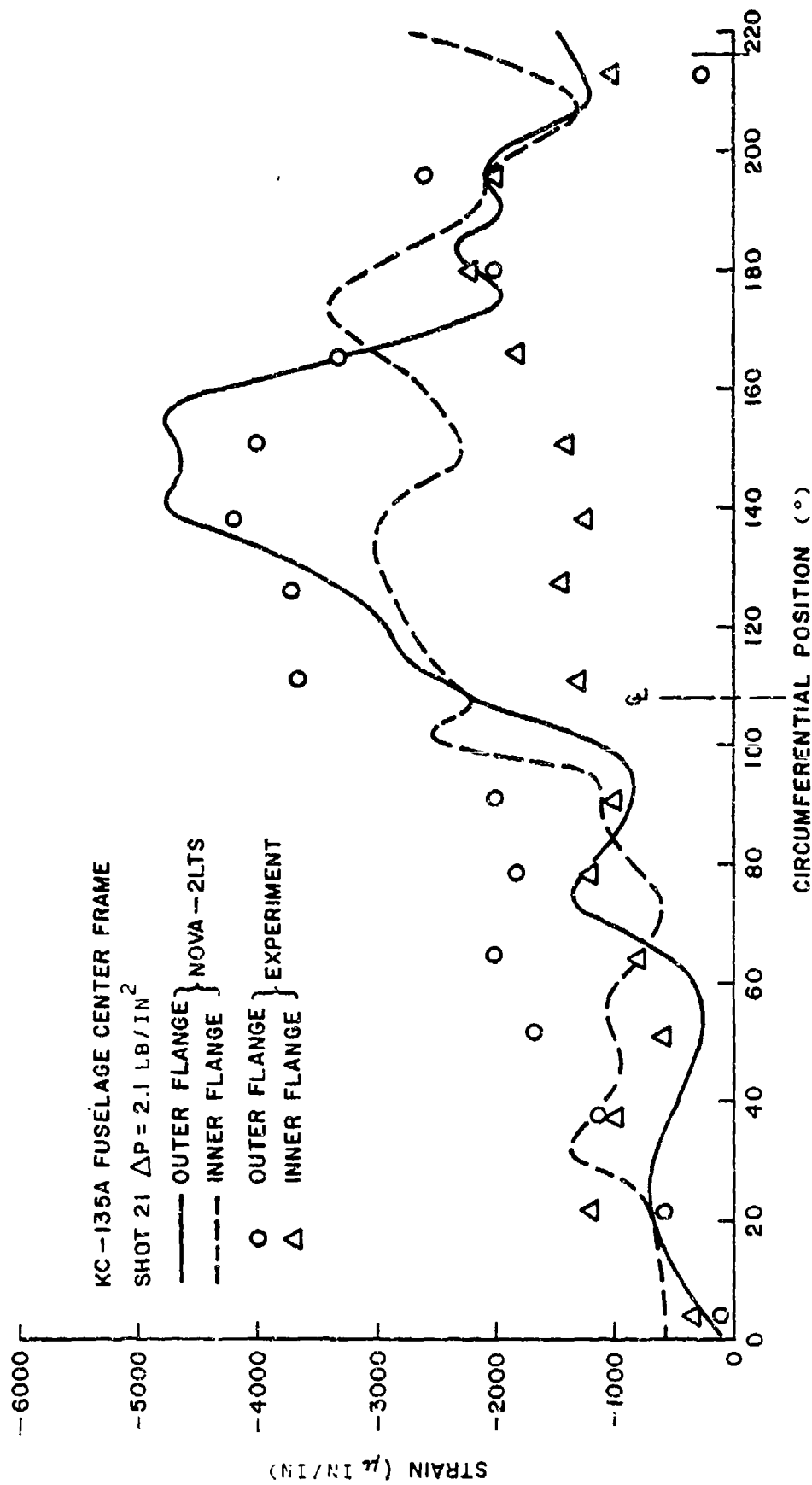


Figure 12. Maximum Compressive Strain Versus Circumferential Position at the 45° Loading Orientation for Shot 21

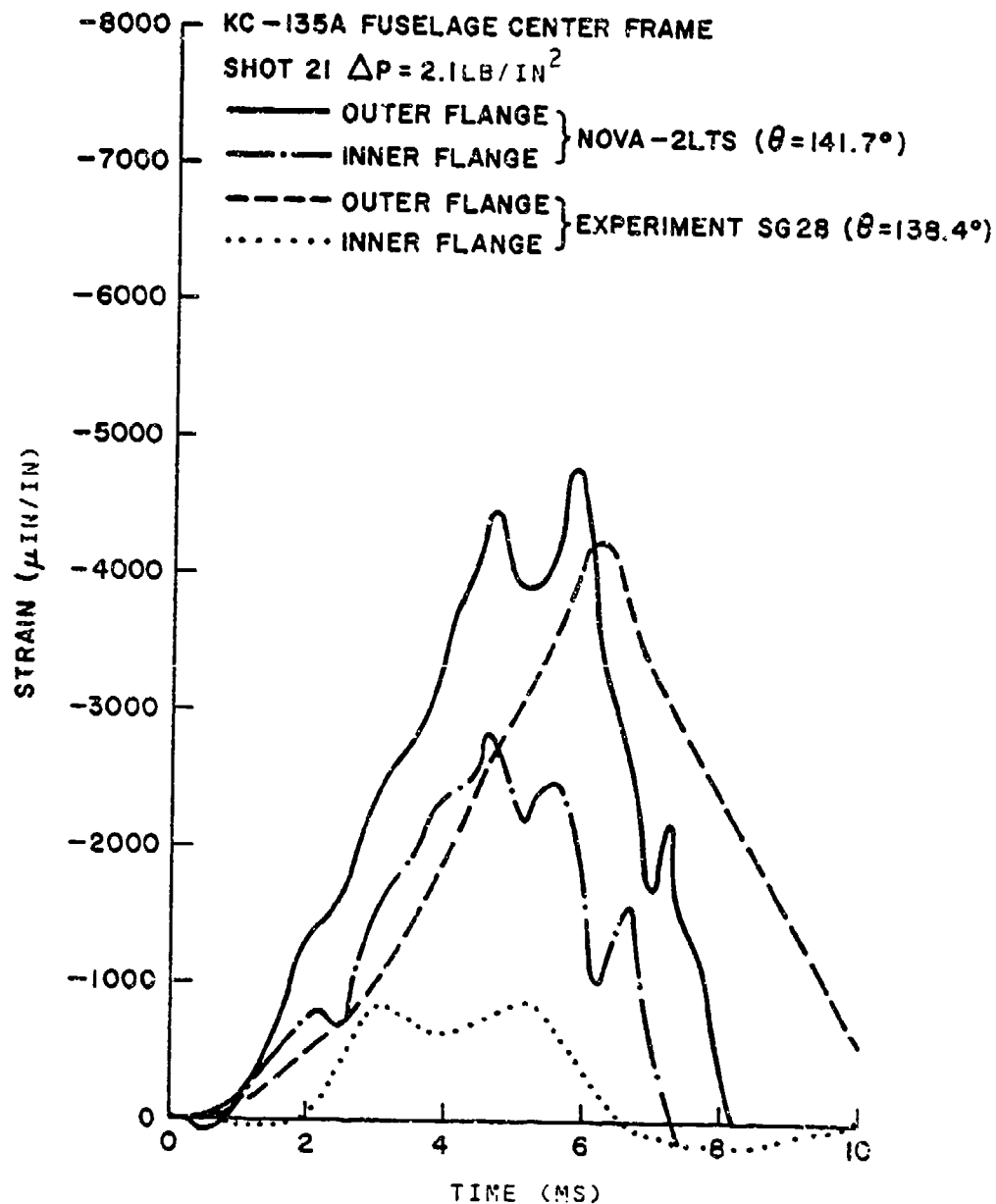


Figure 13. Comparison of Peak Strain Time Histories at the 45° Loading Orientation for Shot 21

In the final shot, 22, (90° orientation) at an incident over-pressure of 3.5 lb/in^2 , the frames went inelastic over a large region of the crown and at four positions severe plastic buckling of the center frame occurred leading to rupture of the frame at three of the positions. Figure 14 illustrates the distribution of strain maximums over the circumference of center frame for the outer and inner flanges. Along the position axis cross marks indicate the locations where plastic buckling of the frame occurred. The experimental strain distribution is misleading in that the severe plastic deformation at three of these positions are not represented on the plot because the strain gages were outside this local area of deformations. At $\theta = 91.4^\circ$ gage GA 19 was located in one of the local buckling areas and large plastic strains (over 4%) were measured before the gage became inoperative. The three other positions (cross marks) would have shown similar plastic response on both flanges if gages had been placed there. The yielding strain value is indicated on the ordinate axis of Figure 14. The experimental and analytical strain distribution are different, although both show a large region of plastic deformation, from 45° to 145° experimentally and from 60° to 216° analytically. Experimentally, the zone of maximum response is shifted more to the left side of the crown which differs from the previous elastic shots 6, 17, and 5. The experimental results show concentrated locations (plastic buckling) of very large plastic strains, (greater than 4%) while the analytical results show a more even distribution in the crown region reaching about 2.5% maximum strain. The NOVA-2LTS model does not at present allow for local buckling of a stiffener, hence without these local failures present in the response calculation the energy is absorbed more evenly over the frames. A method to account for local elastic or plastic buckling of stiffeners in NOVA-2S is discussed in Section V. For those strain measurements not affected by local frame buckling, inelastic strains varied between 0.8 to 1.5%. Analytically, the strain varied from 0.8 to 2.5% in the inelastic region. The analytical results in Figure 14 show that large strains were generated at the right side clamped position. The experimental values near this position are still quite low, as they were

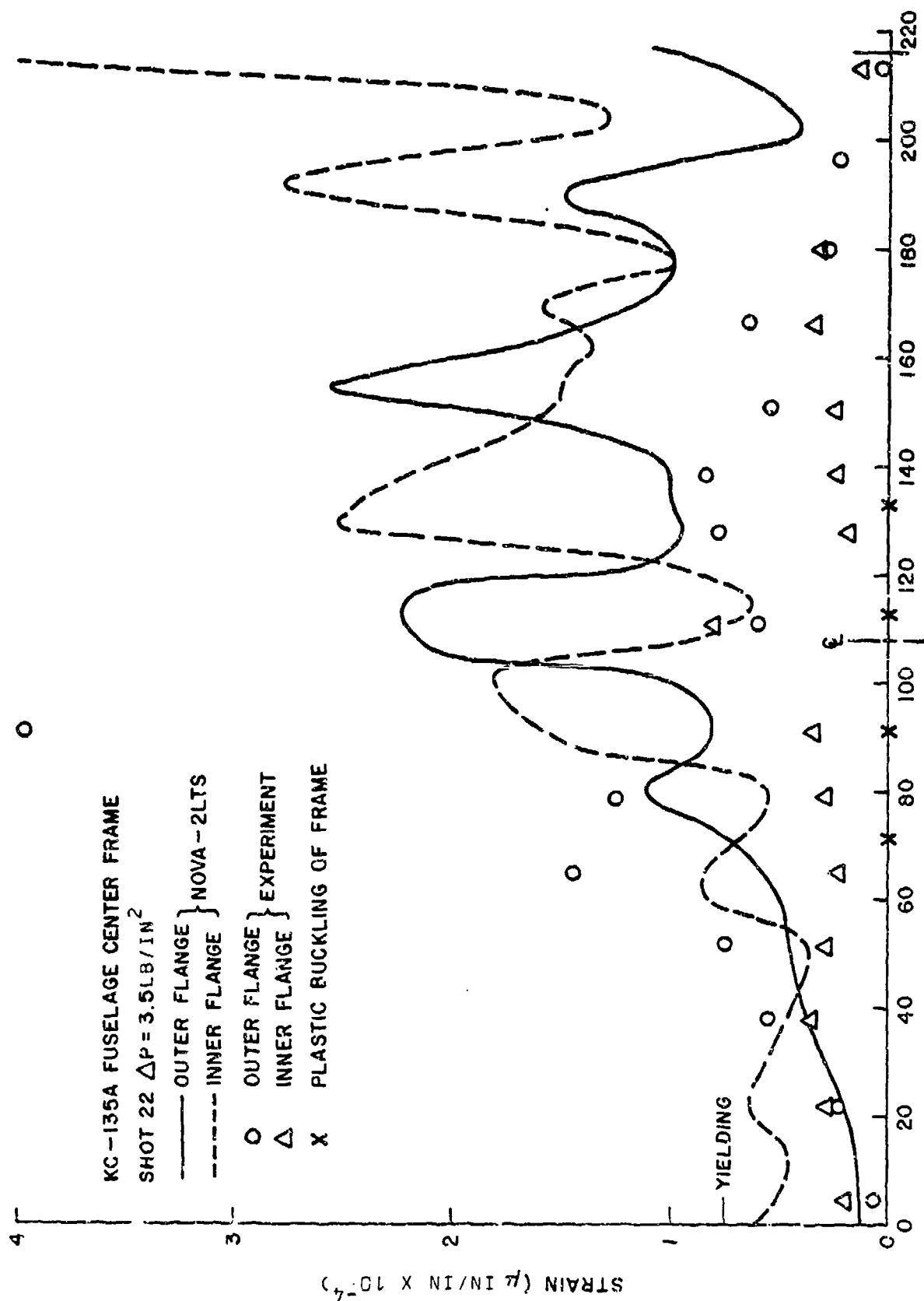


Figure 14. Maximum Compressive Strain Versus Circumferential Position at the 90° Loading Orientation for Shot 22

in the elastic cases. This indicates that for this large deformation response case, the clamped condition does not properly model this boundary. It appears the floor system does not provide the rigidity that was assumed and the frames may be primarily acting as full rings around the entire fuselage. To remedy this situation in the future the entire frame could be modeled. The clamped boundary may still not significantly affect the strain response in the crown region. Figure 15 illustrates selected strain time histories on the outer flange of the center frame. In this figure the two largest measured strains are compared with the two largest analytical strains in the crown region. The time of peak plastic strains compares better than in the elastic response cases.

In shots 16 and 20 for the 90° and 45° loading orientations, respectively, the upper lobe compartment of the fuselage was pressurized at 2.5 and 2.7 lb/in², respectively. In these two pressurized shots the incident overpressure of the blast was at about the 2 lb/in² level which is comparable to the unpressurized shots 17 (90° orientation) and 21 (45° orientation). The pressurization in shots 16 and 20 significantly reduced the strain response in the frames of the fuselage both experimentally and analytically as predicted through NOVA-2LTS. It is recalled that for the unpressurized cases of shot 17 and 21, the maximum measured strains were at the -5000 and -4200 μ in/in level. Table 8 gives the maximum compression and tension strains measured in shot 16 and 20 on the inner and outer flange of the center frame. It can be seen that these strains are significantly less than the corresponding aforementioned values. Shot 16 gives maximum strain values of -1075 and 1100 μ in/in while shot 20 gives values of -1000 and 1300 μ in/in. Table 8 also compares the maximum compression and tension strains predicted by NOVA-2LTS with the corresponding experimental values. It was found that on the inner flanges for both shots the NOVA-2LTS analytical strain maximums were higher than the experimental values, while on the outer flanges the analytical values were lower than the experimental values. Both the experimental and analytical strain distributions had irregular patterns which made a detailed comparison of

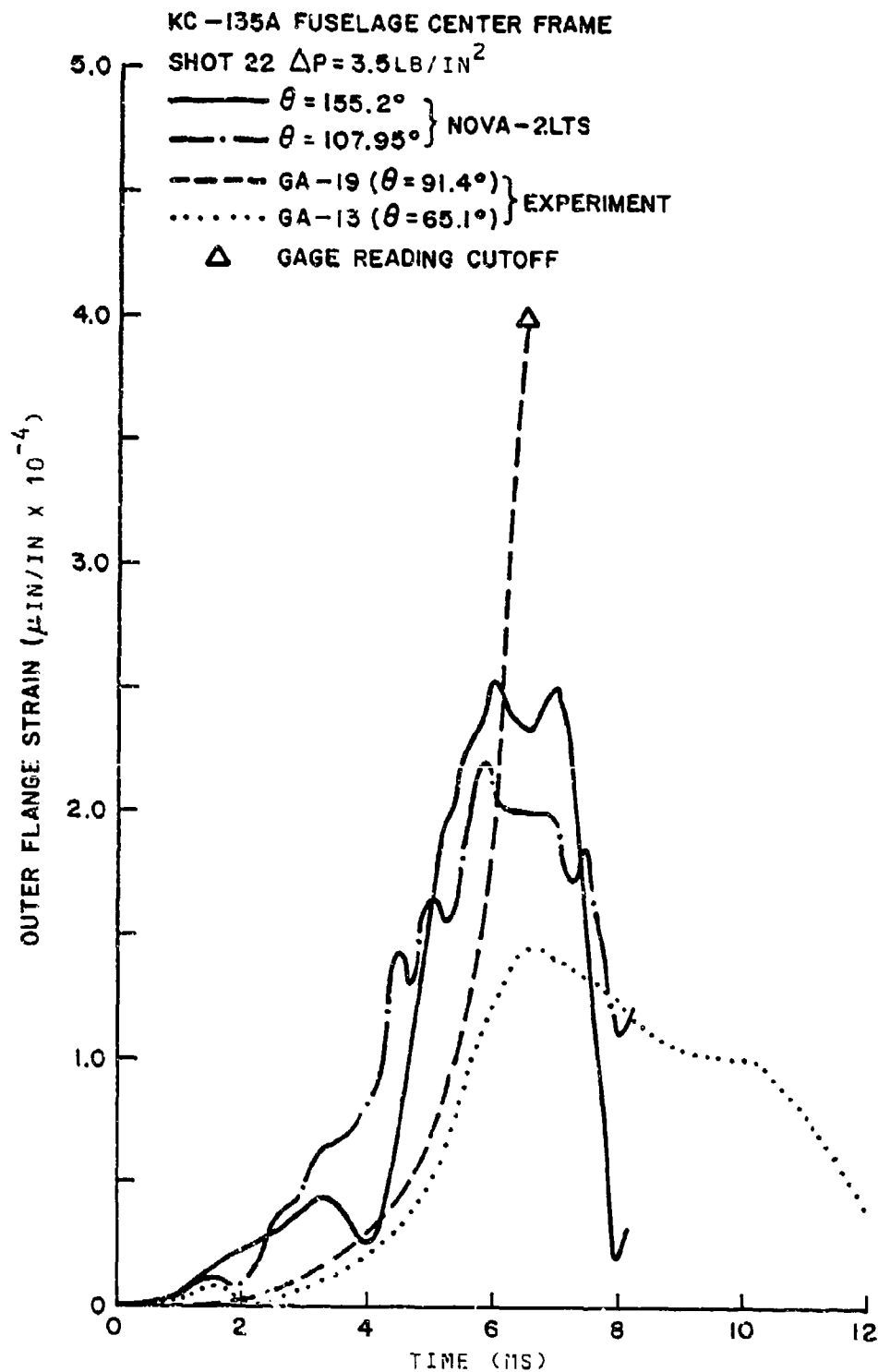


Figure 15. Comparison of Strain Time Histories at the 90° Loading Orientation for Shot 22

TABLE 8

STRAIN COMPARISONS FOR PRESSURIZED KC-135A FUSELAGE
TEST SECTION IN SHOTS 16 and 20

Shot 16 - 90° Loading Orientation
($\Delta p = 2.08 \text{ lb/in}^2$, $p_i = 2.5 \text{ lb/in}^2$)

± Maximum Frame Strains ($\mu\text{in/in}$)		
Position	Experiment	NOVA-2LTS
Inner Flange	1100	1740
	-900	-1085
Outer Flange	700	540
	-1075	-375

Shot 20 - 45° Loading Orientation
($\Delta p = 1.85 \text{ lb/in}^2$, $p_i = 2.7 \text{ lb/in}^2$)

± Maximum Frame Strains ($\mu\text{in/in}$)		
Position	Experiment	NOVA-2LTS
Inner Flange	1300	1925
	-1000	-1570
Outer Flange	920	395
	-800	-464

results unfruitful. The importance of these results is that both the experimental and analytical strains show a significant reduction in magnitude from the internal pressurization. Many of the differences in the results may be the result of unknown structural and geometric anomalies whose presence were suspected from previous unpressurized correlations. Figures 16 and 17 show comparisons of selected analytical and experimental strain time histories for shots 16 and 20, respectively. In Figure 16 for the 90° loading orientation, the analytical strain time histories at the two positions ($\theta = 87.7^\circ$ and 67.5°) of maximum compression and tension strain on the inner flange are compared with the experimental strain time history at the position ($\theta = 110.8^\circ$) for which both the maximum compression and tension strains occurred. These strain responses exhibit higher frequency content than found in the unpressurized response cases. The initial strains at zero time indicate the static preblast state associated with only the internal pressure loading. In Figure 17 for the 45° loading orientation, the analytical strain time history at the position ($\theta = 141.7^\circ$) where the maximum compression strain occurred is compared with the two positions ($\theta = 179.5^\circ$ and 195.7°) at which the maximum compression and tension experimental strains occurred. The positions of the maximum experimental strain are well away from blast loading direction of $\theta = 153^\circ$, while the analytical strain time history occurred near the loading direction.

Although displacements of the fuselage test section were not measured, it is informative to present some of the radial displacement results from the NOVA-2LTS response calculations. Figure 18 shows the maximum inward radial displacement versus the incident overpressure for all seven test cases considered in this effort. For the elastic unpressurized case, the response follows a linear path with increasing overpressure, but becomes nonlinear as inelastic deformations occur. The displacement for the elastic-plastic response case of shot 22 is substantially higher than that of shot 5 which produced response near the threshold of yielding. The maximum displacements of the pressurized cases were low in comparison with the unpressurized cases. Figure 19 illustrates the differences in the radial displacement distributions at

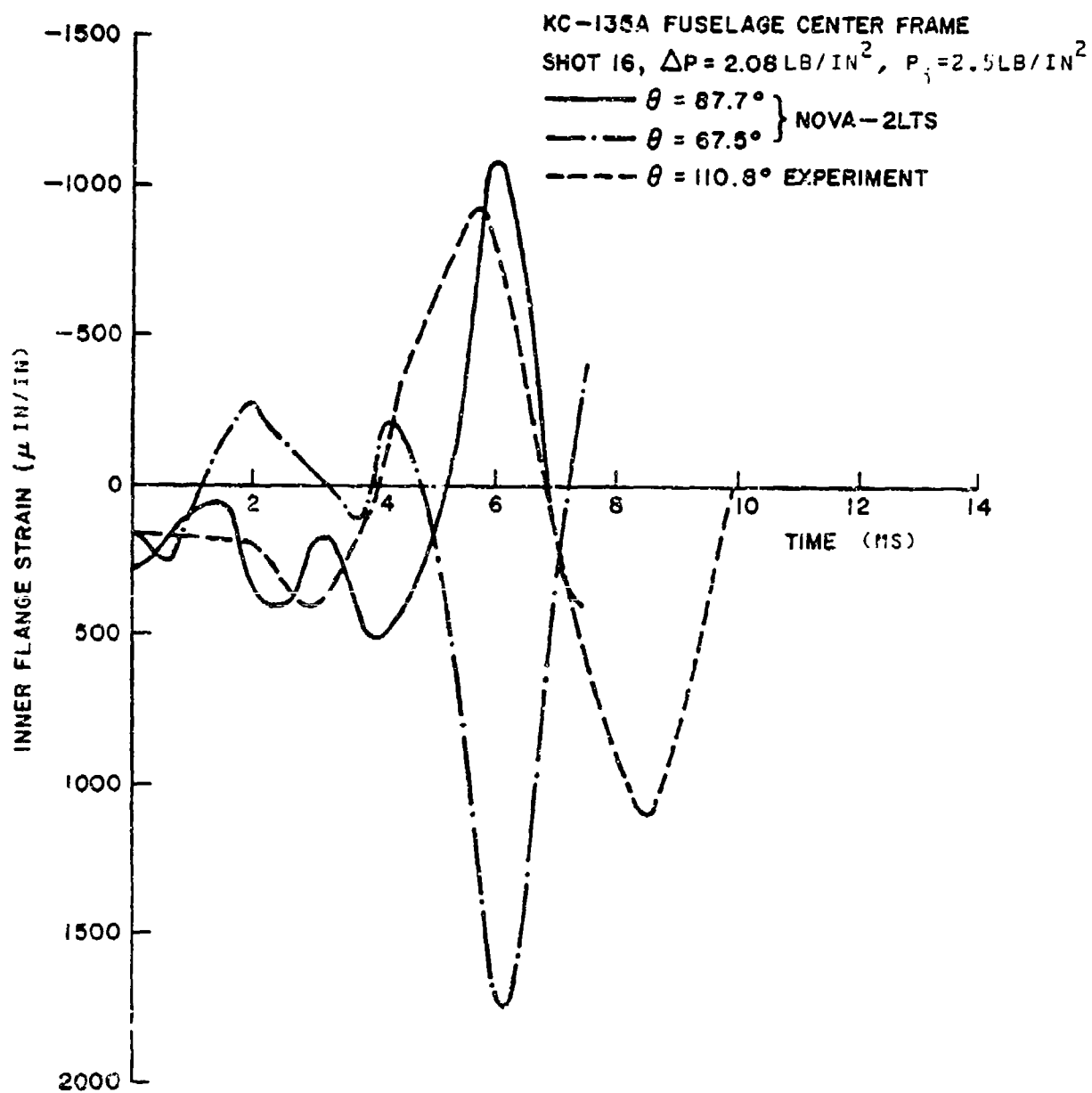


Figure 16. Comparison of Strain Time histories at the 90° Loading Orientation for Shot 16

KC-135A FUSELAGE CENTER FRAME
 SHOT 20, $\Delta P = 1.85 \text{ LB/IN}^2$, $P_1 = 2.7 \text{ LB/IN}^2$
 — $\theta = 141.7^\circ$ NOVA-2LTS
 --- $\theta = 179.3^\circ$ } EXPERIMENT
 $\theta = 195.7^\circ$ }

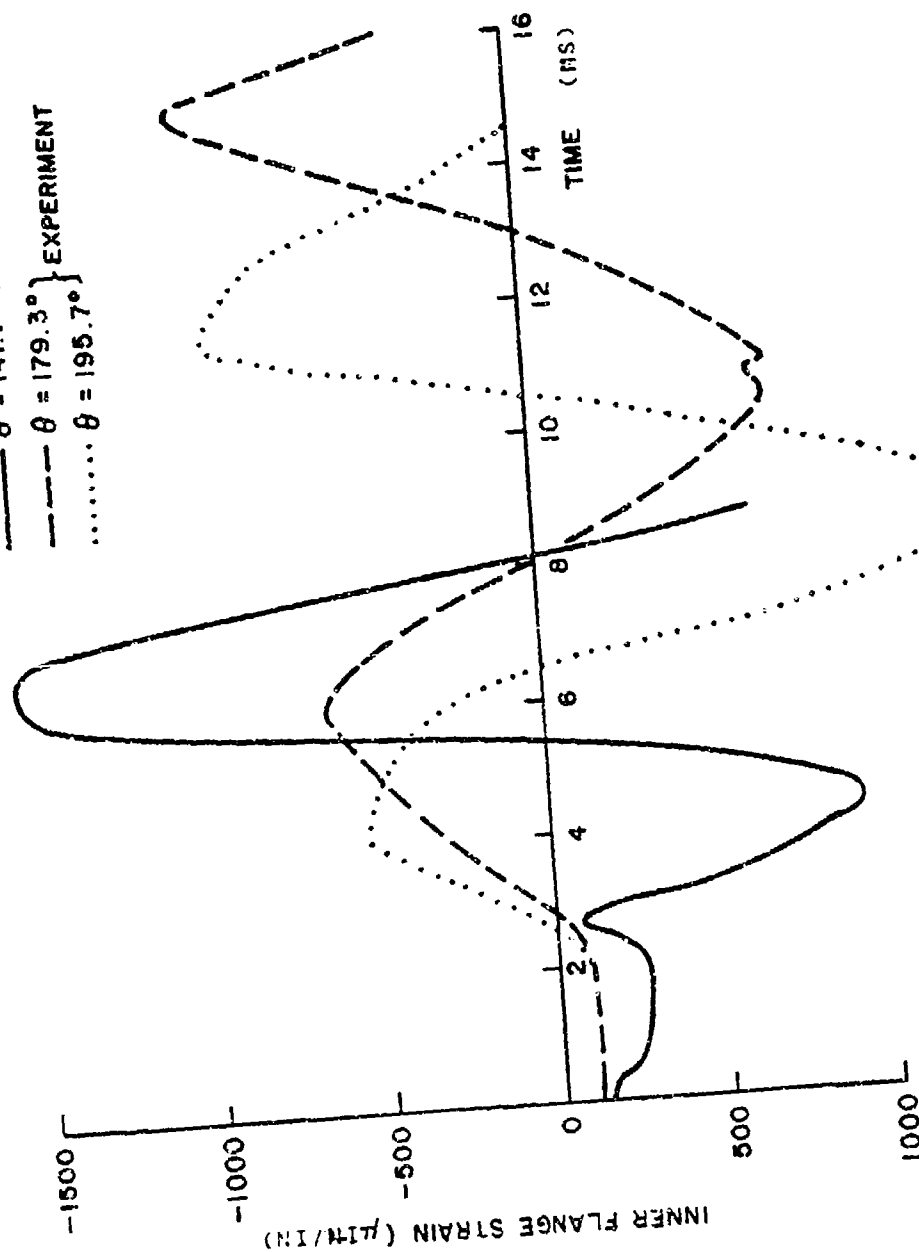


Figure 17. Comparison of Strain Time Histories at the 45° Loading Orientation for Shot 20

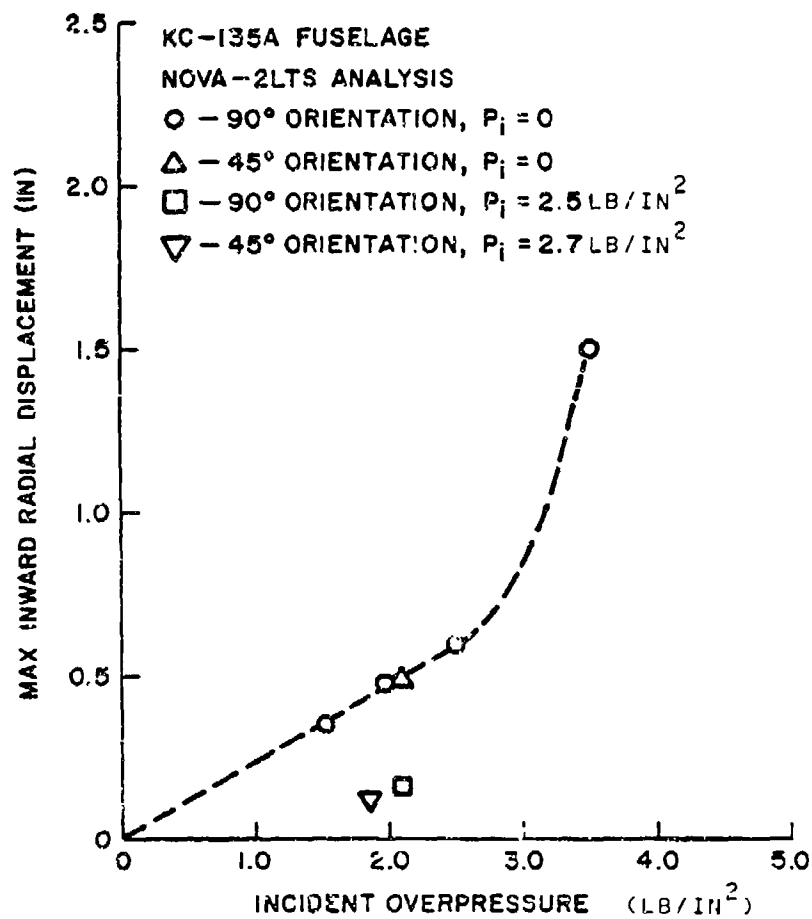


Figure 13. Maximum Inward Radial Displacement Versus Incident Overpressure for all Selected Shots

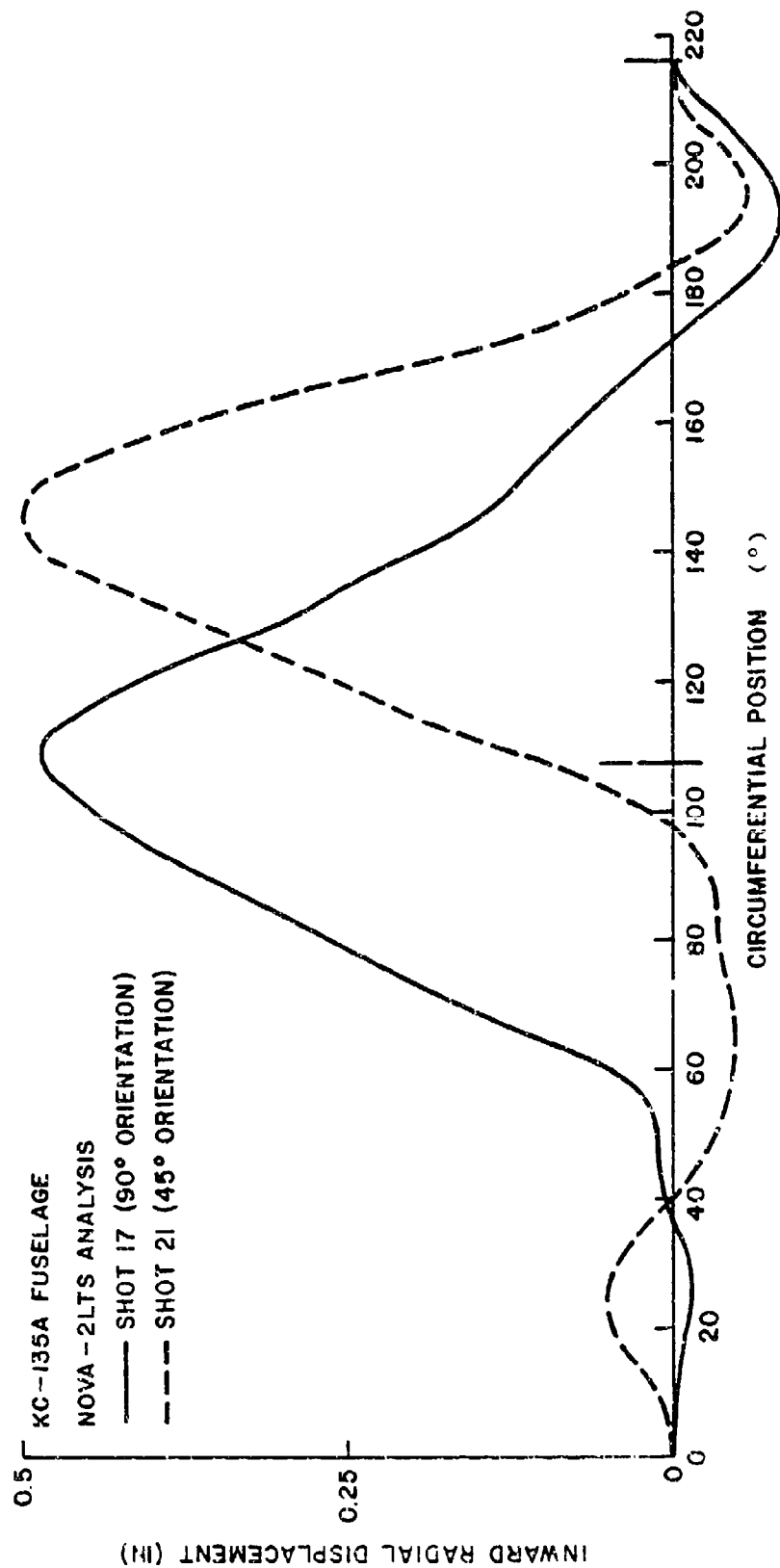


Figure 19. Inward Radial Displacement Circumferential Distribution for Shots 17 and 21

the time of maximum displacement between the 90° and 45° loading orientations for shots 17 and 21. Both peak displacements are very near to the respective positions corresponding to blast loading direction. Figure 20 contrasts the radial displacement time histories for an elastic response case (shot 5) and the elastic-plastic response case (shot 22). Aside from the peak response being much greater, the elastic-plastic response case has a longer period to peak than the elastic response case.

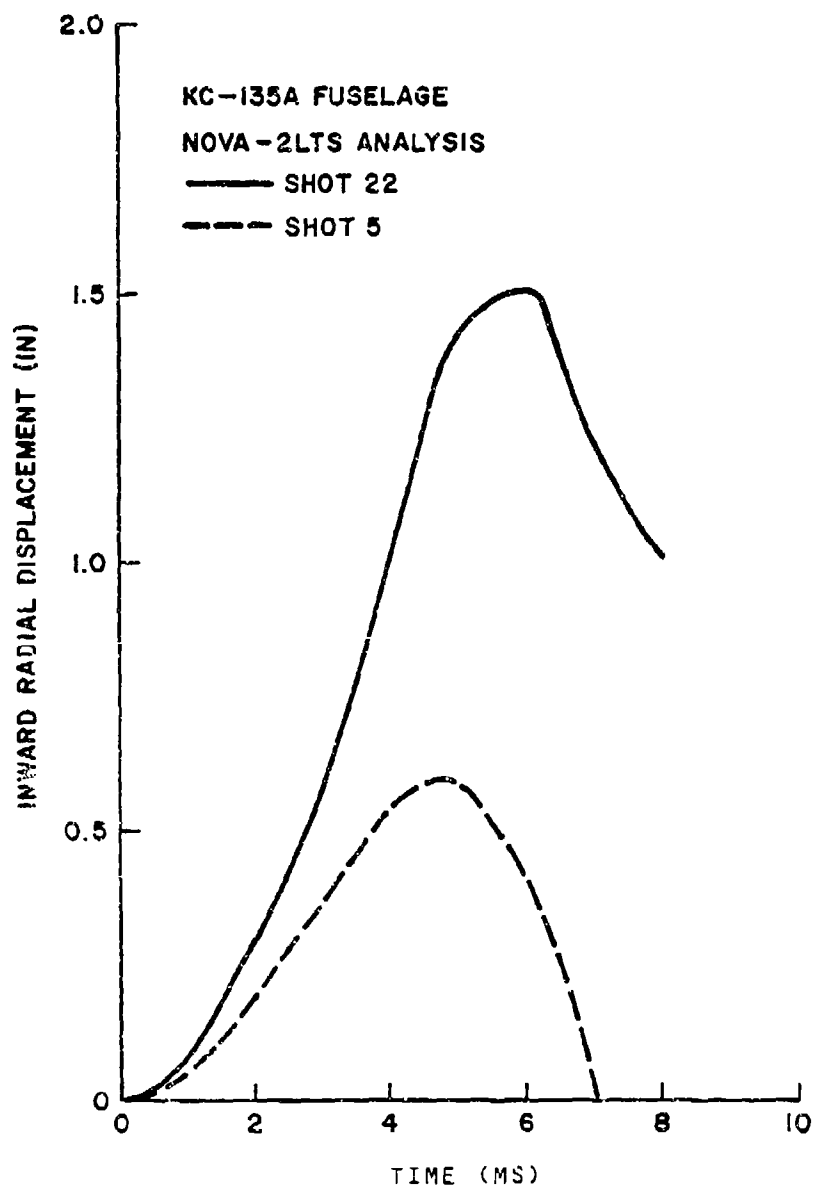


Figure 20. Radial Displacement Time Histories for Shots 5 (Elastic Response) and 22 (Inelastic Response)

SECTION V

EVALUATION OF THE NOVA-2S COMPUTER CODE

In the past the panel subroutine DEPROP in NOVA-2S and NOVA-2LTS has been evaluated successfully through comparison with available experimental results and other nonlinear computer codes. It has been established that NOVA-2S can accurately determine the response of well defined structures within the framework of the theoretical formulation currently programmed in DEPROP. These evaluations have been well documented in References 2, 3, 4, 5, and 8 for unstiffened and stiffened panels. Recently, the correlation of NOVA-2LTS with B-52 aft fuselage results from blast tests performed in a similar manner as the KC-135A fuselage tests has been completed in Reference 4. These results together with the results from this current effort are now employed to assess the validity of using the NOVA-2S stiffened panel option to predict the response of large complex stiffened aircraft sections. It should be noted that the B-52 and KC-135A fuselage sections represent the two major types of fuselage construction, namely, the longeron system and the stringer system, respectively. Thus, the correlation of blast test data from these two types of fuselage construction with NOVA-2LTS structural model response results covers many modeling problems that can be anticipated for actual aircraft sections. It should be noted that some of these modeling problems also apply to any structural code, such as finite element code representations.

From the correlation results of the KC-135A and B-52 fuselage test sections, it was found that the strain response of the frames can be significantly influenced by the boundary conditions, the initial panel geometry, the spatial loading distribution and the local buckling of the thin skin between stringers or frames. In the B-52 aft fuselage correlation in Reference 4 the NOVA-2LTS structural model had to account for the noncircular shape of the fuselage section (through the initial geometric imperfection option), local skin buckling between frames and a boundary being close to the region of maximum strain. All these ingredients were important in correlating successfully with the experimental data using the modeling techniques provided in NOVA-2LTS.

In this current KC-135A fuselage correlation it was found that apparent minor asymmetries in the spatial loading distribution for the 90° orientation were important and therefore, the computer time advantage of double symmetry could not be used. Furthermore, local skin buckling between stringers was very important. For the KC-135A fuselage the panel geometry and the boundary conditions were not major factors in influencing reasonable correlation. The designed geometry of the fuselage was for the most part circular, although the deformation behavior pattern indicated that perhaps out-of-roundness or other structural anomalies were present in this fuselage section. Such possible anomalies could not be defined for modeling by NOVA-2LTS, but the absence of finer geometry definition did not prevent a reasonable correlation. The boundaries of the KC-135A fuselage section were far enough away from the region of maximum strains that the assumed boundary conditions were not an important factor for the elastic response cases. For the inelastic response case the assumed clamped condition at the floor boundary appeared to be too severe. Whether the higher local plastic strains generated at this boundary affected the strains calculated in the crown region was not pursued further, since the more important effect of local plastic buckling of the frames could not presently be modeled by NOVA-2LTS. NOVA-2LTS should be modified to account for local elastic or plastic buckling of stiffeners. This could be accomplished in a similar manner that the skin buckling was handled in NOVA-2LTS. Each cross section segment of a stiffener would have a critical buckling stress parameter modified by a plasticity factor and a stress decay factor, so that the local stiffness of each segment could be altered as buckling progresses through the flanges and web of the stiffener. This is a recommended modification for NOVA-2LTS and NOVA-2S.

In both the KC-135A and B-52 fuselage testing emphasis was placed on measuring the response of the frames since they were the major structural component of the fuselage panels. The thin skins of the fuselages were undergoing buckling or wrinkling during the deformation of the stiffened panel. It should be noted that once the skin is allowed to buckle in NOVA-2LTS through the buckling criterion option the

true strain response of the buckled skin is uncalculable. If accurate strain response of the skin was desired in these large structurally stiffened panels a very fine model, probably producing a prohibitive number of modes and integration points, would result. Whether such a solution would be reasonable on the computer would have to be determined. The same problem faces the finite element method in that a prohibitive number of nonlinear finite elements are probably required to simulate the local buckling patterns between stiffeners. If the computer solution is unreasonable, the finite element method would have to be modified by special birth and death options for the elements to approximately account for skin buckling as was presently done in NOVA-2S. It should be noted that even if the skin responses were directly modeled, the undefined initial geometric imperfections of the thin curved skin would probably prevent an accurate determination of the strain response of the buckled skin.

The correlation results from this KC-125A fuselage investigation and the previous B-52 aft fuselage effort demonstrated that the NOVA-2S or NOVA-2LTS computer code can predict the peak response of actual large stiffened aircraft sections with reasonable accuracy (error less than 10%) in the elastic response region. Thus, for the threshold of permanent damage criterion in NOVA-2S based on the onset of yielding, the NOVA-2S peak strain response would result in a good prediction. In the inelastic response region leading to catastrophic damage based on a fracture strain criterion, the evaluation is more complicated. In the B-52 aft fuselage tests, the frames failed under tension strain on the inner flanges. This failure appeared (the strain gage failure at about 1% strain) to be premature for this fuselage test section and resulted from small holes that were present in the inner flanges which probably held cable harnesses in the actual aircraft. One longitudinal set of holes in the inner flanges of the frames was very near the position of peak tension strain induced by the blast loading and all fractures on the frames occurred through these holes. Thus, the fracturing of the frames occurred prematurely as the result of stress concentrations around the holes. How to account for such irregularities in the structure (usually unknown) is a question that can not be addressed in

this effort. If the holes were not present in the frame, NOVA-2S could give a good prediction for the B-52 fuselage of the peak inelastic response into the strain region where fracture would normally occur through a tension mechanism. Experience is needed in selecting the fracture strain for the catastrophic criterion. In the inelastic deformation shot for the KC-135A fuselage section, the severe damage to the frames was caused by local compressive failures (plastic buckling of the frame) which led to fractures after severe buckling deformations had occurred across the frame's cross section. This catastrophic compressive failure mechanism cannot presently be predicted by NOVA-2S. The NOVA-2LTS results of shot 22 showed peak compressive strains at the 2.5% level and no significant tension strains. Therefore, under the present catastrophic criterion based on tension strains, NOVA-2S could not predict this catastrophic failure of the KC-135A fuselage. Thus, there is a real need for a compressive catastrophic failure criterion in NOVA-2S along with a method to permit local buckling of the stiffeners as discussed before.

The usual clamped and simply supported boundary conditions permitted in any structural response code can only approximate the true boundary conditions found in actual large aircraft sections. Further refinement can be achieved by introducing other flexibilities at the boundaries through translational and torsional springs to simulate the stiffness of the adjacent structure outside the boundary. In this method the difficulty is estimating a priori the proper spring constants. The other approach would entail modeling the structure beyond the apparent boundary of interest. This method which is certainly more accurate has a significant computer time penalty. The NOVA-2S computer code has presently the capability to pursue all of these options, if required to obtain reasonable results. From the correlation efforts involving the KC-135A and B-52 fuselages, it appears that good results can be obtained if the boundary approached either a clamped or pinned condition. If the region of maximum strain is far removed from the boundary, the effect of the boundary is minimized for elastic response of the structure. If the peak response is occurring near a boundary it is important to know whether the actual condition approaches clamped or

pinned. When the displacements of the fuselage sections become large when inelastic deformations occur, the boundary conditions become more significant, but more evidence is needed to assess the overall importance in predicting peak response away from the boundary.

In analyzing large stiffened panel sections from aircraft uselages, it is important to be able to handle noncircular geometry. With the use of the initial geometric imperfection option in NOVA-2S, arbitrary geometry of a panel can be approximated. This method worked well for the B-52 fuselage panel which had a very irregular geometry in the circumferential direction as shown in Reference 4. The method for computing the necessary radial displacement coefficients for a surface which deviates from a specified circular shape should be incorporated directly in the NOVA-2S code. It would also improve the geometry capability of NOVA-2S to introduce a conical panel option that would permit better modeling of a nose radome type of structure when used in conjunction with the initial geometric imperfection option. The conical shell theoretical formulation already exists as an option in the DEPICS cylindrical shell code from which DEPROP was originally developed as a cylindrical panel code.

With the increased usage of composite materials in aircraft design, the elastic material model available in NOVA-2S could be refined to include a more general anisotropic material. The present orthotropic material model has been adequate in the past since the material properties for the composite material are usually approximated by specifying the material in terms of the orthotropic material constants. A more accurate description of a composite skin would contain constants beyond the five orthotropic constants and they could be computed if the detailed laminar construction of the skin is specified. It would also be helpful in establishing better failure criteria for composites in NOVA-2S, if the interlaminar shear stresses would also be computed for the composite.

The pressure loadings on the panels generated in NOVA-2S from the nuclear encounter should be reviewed and modified where necessary for the various aircraft components. At present, for panel analysis in

NOVA-2S the pressure time history of the blast loading is computed at the center of the panel and the distribution is assumed to be uniform over the panel. This assumption was established when only small panel components were being considered. Now for large stiffened fuselage panel sections, the actual distribution of the pressure loading over the panel becomes important. Thus, a new spatial loading distribution over the large panel needs to be defined in NOVA-2S.

SECTION VI

CONCLUSIONS AND RECOMMENDATIONS

The general conclusions emanating from this NOVA-2S correlation effort with the KC-135A fuselage test results are delineated as follows:

- (1) It was found that the maximum strain response on the center frame in the crown region of the KC-135A fuselage was most sensitive to the local skin buckling between stringers and the asymmetries in the pressure distribution over the fuselage's surface. Both of these effects were taken into account in the NOVA-2LTS structural and loading model. The skin buckling effect required a special modification to the NOVA-2S program which is documented in this report.
- (2) In the new skin buckling criterion option in NOVA-2S it was found that the peak strain response was more sensitive to the stress decay rate in the buckled skin than the critical buckling stress.
- (3) By examining the experimental strain behavior, it is suspected that structural anomalies (most likely out-of-roundness) were present in the crown region of this fuselage test section which had previously been subjected to fatigue testing. Because such structural anomalies were not defined for the fuselage, they could not be accounted for in the NOVA-2LTS model; however, the assumed perfect circular geometric shape still produced reasonable analytical and experimental strain comparisons.
- (4) The main difference between the analytical and experimental results, which could be attributed to out-of-roundness, was that the experimental strain distribution across the frames had more bending content than the analytical results exhibited.

- (5) The structural model employed in this effort represented the upper lobe compartment of the fuselage where the boundaries at the floor intersection were assumed clamped. This model was quite adequate for the elastic response cases, especially since the maximum strains occurred in the crown region far removed from these boundaries. However, in the inelastic case where large deformations of the fuselage occurred, this clamped condition appeared too rigid. It appears that the floor system does not provide full rigidity, since the main floor beam members are longitudinally oriented. The frames are continuous through this floor joint, so that the assumed clamped condition is better than a pinned condition, but there is an undetermined flexibility at this boundary. This flexibility could be approximated by other boundary options in NOVA-2S, if the joint stiffness was known apriori. The most accurate method would be to model the whole fuselage and absorb the computer cost penalty.
- (6) NOVA-2LTS predicted the maximum strains which occurred on the outer flange of the center frame very well (within 10%) for the unpressurized elastic response case at the 90° loading orientation. For the 45° loading case, NOVA-2LTS predicted the change in strain distribution along the circumference and the maximum strain quite well. For the pressurized cases, NOVA-2LTS indicated the significant decrease in the strain level that has occurred experimentally. At these lower strain levels the comparisons of the maximum did not show the accuracy demonstrated in the unpressurized cases. This is not unexpected since low level strain response is usually more sensitive to structural anomalies.
- (7) NOVA-2LTS time histories of the maximum strains compared well in general shape, but the phasing was off by about 2 ms. The experimental time to peak was always longer which could be caused by the greater bending content across the cross section of the frame in the experimental results. Bending is a lower frequency response than membrane action.

- (8) For the elastic response case in which the frames failed, NOVA-2LTS could not predict the local plastic buckling of the frames. Analytically, the energy was absorbed more evenly over the frames and the compressive strain levels reached about 2.5%, while experimentally strain levels become very high at local positions and resulted in rupturing of the frame at several circumferential positions.
- (9) Overall, complex aircraft stiffened panels can be modeled by NOVA-2S or NOVA-2LTS with confidence provided the user can define all important structural factors involved in the real structure and has a thorough understanding of all the modeling options now available in NOVA-2S and how to apply them to represent the real structure. For these large structures the dimensions of the program had to be extended and the computer time for a response run increased.

Based on the results of this effort the following recommendations are given as follows:

- (1) With all the modifications introduced into NOVA-2S over the last few years, it is important to generate a new User's Manual that contains a complete group listing, gives advice on how to use the new modifications and gives information on how to redimension the program for modeling the larger complex aircraft components. In addition, some of the modifications require that changes be made in the strain and stress output format of the program.
- (2) NOVA-2S should be modified to handle local buckling of the stiffeners elastically and plastically. In addition, the criteria in NOVA-2S should be revised for catastrophic damage to include a compressive type of failure through buckling.
- (3) The blast induced pressure loading formulation used in NOVA-2S should be reviewed and modified if necessary, especially in specifying a non-uniform pressure distribution for large panel structures. There are other less important modifications that could be made to NOVA-2S and these were discussed in Section V.

- (4) Many of the new additions to NOVA-2S should be more thoroughly checked out by benchmark solutions using other structural codes.

REFERENCES

1. "NOVA - A Digital Computer Program for Calculating the Response of Aircraft to the Overpressure from a Nuclear Explosion," AFWL-TR-72-115, Volume I, Kaman Avidyne, Air Force Weapons Laboratory, Kirtland Air Force Base, NM, July 1973.
2. Lee, W.N. and Mente, L.J., "NOVA-2 - A Digital Computer Program for Analyzing Overpressure Effects on Aircraft", AFWL-TR-75-262, Parts 1 and 2, Air Force Weapons Laboratory, Kirtland Air Force Base, NM, August 1976.
3. Mente, L.J. and Lee, W.N., "NOVA-2S - A Stiffened Panel Extension of the NOVA-2 Computer Program", AFWL-TR-78-182, Air Force Weapons Laboratory, Kirtland AFB, NM, December 1978.
4. Mente, L.J., Lee, W.N. and Stagliano, T.R., "NOVA-2S Modifications and Correlation with B-52 Shock Tube Test Results (U)", DNA 5983F, Defense Nuclear Agency, Washington, DC, April 1982, Secret.
5. Mente, L.J. and Lee, W.N., "Dynamic Elastic-Plastic Response of Unstiffened and Stiffened Panels to Pressure Loadings", AMMRC MS 80-4, Army Materials and Mechanics Research Center, Watertown, MA, Proceedings of the Army Symposium on Solid Mechanics, 1980, September 1980.
6. Syring, R.P., "The Effect of Internal Pressurization on the Blast Response Characteristics of the KC-135A Fuselage", AFWL-TR-78-159, Air Force Weapons Laboratory, Kirtland AFB, NM, February 1979.
7. Bruhn, E.F., Analysis and Design of Flight Vehicle Structures Tri-State Offset Company, 1973.
8. Stagliano, T.R. and Mente, L.J. "An Evaluation of the ADINA Finite Element Program for Application to Aircraft Overpressure Vulnerability" DNA 4876F, Defense Nuclear Agency, Washington, DC, February 1979.

APPENDIX

CHANGES IN THE NOVA-2S PROGRAM LISTING

This Appendix gives the routines in NOVA-2S and NOVA-2LTS that were modified for increasing the program dimensions and incorporating the buckling criterion method. The COMMON subroutine in the Appendix reflects the dimension changes that were made to accommodate the structural models generated in this effort. The inclusion of the buckling criterion method required modifications in subroutines DERV1, DERV2, DSET1, DSET3, SIGMA, and SIGMAB which are given in the Appendix.

*COMMON DECK DROVA

```
COMMON/DROVA/ ALFAA,ALFAF,ALTI,BAF,CORO,CO,ORDX,HR,HG,HI,INC,
1 IUL,KF,KGRD,KGRD0,NEL,NFF,NFS,NLEHT,NLEVT,NLEN,ROE,NORMAX,
2 NORI,NTERT,NTFVI,NTFV,NTF1,OUT(8),PINT,P0,RCRIT(100),
3 REST(30),RF(20),RH00,SL,SSFAN,ST,THETAR,TWP(1000),VEL,WKT,
4 WP(1000),XB(20),XBF,XCC(20),XCK,XLE(5),XLEHT(5),XLEVT(5),
5 XLEN(5),XLL,XNUSE,XOSRH(30),XOSRO(30),XP,XSA,XSCRIT(100),
6 XTAL,XTE(5),XTEHT(5),XTEVT(5),XTFV(5),XTL,YCC(20),YF,
7 YLE(5),YLEHT(5),YLEV(5),YOSPB(30),YOSRO(30),YP,YSA,
8 YSCRIT(100),YSN,YTE(5),YTEHT(5),YTEV(5),ZCC(20),ZF,
9 ZLEVT(5),ZOSRH(30),ZOSRO(30),ZP,ZSA,ZSCRIT(100),ZTEVT(5),ZZ2(9)
DIMENSION FP(10,40),TFP(10,40)
EQUIVALENCE (FP(1,1),*P(1)),(TFP(1,1),IWP(1))
```

*COMMON CTIX

```
COMMON/CTIX/ HX,ILX
```

*COMMON PBI

```
COMMON/PBI/ AMPG,AMP1,DUMA,DUMB,DUM1,DUM2,DUM3,DUM4,DUM5,
1 DUM6,DUM7,DUM8,DUM9,GNF1,P1,SNA,SNG,IND1,IND2,IND3,IND4,
2 IND5,TAU0P1
```

*COMMON REFRA

```
COMMON/REFRA/ DA(17),DB(17),DPAX(150),DPOLF,ELA(41),
1 FLB(41),FLMAX(200),FCOPE,FJEM1,H,HI,HT(150),IE,IE1,IE2,
2 ITIM(200),IDAK(150),MI,MCPA(41),MCPB(41),NT,NTAPE,NTM,NTI,
3 OUTD(5),FA(16,40),PB(16,40),PRA(40),PRB(40),PSA(16),
4 PSB(16),PSI(150),PO,PHDA(16,40),RHOB(16,40),RHOKA(40),
5 RHORB(40),RHOSA(16),RHOSH(16),RHOD,KI(150),RTD,SED(5),
6 TAPTE(150),TADD,TAUTK(200),TIMES(200),TR,TS,
7 URA(16,40),URE(16,40),UREA(40),URRB(40),URSA(16),
8 URSH(16),UA(16,40),UB(16,40),YFA(40),YRB(40),YSA(16),
9 YSH(16)
```

*COMMON RIK2

```
COMMON/RIK2/ ACC0V(45),ACC0Y(45),AFL(8,46),AMP,
1 ARSL(5,4),F1B(45),F1G(45),F1G3,CORIT(8),CINST(8),
2 CGSG(44),COST(45),CPTIM,CIN2,C6(45),DELTAS(45),
3 DELTS(45),DELTSB(45),DELTSO(45),DELT1(45),DELT1K(45),
4 DELT1O(45),DIS(44),DUMA,FCAX1(8),FCAXO(8),EI(40),ELI,
5 EPSIL(45),EPSIL1(45),EPN,FINAT(8),EINXO(8),
6 F1(5,21,46),F1H(4),F1X,FSK10,FY(45),FZ(45),
7 H(8,46),H1(45),IL1(2),IL2,IPR0P(8),IUI(2),IU2,IY(45),IY1,
8 IY2,ITIM,AFL,KEYB1,KEYB2,KEYB6,KEYB8,KIS,KMAX,KSUB,KREF,
9 LMAX,LSCHX1(8),LSCHXO(8),LSTAX1(8),LSTAXO(8),LAXF,MAXLK
COMMON/RIK2/ MAXSE,MAXX,MPH1T,MTAPE,MYIELD,B1,B2,...
1 LAY(40),LCP,LEP0R,M,MLL,MSL,FSK10,NSL(8),SSSL(8),
2 SSST1(8),LTAPE,MYIELD,B1(2,B1,LI45),KAT10(8),REF,REF,
3 RH0(8),SD(15,6),SCAX1(8),SCAXO(8),SING(44),SINT(45),
4 SA(46),SASSE,SSASST,SSS(8,6),SSS1(6,6),STH2,
5 STH(5,4),STH1(8),STXO(8),STH4(8,5),STRMAT(8,5),
6 STRSO(8,5),STRSO1(8,5),SC0P(8),ICN1(8),TH,THE1(45),THE1A1,
7 THETA2,ISCHX1(8),ISCHXO(8),ISTEX1(8),ISTEXO(8),V(45),
8 VM(45),V1(45),V1V2,A(45),B(45),C(45),AR(8,46),
9 KAT1(8),B1(2,B1,LI45),YCNL,YCN1(46),ZETA(21,46)
COMMON/RIK2/ ZETAL(46),ZETAR(46)
```

*COMMON RIK3

```
COMMON/RIK3/ DELT1(45),DELT1O(45),DELT3,ERRR(90),IL,
1 KS,FCOPE,FCOPE1,FCOPE2,FCOPE3,FCOPE4,FCOPE5,RES(90),SINTE(45),
2 SINTO(45),SSS(8,6),V2X,V2O,V2P,V2Q,V2R,V2S
```

Reproduced From
Best Available Copy

```

*COMDECK BLK4
  COMMON /BLK4/ IP(90),PRES(90),PX(90),PRES(90),SIGX(90),
1  XRES(90,90),XX(90)
*COMDECK BLK5
  COMMON /BLK5/ PRES(3),PX(3),PRES(3),XRES(3,3),XX(3)
*COMDECK BLK6
  COMMON /BLK6/ SAV(10,2),SBV(10,2),BIGMP(2),BMP1(2),
1  CEA(2),CEZA(2),CEZ2A(2),CTET(11,2),CTP1(10,2),CT2,
2  DEN(2),ER(3),HF(2),HP1(2),MCDDND,NT1(2),SAV(10,2),
3  SAVP1(10,2),SBV(10,2),SBVP1(10,2),STET(11,2),
4  STR1(10,2),STRA(5,21,20),ST1,ST2,TEND1,TEND2,TETA(11),
5  VF(2),VP1(2),X(11),Y(11)
*COMDECK CHLK1
  COMMON /CHLK1/ A,KCOUP,KPG(50),KPB(50),KZ,LBAR,LMAX,RP,RBAR,
1  MG,MGA(13),MGB,MGB2,MUSE(20,20),NB,NBAR,PRR(20),LEND,GBT,
2  FDERV,MG,MGB,MGB2,NGT,DEP,DELT,PSYMB,MSYMB,MUSE(129,55),
3  PI,XR(129),XG(55),NRND1,IPND2,NSPR,IDIR(30),NSPG(30),
4  NSPG(30),BIGK(30),XLP3,XLP4,XLP5,RTSC,ISLOC(736),KTSGB(736),
5  BIGC(736),TG1,TG2,TR1,TR2,NRUV,NRUV1,NRUV2,BFI(4),PIPE,
6  FIP(10,4),TIP(10,4),JLIP(4),SFIP(129,4),XLP6,NBUCK,KBUCKS,BUCK
*COMDECK CHLK2
  COMMON /CHLK2/ PLTR(129),CP(6),CPRT,CPRT1,FP1(550),FP2(550),
1  FP3(550),FP5(2580),FP6(2580),FP7(2580),GAM(55),KC,
2  HJ(55),PK(129),PLMA(55),PLMA(129),XJ,XJ2,XJ3,XJ4,XJ5,XL,
3  XLF,XLF1,XLF2,XL1,XL2,XL3,XL4,XL5,XL7,PRLU(100),PRLV(100),
4  PRL(100),F01(550),F02(550),F03(2580),F04(2580),FV1(550),
5  FV2(550),FV3(2580),FV4(2580),OTG(13),OTR(20)
*COMDECK CHLK3
  COMMON /CHLK3/ GA(6),HGO(6)
*COMDECK CHLK4
  COMMON /CHLK4/ M2,PMS(300),VX(300),XX(300),YY(300)
1  ,PSM
*COMDECK CHLK5
  COMMON /CHLK5/ FR(8),ERR(300),FG(20,13),FM(8),FOOT(300),
1  NGUT(300),HMD(8),FI(20,13),VI(20,13),WI(20,13)
*COMDECK CHLK6
  COMMON /CHLK6/ ALTI(1235),ALXT(1235),ALXX(1235),BE1(1235),
1  BE2(1235),BE3(1235),FB0(1235),ETI1(1235),EXT1(1235),
2  EXX1(1235),SIG1(1235),SIGT1(1235),SIGXX1(1235),TT(20)(1235)
*COMDECK CHLK7
  COMMON /CHLK7/ C01,C02,C03,C02,C03,C04,C05,C06,C07,FI,FP,
1  FFO,FPP,H,IFIRST,JFIRST,LC,LCMAX,KFLP,STGO,SIGC2,T00,T00S
*COMDECK CHLK8
  COMMON /CHLK8/ DISC,XX3(300)
*COMDECK CHLK9
  COMMON /CHLK9/ SIL(8),RXL(8),CCRT(8),CCRTB(6),CCRTG(31),
1  CIOST(8),CISTG(31),CIST(3),FI(8),FX(8),GXT(8),LBP,LGP,LSBP(2),
2  LSGP(2),I12(16),STEC(2),TECO,LZP,SAC(8),SAT(8),MAX,SIMAX(2),
3  ICRT(8),ICRTB(6),ICRTG(31),TH(8),TMAX,TSAX(2),XX(8),
4  ZC(16)
*COMDECK CHLK10
  COMMON /CHLK10/ G(7095),F(7095),H(7095),PI(7095),
1  BE(7095),BE1(7095),V(7095),G(7095),V6(7095),G(7095),PI(7095),
2  LBP(7095),LGP(7095),LSBP(7095),LSGP(7095)
*COMDECK CHLK11
  COMMON /CHLK11/ C011,C012,C022,C033,C011,C012,C022,C033,FR11,

```

```

1 FM12,FM22,FM33
*COMDECK CBLK12
COMMON/CBLK12/ DELX(1),IP(1),PRES(1),PX(1),PRES(1),
1 SIGX(1),XRES(1,1),XX1(1)
*COMDECK CBLK13
COMMON/CBLK13/ DC,EC,EPSIF,GC,HBAR,NL,NNOUT,RHO,THETA0
*COMDECK CBLK15
COMMON/CBLK15/ AASB(8,129,3),AASG(8,31),ASB(129,3),ASG(31),BETC
1(129,3),RIGJB(129,3),RIGJG(31),ASTB(8,129,3),BSTG(8,31),CA1,CA2
2(31),CA3(3),C11G(31),C22B(129,3),D11G(31),D22B(129,3),D33B(129,3)
3,D33G(31),EPOB(3),EPOG(31),EPSB(3),EPSG(31),ESTRB(3),ESTRG(31),
4ETSTRB(3),ETSTRG(31),F11G(31),F22B(129,3),GBARB(3),GBARG(31),HOB
5(129,3),HOG(31),HSTB(8,129,3),HSTG(8,31),KSB(3),KSBX(129),KSG(31)
6,KSGX(129),KSTIF,KSUMB(2092),KSUPB(3),KSUPG(31),KYX(4895),LXMAX,
7MFIRST,MFJRST,NSH,NSEGB(3),NSEGG(31),MSG,NSGMB,NSMAX,NSTR(3),
8RHOSTB(3),RHOSTG(31),SIDEB(3),SIDEG(31),SIGOBC(3),SIGOBT(3),
9SIGOGC(31),SIGOGT(31),SX(4895),ZFB(8,418),ZSTB(2,129,3),ZSTG(2,31)
*COMDECK CBLK16
COMMON/CBLK16/ ALX(4895),BEX(4895),EX1(4895),SIX1(4895)
*COMDECK CBLK17
COMMON/CBLK17/ AU(100,100),AV(100,100),AW(100,100)
*COMDECK CBLANK
COMMON/CBLANK/ CN10,CN11,CN8,CN9,EPHO(1235),ETT,EXT,EXX,
1 INZ(2),KSUMA(7095),KY(1235),STT(1235),SXT(1235),SXX(1235),
2 S1A(7095),S2A(7095),S3A(7095),S4A(7095),S5A(7095),S6A(7095),
3 UU(20,13),VV(20,13),WW(20,13),XKTT,XKXT,XKXX,X1A(7095),
4 X2A(7095),X3A(7095),X4A(7095),X5A(7095),X6A(7095),
5 ZA(2),ZB(2),ZF(6),ZG(6),ZH(6)
*COMDECK CBLK18
COMMON/CBLK18/ AWEBG(31),AWEHB(129,3),C,CUR,FTZ1(230),FTZ2(230),
1 FTZ3(230),FTZ4(230),FXZ1(230),FXZ2(230),FXZ3(230),FXZ4(230),
2 GB,GG,LOUT,LHBAK,LRG(10),LRGOUT(99),LSR(10),LSHAK,LSOUT(99),
3 LUSE(10,10),NSHEAR,PESTZB(361),PESTZG(361),PESXZB(361),
4 PESXZG(361),RSL(10,10),RSLP(10,10),RSM(10,10),RSMPL(10,10),
5 XLP7,XLP8,XSTZ(361),XSXZ(361)
*DECK DERV1
SUBROUTINE DERV1

*CALL CBLK1
*CALL CBLK2
*CALL CBLK4
*CALL CBLK10
*CALL CBLK11
*CALL CBLK15
*CALL CNOVA
*CALL CBLANK
*CALL CBLK18

```

Reproduced From
Best Available Copy

```

I=1
DO 100 M=1,NG
DO 100 N=1,NB
IF(MUSE(N,M).EQ.0) GO TO 100
UU(N,M)=XX(I)
VV(N,M)=XX(MGB+I)
WW(N,M)=XX(MGB+2+I)
I=I+1

```

```

100  CONTINUE
      K=0
      DO 500 I=1,NGT
      DO 500 J=1,NBT
      IF(NUSE(J,I).EQ.0) GO TO 500
      K=K+1
      SS1=0.0
      SS2=0.0
      SS3=0.0
      SS4=0.0
      SS5=0.0
      SS6=0.0
      SS7=0.0
      SS8=0.0
      SS9=0.0
      SS10=0.0
      SS11=0.0
      SS12=0.0
      DO 400 M=1,MB
      MM= (M-1)*NGT+I
      FU11 = FU1(MM)
      FU22 = FU2(MM)
      FV11 = FV1(MM)
      FV22 = FV2(MM)
      T1 = FP1(MM)
      T2 = FP2(MM)
      T3 = FP3(MM)
      S1=0.0
      S3=0.0
      S4=0.0
      S6=0.0
      S7=0.0
      S9=0.0
      S11=0.0
      DO 200 N=1,NB
      IF(MUSE(N,M).EQ.0) GO TO 200
      NN= (N-1)*NBT+J
      UMN=UU(N,M)
      VMN=VV(N,M)
      WMN=WW(N,M)
      S1 = UMN*FU3(NN) + S1
      S3 = UMN*FU4(NN) + S3
      S4 = VMN*FV3(NN) + S4
      S6 = VMN*FV4(NN) + S6
      S7 = WMN*FP5(NN) + S7
      S9 = WMN*FP6(NN) + S9
      S11 = WMN*FP7(NN) + S11
200  CONTINUE
      SS1 = S1*FU11 + SS1
      SS2 = S1*FU22 + SS2
      SS3 = S3*FU11 + SS3
      SS4 = S4*FV11 + SS4
      SS5 = S4*FV22 + SS5
      SS6 = S6*FV11 + SS6
      SS7 = S7*T1 + SS7
      SS8 = S7*T2 + SS8

```

Reproduced From
Best Available Copy


```

      SS9 = S9*T1 + SS9
      SS10 = S7*T3 + SS10
      SS11 = S11*T1 + SS11
      SS12 = S9*T2 + SS12
400  CONTINUE
      U(K)=SS1
      UG(K)=SS2
      UB(K)=SS3
      V(K)=SS4
      VG(K)=SS5
      VB(K)=SS6
      W(K)=SS7
      WG(K)=SS8
      WB(K)=SS9
      WGG(K)=SS10
      WBB(K)=SS11
      WGB(K)=SS12
500  CONTINUE

```

Reproduced From
Best Available Copy

COMPUTE STRAINS AND STRESSES

```

      K=0
      DO 700 I=1,MGT
      K2 = KSRX(I)
      DO 700 J=1,NBT
      IF(NUSE(J,I).EQ.0) GO TO 700
      K1 = KSGX(J)
      K=K+1
      UGF=UG(K)
      UBF=UB(K)
      VF=V(K)
      VGF=VG(K)
      VBF=VB(K)
      WF=W(K)
      WGF=WG(K)
      WBF=WB(K)
      DWGF=DWG(K)
      DWBF=DWB(K)
      EXX=XL1*(UGF+XL1*(WGF*DWGF+0.5*(WGF**2+VGF**2+UGF**2)))
      ETT=XJ*(VBF+XJ*(WBF*DWBF+0.5*(WBF**2+VBF**2+UBF**2)))
      EXT=XJ*UBF+XL1*(VGF*(1.0+XJ*VBF)+XJ*(WGF*(WBF+DWBF)+DWGF*VBF+UBF*
1UGF))
      AC = XJ*VBF + XL1*UGF + 1.0
      WGGF = WGG(K)
      WBBF = WBB(K)
      WGBF = WGB(K)
      XKXX = XL7*WGGF*AC
      XKTT = XJ2*WBBF*AC
      XKXT = XJ5*WGBF*AC
      IF(NPLT.EQ.0) GO TO 600
      ETT=ETT-WF*(1.0+XJ*VBF-0.5*VF)+VF*(XJ*WBF+0.5*VF)
      EIT=ETT+VF*DWG(K)
      EXT=EXT+XL1*(WGF*VF-VGF*WF)
      YKTT=XKTT+XJ4*VBF+XL1*UGF-WF
      XKXT=XKXT+XL1*VGF
      AC = XJ*WBF + VF

```

```

      XKXX = XKXX - XL7*WGGF*WF
      XKTT = XKTT + XJ*VBF*(XJ*VBF - WF) - XJ2*WF*WBBF +
1    (XJ*VBF - WF)**2 + AC*(AC + XJ*WBF)
      XKXT = XKXT - XJ5*WGBF*WF + XL3*WGF*AC
600 IF (NSHEAR.EQ.0) GO TO 605
      X1 = XSX7(K)
      X2 = XSTZ(K)
      EXX = EXX + X1*(0.5*X1 - XL1*WGF)
      ETT = ETT + X2*(0.5*X2 - XJ*WBF - CUR*VF)
      EXT = EXT - XL1*WGF*X2 + X1*(X2 - XJ*WBF - CUR*VF)
      XKXX = XKXX - XL1*PESXZG(K)
      XKTT = XKTT - XJ*PESTZB(K)
      XKXT = XKXT - XJ*PESXZR(K) - XL1*PESTZG(K)
605 IF (NDERV.EQ.2) GO TO 640
      CS11 = CM11
      DS11 = DM11
      FS11 = FM11
      CS22 = CM22
      DS22 = DM22
      FS22 = FM22
      DS33=DM33
      SIG = 1.0
      IF (K1.EQ.0) GO TO 610
      CS11 = CM11 + C11G(K1)
      FS11 = FM11 + F11G(K1)
      DS11 = DM11 + D11G(K1)
      DS33=DS33+D33G(K1)
      SIG = SIG*SIDEK(K1)
610 IF (K2.EQ.0) GO TO 620
      CS22=CM22+C22B(J,K2)
      FS22=FM22+F22B(J,K2)
      DS22=DM22+D22B(J,K2)
      DS33=DS33+D33B(J,K2)
      SIG = SIG*SIDEK(K2)
620 S1A(K) = CS11*EXX + CM12*ETT + FS11*XKXX + FM12*XKTT
      S2A(K) = CS22*ETT + CM12*EXX + FS22*XKTT + FM12*XKXX
      S3A(K) = CM33*EXT + FM33*XKXT
      IF (NBUCK.EQ.0.OR.NCALL.GT.0) GO TO 625
      G2 = CM22*ETT + CM12*EXX + FM22*XKTT + FM12*XKXX
      IF (G2.GT.BUCKS) GO TO 625
      S1A(K) = CS11*EXX + FS11*XKXX
      S2A(K) = (CS22-CM22)*ETT+(FS22-FM22)*XKTT+BUCKS*(BUCKS/G2)**1.00
      S3A(K) = CM33*EXT
625 IF (SIG.EQ.0.0) GO TO 630
      S4A(K) = DS11*XKXX + DM12*XKTT + FS11*EXX + FM12*ETT
      S5A(K) = DS22*XKTT + DM12*XKXX + FS22*ETT + FM12*EXX
      S6A(K)=DS33*XKXT+FM33*EXT
      IF (NBUCK.EQ.0.OR.NCALL.GT.0) GO TO 660
      IF (G2.GT.BUCKS) GO TO 660
      S4A(K) = DS11*XKXX + FS11*EXX + DM12*XKTT + FM12*ETT
      S5A(K) = DS22*XKTT + FS22*ETT + DM12*XKXX + FM12*EXX
      S6A(K) = DS33*XKXT + FM33*EXT
      GO TO 660
630 S4A(K) = 0.0
      S5A(K) = 0.0
      S6A(K) = 0.0

```

Reproduced From
Best Available Copy

```

      GO TO 660

640  CALL SIGMA (J,I,K)
      IF (K1.GT.0) CALL SIGMAR (K1,0,J,I,K)
      IF (K2.GT.0) CALL SIGMAR (0,K2,J,I,K)
660  X1A(K) = EXX
      X2A(K) = ETT
      X3A(K) = EXT
      X4A(K) = XKXX
      X5A(K) = XKTT
      X6A(K) = XKXT
700  CONTINUE
      RETURN
      END
*DECK DERV2
      SUBROUTINE DERV2

*CALL CBLK1
*CALL CBLK2
*CALL CBLK3
*CALL CBLK4
*CALL CBLK10
*CALL CBLK15
*CALL CBLK17
*CALL CNOVA
*CALL CBLANK
*CALL CBLK18

900  IZ=0
      DO 1800 IR=1,MG
      MM0=(IR-1)*NGT
      DO 1800 IS=1,MB
      IF (MUSE(IS,IR).EQ.0) GO TO 1800
      NN0=(IS-1)*MBT
      IZ=IZ+1
      SURS=0.0
      SVRS=0.0
      SWRS=0.0
      K=0
      DO 1700 I=1,NGT
      MM=MM0+I
      FU11 = FU1(MM)
      FU22 = FU2(MM)
      FV11 = FV1(MM)
      FV22 = FV2(MM)
      T1 = FP1(MM)
      T2 = FP2(MM)
      T3 = FP3(MM)
      SU = 0.
      SV = 0.
      SW = 0.
      PWLM = P1WA(I)
      DO 1600 J=1,NB1
      IF (MUSE(J,I).EQ.0) GO TO 1600
      K = K + 1

```

Reproduced From
Best Available Copy

```

IF (NUSE(J,1).EQ.1) GO TO 1600
PRLN = PTNA(J)
NN=NN0+J
UGF=UG(K)
UBF=UB(K)
VF=V(K)
VGF=VG(K)
VBF=VB(K)
WF=W(K)
WGF=WG(K)
WBF=WB(K)
WGGF = WGG(K)
WBBF = WBB(K)
WGBF = WGB(K)
DWGF=DWG(K)
DWBF=DWB(K)
IF (NU.EQ.0) PPP=PA(K)
PU = FU11*FU3(NN)
PUG = FU22*FU3(NN)
PUB = FU11*FU4(NN)
PV = FV11*FV3(NN)
PVG = FV22*FV3(NN)
PVB = FV11*FV4(NN)
PW = T1*FP5(NN)
PWG = T2*FP5(NN)
PWB = T1*FP6(NN)
PWGG = T3*FP5(NN)
PWBB = T1*FP7(NN)
PWGB = T2*FP6(NN)
1100 PEXXU=XL1*PUG*(1.0+XL1*UGF)
PEXXV=XL7*VGF*PVG
PEXXW=XL7*PWG*(WGF+DWGF)
PETTU=XJ2*UBF*PUB
PETTV = XJ*PVB*(1.0 + XJ*VBF)
PETTW = XJ2*PWB*(WBF + DWBF)
PEXTU=XJ*(PUB*(1.0+XL1*UGF)+XL1*UBF*PUG)
PEXTV = XL1*(PVG*(1.0 + XJ*VBF) + XJ*VGF*PVB)
PEXTW = XJ3*(PWB*(WGF+DWGF) + PWG*(WBF+DWBF))
PKXXV=XL7*PWGG
PKTTW=XJ2*PWBB
PKXTW=XJ5*PWGB
AC = XJ*VBF + XL1*UGF
PKXXU = XL1*XL7*WGGF*PUG
PKXXV = XJ*XL7*WGGF*PVB
PKXXW = PKXXW + XL7*PWGG*AC
PKTTU = XJ2*XL1*WBBF*PUG
PKTTV = PVB*XJ*XJ2*WBBF
PKTTW = PKTTW + PWBB*XJ2*AC
PKXTU = XJ4*XL7*WGBF*PUG
PKXTV = XL3*XJ2*WGBF*PVB
PKXTW = PKXTW + XJ5*PWGB*AC
IF (NSHFAK.EQ.0) GO TO 1160
X1 = XSX7(K)
X2 = XSTZ(K)
PEXXW = PEXXW - XL1*X1*PUG
PETTV = PETTV - CUB*X2*PV

```

Reproduced From
Best Available Copy

```

      PETTW = PETTW - XJ*X2*PWB
      PEXTV = PEXTV - CUR*X1*PV
      PEXTW = PEXTW - XL1*X2*PWG - XJ*X1*PWB
1180 S1 = 0.9
      S2=0.0
      IF(NPL7.EQ.0) GO TO 1200
      PETTV=PETTV+PV*(VF+XJ*WBF) - XJ*WF*PVB
      PETTW=PETTW - PW*(1.0+XJ*VBF-WF) + XJ*VF*PWB
      PEXTV=PEXTV + XL1*(WGF*PV-WF*PVG)
      PEXTW=PEXTW + XL1*(VF*PWG-VGF*PW)
      PKTTU = XL1*PUG + PKTIU
      PKTTV=XJ4*PVB + PKTIV
      PKTTW=PKTTW - PW
      PKXTV=XL1*PVG + PKXTV
      PKXXW = PKXXW - XL7*(PWGG*WF + PW*WGGF)
      PKTIV = PKTIV + XJ*PVB*(4.*XJ*VBF - 3.*WF) +
1      PV*(3.*XJ*WBF + 2.*VF)
      PKTTW = PKTTW + XJ2*PWB*( -WF + XL1*UGF) + PW*(2.*WF -
1      3.*XJ*VBF - XJ2*WBF) + PWB*XJ*(4.*XJ*WBF + 3.*VF)
      PKXTV = PKXTV + XL3*PV*WGF
      PKXTW = PKXTW - XJ5*(PWGB*WF + PW*WGBF - PWB*WGF) +
1      PWG*XL3*(XJ*WBF + VF)
      S1 = DW0(K) + WF
      S2 = VF
1200 PU = XLP2*PPP*PU*(WGF + DWGF)
      PV = XLP1*PPP*PV*(XJ*(WBF + DWBF) + S2)
      PW = XLP1*PPP*PW*(S1 - XL1*UGF - XJ*VBF - 1.0)

      FUX = 0.
      FVX = 0.
      FWX = 0.
      SIG=1.0
      IF (NDERV.EQ.1) GO TO 1280
      IF (KSTIF.EQ.0) GO TO 1270
      STIFFENERS.
      K1 = MSGX(IJ)
      K2 = MSRX(I)
      IF (K1.EQ.0) GO TO 1230
      SIG=SIGEG(K1)
      IJ = (K1-1)*NMAX + 1
      KSUM = KSUMB(IJ)
      NS = NSEGG(K1)
      IF (KSUM.LT.NS) GO TO 1210
      ELASTIC = GAMMA.
      G1 = C11G(K1)*X1A(K) + F11G(K1)*X4A(K)
      G4 = D11G(K1)*X4A(K) + F11G(K1)*X1A(K)
      G5=D33G(K1)*X6A(K)
      FUX=(PEXXU*G1+PKXXU*G4+G5*PKXTU)*CA1+FUX
      FVX=(PEXXV*G1+PKXXV*G4+G5*PKXTV)*CA1+FVX
      FWX=(PEXXW*G1+PKXXW*G4+G5*PKXTW)*CA1+FWX
      GO TO 1230
      INELASTIC = GAMMA.
1210 FS1 = 0.
      FS2 = 0.
      FS3 = 0.
      LU = NSMAX*(IJ-1)

```

Reproduced From
Best Available Copy

```

DO 1220 KK=1,NS
  L = LO + KK
  G1 = AASG(KK,K1)*SX(L)
  Z1 = ZFR(KK,K1)
  FS1 = G1*(PEXXU + Z1*PKXXU) + FS1
  FS2 = G1*(PEXXV + Z1*PKXXV) + FS2
1220 FS3 = G1*(PEXXW + Z1*PKXXW) + FS3
  G2=CA1*D33G(K1)*X6A(K)
  FUX=FS1*CA2(K1)+G2*PKXTU+FUX
  FVX=FS2*CA2(K1)+G2*PKXTV+FVX
  FWX=FS3*CA2(K1)+G2*PKXTW+FWX

1230 IF (K2.EQ.0) GO TO 1270
  SIG=SIG*SIDER(K2)
  IJ = NSGMB + (K2-1)*NBAR + J
  KSUM = KSUMB(IJ)
  NS = NSEGR(K2)
  IF (KSUM.LT.NS) GO TO 1240
  ELASTIC = BETA.
  G2=C22B(J,K2)*X2A(K)+F22B(J,K2)*X5A(K)
  G5=D22B(J,K2)*X5A(K)+F22B(J,K2)*X2A(K)
  G6=D33B(J,K2)*X6A(K)
  FUX=(PETTU*G2+PKTTU*G5+PKXTU*G6)*CA1+FUX
  FVX=(PETTV*G2+PKTTV*G5+PKXTV*G6)*CA1+FVX
  FWX=(PETTW*G2+PKTTW*G5+PKXTW*G6)*CA1+FWX
  GO TO 1270
  INELASTIC = BETA.
1240 FS1 = 0.
  FS2 = 0.
  FS3 = 0.
  KKK=NSG+(K2-1)*NBAR+J
  LO = NSMAX*(IJ-1)
  DO 1250 KK=1,NS
    L = LO + KK
    G1=AASB(KK,J,K2)*SX(L)
    Z1=ZFB(KK,KKK)
    FS1 = G1*(PETTU + Z1*PKTTU) + FS1
    FS2 = G1*(PETTV + Z1*PKTTV) + FS2
1250 FS3 = G1*(PETTW + Z1*PKTTW) + FS3
    G2=CA1*D33B(J,K2)*X6A(K)
    FUX=FS1*CA3(K2)+G2*PKXTU+FUX
    FVX=FS2*CA3(K2)+G2*PKXTV+FVX
    FWX=FS3*CA3(K2)+G2*PKXTW+FWX

1270 J1 = LPAR*(K-1)
  KSUM = KSUMA(K)
  IF (KSUM.LT.LPAR) GO TO 1300
  IF (KTYPE.EQ.3) GO TO 1300
1280 G1 = S1A(K)
  G2 = S2A(K)
  G3 = S3A(K)
  G4 = S4A(K)
  G5 = S5A(K)
  G6 = S6A(K)
  F1 = PEXXU*G1 + PETTU*G2 + PEXTU*G3
  F2 = PKXXU*G4 + PKTTU*G5 + PKXTU*G6

```

Reproduced From
Best Available Copy

```

F3 = PEXXV*G1 + PETTV*G2 + PEXTV*G3
F4 = PKXXV*G4 + PKTTV*G5 + PKXTV*G6
F5 = PEXXW*G1 + PETTW*G2 + PEXTW*G3
F6 = PKXXW*G4 + PKTTW*G5 + PKXTW*G6
FU = CN10*F1 + CN11*F2
FV = CN10*F3 + CN11*F4
FW = CN10*F5 + CN11*F6
GO TO 1500

```

```

1300 TOTUM=0.0
TOTVM=0.0
TOTWM = 0.0
TOTUB = 0.0
TOTVB = 0.0
TOTWB = 0.0
DO 1400 KK=1, LBAR
L = JI + KK
S1 = HGO(KK)
S2 = GX(KK)*S1
G1 = SXX(L)
G2 = STT(L)
G3 = SXT(L)
TOTUM = TOTUM + S1*(PEXXU*G1 + PETTU*G2 + PEXTU*G3)
TOTUB = TOTUB + S2*(PKXXU*G1 + PKITU*G2 + PKXTU*G3)
TOTVM = TOTVM + S1*(PEXXV*G1 + PETTV*G2 + PEXTV*G3)
TOTVB = TOTVB + S2*(PKXXV*G1 + PKITV*G2 + PKXTV*G3)
TOTWM = TOTWM + S1*(PEXXW*G1 + PETTW*G2 + PEXTW*G3)
1400 TOTWB=TOTWB+S2*(PKXXW*G1+PKITW*G2+PKXTW*G3)
FU = CN8*TOTUM + CN9*TOTUB*SIG
FV = CN8*TOTVM + CN9*TOTVB*SIG
FW = CN8*TOTWM + CN9*TOTWB*SIG

1500 SU = (FU + PU + FUX)*PRLN + SU
SV = (FV + PV + FVX)*PRLN + SV
SW = (FW + PW + FWX)*PRLN + SW
1600 CONTINUE
SURS = SURS + PRLN*SU
SVRS = SVRS + PRLN*SV
SWRS = SWRS + PRLN*SW
1700 CONTINUE
ELASTIC SPRINGS.
IF (NSPR.EQ.0) GO TO 1740
DO 1730 L12 = 1, NSPR
L1 = NSPR(L12)
L2 = NSPR(L12)
K = (L1-1)*NBT + L2
RIGKL = RIGK(L12)*XLP3
IF (IDIN(L12) = 2) 1710, 1720, 1725
1710 SURS = RIGKL*D(N)*F01(MMO+L1)*F03(NNO+L2) + SURS
GO TO 1730
1720 SVRS = RIGKL*V(N)*FV1(MMO+L1)*FV3(NNO+L2) + SVRS
GO TO 1730
1725 SWRS = RIGKL*W(N)*FP1(MMO+L1)*FP5(NNO+L2) + SWRS
1730 CONTINUE
TORSIONAL SPRINGS.
1740 IF (NTSC.EQ.0) GO TO 1750

```

Reproduced From
Best Available Copy

```

DO 1746 I=1,NTSC
J = ISLOC(I)
II = KTSGB(I)
GO TO (1742,1743,1744,1745), J
1742 K = II
SWRS = SWRS+XLP4*BIGC(I)*WG(K)*FP2(MMO+1)*FP5(NNO+II)*HK(II)
GO TO 1746
1743 K = (NGT-1)*NBT + II
SWRS = SWRS+XLP4*BIGC(I)*WG(K)*FP2(MMO+NGT)*FP5(NNO+II)*HK(II)
GO TO 1746
1744 K = (II-1)*NBT + 1
SWRS = SWRS+XLP5*BIGC(I)*WB(K)*FP1(MMO+II)*FP6(NNO+1)*HJ(II)
GO TO 1746
1745 K = II*NBT
SWRS = SWRS+XLP5*BIGC(I)*WB(K)*FP1(MMO+II)*FP6(NNO+NBT)*HJ(II)
1746 CONTINUE
1750 IF (NIPF.EQ.0) GO TO 1780
DO 1770 I=1,4
IF (NFI(I).EQ.0) GO TO 1770
IN-PLANE EXTERNAL FORCES.
CALL INFORC (FIP(1,I),TIP(1,I),JLIP(I),NFI(I),TIME,F)
IF (I-2) 1752,1754,1760
1752 F = F*XLP6*FU1(MMO+1)
GO TO 1756
1754 F = -F*XLP6*FU1(MMO+NGT)
1756 DO 1758 J=1,NBT
1758 SURS = SURS - F*SFIP(J,I)*FU3(NNO+J)
GO TO 1770

1760 IF (I.EQ.4) GO TO 1762
F = F*XLP6*FV3(NNO+1)
GO TO 1764
1762 F = -F*XLP6*FV3(NNO+NBT)
1764 DO 1766 J=1,NGT
1766 SVRS = SVRS - F*SFIP(J,I)*FV1(MMO+J)
1770 CONTINUE
1780 IF (ABS(SWRS).GT.1.0E20) GO TO 2150
IF (KCOUP.GT.0) GO TO 1790
YY(IZ) = SURS*PRLU(IZ)
YY(IZ+MGMB) = SVRS*PRLV(IZ)
YY(IZ+MGMB2) = SVRS*PRLW(IZ)
GO TO 1800
1790 RHS(IZ) = SURS
RHS(IZ+MGMB) = SVRS
RHS(IZ+MGMB2) = SVRS
1800 CONTINUE
IF (KCOUP.EQ.0) GO TO 2200
DO 1900 M=1,MGMB
D1 = 0.
D2 = 0.
D3 = 0.
DO 1850 N=1,MGMB
D1 = RHS(N)*AV(N,M) + D1
D2 = RHS(N+MGMB)*AV(N,M) + D2
1850 D3 = RHS(N+MGMB2)*AV(N,M) + D3
YY(M) = D1

```



```

      YY(M+MGMB1) = D2
1900 YY(M+MGMB2) = D3
      GO TO 2200

```

Reproduced From
Best Available Copy

```

2150 KERR = 1
      WRITE (6,2151)
2151 FORMAT (30HOSOLUTION DIVERGING IN DEPROP )

2200 RETURN
      END
*DECK DSET1
      SUBROUTINE DSET1

*CALL CBLK1
*CALL CBLK2
*CALL CBLK3
*CALL CBLK4
*CALL CBLK5
*CALL CBLK7
*CALL CBLK9
*CALL CBLK10
*CALL CBLK11
*CALL CBLK13
*CALL CBLK15
*CALL CNOVA
*CALL CBLANK
*CALL CBLK18

```

INPUT DATA

```

      READ(5,7000) MG,MB,MHAR,NBAR,LBAR
      READ (5,7000) (MG(I),I=1,MG)
      READ (5,7000) (MB(I),I=1,MB)
      READ (5,7000) NSYMG,NSYMB,NBUV
      IF (NBUV.EQ.0) NBUV = 11
      READ (5,7000) DPLT,NHND,NDEPV,NSG,NSB,KCOUP
      READ(5,7000) NMOUT
      IF(NMOUT.EQ.0) GO TO 70
      DO 50 I=1,NMOUT
50  READ(5,7000) MOUT(I),NMOUT(I)
      70 READ(5,7000) NKP
      IF (NKP.EQ.0) GO TO 90
      DO 80 I=1,NKP
80  READ(5,7000) KPG(I),KPB(I)
      90 IF(KDAM.EQ.1.AND.KTYPE.EQ.1) NDERV=2
      IF (KDAM.EQ.1.AND.KTYPE.EQ.3) NDERV = 2
      IF (NDERV.EQ.1) LBAR = 1
      READ(5,7000) NL,NSHEAR,NBUCK
      IF ((KTYPE+1)/2.EQ.2) NSHEAR = 0
      LRBAR = 1
      IF (KTYPE.LT.5) NL = 3
      IF (KTYPE.LT.3) NL = 1
      READ(5,7100) XLP,THETA0,A
      IF(NPL1.EQ.0) A=1.0
      IF (NDERV.EQ.1) GO TO 150
      DO 100 I=1,NL

```

```

100 READ(5,7100) HM(I),RHOM(I),EM(I)
    READ (5,7100) TNU,SIGO,EP,EPSIF
    GO TO 190
150 DO 160 I=1,NL
    READ (5,7100) HM(I),RHOM(I)
    READ (5,7100) EX(I),ET(I),XXNU(I),THNU(I),GXT(I)
160 READ (5,7100) SAT(I),SAC(I)
    IF (KTYPE.NE.3.AND).KTYPE.NE.4) GO TO 190
    IF (KCAM.NE.0) GO TO 190
    READ (5,7100) EC,GC,DC
190 READ (5,7000) NSPR,NTSC,(NFI(I),I=1,4)
    IF (NSPR.EQ.0) GO TO 205
    DO 200 I=1,NSPR
200 READ (5,7110) IOIR(I),NSPG(I),NSPB(I),BIGK(I)
205 IF (NTSC.EQ.0) GO TO 211
    DO 210 I=1,NTSC
210 READ (5,7120) ISLOC(I),KTSGB(I),BIGC(I)
211 NIPF = 0
    DO 213 I=1,4
    NFIX = NFI(I)
    IF (NFIX.EQ.0) GO TO 213
    NIPF = NIPF + 1
    NFIXX = IABS(NFIX)
    READ (5,7100) (TIP(J,I),J=1,NFIXX)
    READ (5,7100) (FIP(J,I),J=1,NFIXX)
    NSF = MBAR
    IF (I.GT.2) NSF = MBAR
    NSFX = NSF
    IF (NFIX.LT.0) NSFX = 1
    READ (5,7100) (SFIP(J,I),J=1,NSFX)
    IF (NSFX.GT.1) GO TO 213
    DO 212 J=2,NSF
212 SFIP(J,I) = SFIP(1,I)
213 CONTINUE
    KSTIF = IABS(NSG) + IABS(NSB)
    IF (KSTIF.EQ.0) KCUP = 0
    LBAR = 1
    IF (NSHEAR.EQ.0) GO TO 216
    READ (5,7100) C,GG,GR
    READ (5,7000) LBAR,LSBAR,LOUT
    READ (5,7000) (LRG(I),I=1,LBAR)
    READ (5,7000) (LSB(I),I=1,LSBAR)
    IF (LOUT.EQ.0) GO TO 216
    DO 214 I=1,LOUT
214 READ (5,7000) LROUT(I),LSOUT(I)
216 BUCKS=0.0
    IF (NBUCK.GT.0) READ(5,7100) BUCKS
    IF (KSTIF.EQ.0) GO TO 400
    IF (MSG.EQ.0) GO TO 260
    NSGY = IABS(NSG)
    READ (5,7000) (KSG(I),I=1,NSGY)
    NSGX=MSG
    IF (MSG.LT.0) NSGX = 1
    DO 220 I=1,NSGX
    READ(5,7100) SIDE(I),ESTRG(I),GRAPG(I),RHOSTG(I),
1      SIGOUT(I),SIGOGC(I)

```

```

ETSTRG(I) = 0.
EPSG(I) = 0.
IF (NDERV.EQ.2) READ (5,7100) ETSTRG(I),EPSG(I)
READ(5,7000) NSEGG(I),KSUPG(I)
IF (SIDEG(I).EQ.2.0) KSUPG(I) = 0
NS = NSEGG(I)
READ (5,7100) BIGJG(I),HOG(I),AWEBG(I)
DO 220 L=1,NS
READ (5,7100) HSTG(L,I),BSTG(L,I)
220 CONTINUE
IF (MSG.GT.-2) GO TO 260
DO 250 I=2,NSGY
SIDEG(I)=SIDEG(1)
ESTRG(I)=ESTRG(1)
GBARG(I)=GBARG(1)
RHOSTG(I)=RHOSIG(1)
SIGUGT(I) = SIGUGT(1)
SIGOGC(I) = SIGOGC(1)
ETSTRG(I)=ETSTRG(1)
EPSG(I) = EPSG(1)
NSEGG(I)=NSEGG(1)
KSUPG(I) = KSUPG(1)
NS=NSEGG(1)
BIGJG(I)=BIGJG(1)
HOG(I)=HOG(1)
DO 240 L=1,NS
HSTG(L,I)=HSTG(L,1)
240 BSTG(L,I)=BSTG(L,1)
250 CONTINUE

260 IF (NSB.EQ.0) GO TO 400
NSBY = IABS(NSB)
READ (5,7000) (KSB(I),I=1,NSBY)
NSRX=NSB
IF (NSB.LT.0) NSBX = 1
DO 300 I=1,NSBX
READ(5,7100) SIDEB(I),ESTRB(I),GBARB(I),RHOSTB(I),
1 SIGUBT(I),SIGOBC(I)
ETSTRB(I) = 0.
EPSB(I) = 0.
IF (NDERV.EQ.2) READ (5,7100) ETSTRB(I),EPSB(I)
READ(5,7000) NSEGB(I),KSUPB(I),NSTB(I)
IF (SIDEB(I).EQ.2.0) KSUPB(I) = 0
NS = NSEGB(I)
NSTBX=NSTB(I)
DO 300 K=1,NSTBX
READ (5,7100) BIGJB(K,I),HOB(K,I),BETC(K,I),AWEBB(K,I)
DO 300 L=1,NS
READ(5,7100) HSTB(L,K,I),BSTB(L,K,I)
300 CONTINUE
IF (NSB.GT.-2) GO TO 400
DO 350 I=2,NSBY
SIDEB(I)=SIDEB(1)
ESTRB(I)=ESTRB(1)
GBARB(I)=GBARB(1)
RHOSTB(I)=RHOSTB(1)

```

Reproduced From
Best Available Copy

```

SIGOBT(I) = SIGOBT(I)
SIGORC(I) = SIGORC(I)
ETSTRB(I)=ETSTRB(I)
EPSB(I) = EPSB(I)
NSEGB(I)=NSEGB(I)
KSUPB(I) = KSUPB(I)
NSTB(I)=NSTB(I)
NS=NSEGB(I)
NSTBX = NSTB(I)
DO 330 K=1,NSTBX
  BIGJB(K,I)=BIGJB(K,I)
  HOB(K,I)=HOB(K,I)
  RETC(K,I)=RETC(K,I)
DO 330 L=1,NS
  HSTB(L,K,I)=HSTB(L,K,I)
330 HSTB(L,K,I)=HSTB(L,K,I)
350 CONTINUE

400 READ (5,7100) ((FG(I,J),I=1,MB),J=1,MG)
  READ(5,7100) DELTIM,TSTOP,PRINT
  IF(INOUT.EQ.0) GO TO 2100
  PRINT OUT THE INPUT
  WRITE(6,7170)
  WRITE (6,7200) MG,MB,MBAR,NBAR,LBAR
  WRITE (6,7210) (MG(I),I=1,MG)
  WRITE (6,7220) (NBN(I),I=1,MB)
  WRITE(6,7225) NSYMG,NSYMB,NPLT,NBUV,NEND,NDERV
  WRITE (6,7600) NSG,NSB,KCOUP
  WRITE (6,7150) NNOUT
  IF(NNOUT.GT.0) WRITE(6,7180) (NOUT(I),NOUT(I),I=1,NNOUT)
  WRITE (6,7185) NKP
  IF (NKP.GT.0) WRITE (6,7180) (KPG(I),KPB(I),I=1,NKP)
  WRITE(6,11600) NL,NSHEAR,KBUCK,XLP
  IF(NPLT.EQ.0) WRITE(6,7230) THETA0
  IF(NPLT.EQ.1) WRITE(6,7260) THETA0,A
  IF (NDERV.EQ.2) GO TO 1180
  DO 1160 I=1,NL
1160 WRITE (6,11700) I,HM(I),RHOM(I),EX(I),ET(I),XXNU(I),THNU(I),
  1 GXT(I),SAT(I),SAC(I)
  IF (KTYPE.NE.3.AND.KTYPE.NE.4) GO TO 1190
  IF (KDAM.NE.0) GO TO 1190
  WRITE (6,11900) EC,GC,OC
  GO TO 1190
1180 WRITE (6,7280) (HM(I),RHOM(I),EM(I),I=1,NL)
  WRITE (6,7300) THU,SIGO,EP,EPSTF
1190 WRITE (6,12000) NSPR
  IF (NSPR.EQ.0) GO TO 1210
  WRITE (6,12200)
  DO 1200 I=1,NSPR
1200 WRITE (6,12100) IGIR(I),NSPG(I),NSPR(I),BIGK(I)
1210 WRITE (6,12300) NTSC
  WRITE (6,12600) (CFI(I),I=1,4)
  IF (NTSC.EQ.0) GO TO 1225
  WRITE (6,12400)
  DO 1220 I=1,NTSC
1220 WRITE (6,12500) ISLOC(I),KTSGR(I),BISC(I)

```

```

1225 IF (NIPF.EQ.0) GO TO 1240
    DO 1230 I=1,4
        NFIX = IABS(NFI(I))
        WRITE (6,12700) I, (TIP(J,I),J=1,NFIX)
        WRITE (6,12800) (FIP(J,I),J=1,NFIX)
        NSFX = NBAR
        IF (I.GT.2) NSFX = MBAR
        IF (NFI(I).LT.0) NSFX = 1
        WRITE (6,12900) (SFIP(J,I),J=1,NSFX)
        NFI(I) = NFIX
        IF (NFI.GT.1) GO TO 1230
        TIP(2,I) = 1.E6
        FIP(2,I) = FIP(1,I)
1230 CONTINUE
1240 IF (NSHEAR.EQ.0) GO TO 1245
    WRITE (6,13000) C,GG,GB
    WRITE (6,13100) LRBAR,LSBAR,LOUT
    WRITE (6,13200) (LRG(I),I=1,LRBAR)
    WRITE (6,13300) (LSR(I),I=1,LSBAR)
    IF (LOUT.GT.0) WRITE (6,13400) (LROUT(I),LSOUT(I),I=1,LOUT)
1245 IF (NBUCK .GT. 0) WRITE(6,13500) BUCKS
    IF(NSG .EQ. 0) GO TO 1300
    WRITE (6,7700) (KSG(I),I=1,NSGY)
    DO 1250 I=1,NSGX
        WRITE(6,7800) SIDE(I),ESTRG(I),GBARG(I),RHOSTG(I),SIGOGT(I),
1    SIGOGC(I)
        IF (NDETV.EQ.2) WRITE (6,7830) ETSTRG(I),EPSG(I)
        WRITE (6,7850) NSEGG(I),KSUPG(I),RIGJG(I),HOG(I),AWEHG(I)
        NS = NSEGG(I)
        DO 1250 L=1,NS
            WRITE (6,7900) HSTG(L,I),BSTG(L,I)
1250 CONTINUE
1300 IF (NSB.EQ.0) GO TO 1400
    WRITE (6,8000) (KSB(I),I=1,NSBY)
    DO 1350 I=1,NSBX
        WRITE(6,8050) SIDRB(I),ESTRB(I),GBARB(I),RHOSTB(I),SIGORT(I),
1    SIGORC(I)
        IF (NDETV.EQ.2) WRITE (6,8070) ETSTRB(I),EPSB(I)
        WRITE (6,8090) NSEGB(I),KSUPB(I),NSTB(I)
        NS = NSEGB(I)
        NSTBX=NSTB(I)
        DO 1350 K=1,NSTBX
            WRITE (6,8300) K,BIGJB(K,I),HOB(K,I),RETC(K,I),AWEHB(K,I)
        DO 1350 L=1,NS
            WRITE(6,7900) HSTB(L,K,I),BSTB(L,K,I)
1350 CONTINUE
1400 WRITE (6,7400) ((FG(I,J),I=1,NB),J=1,MG)
    WRITE(6,8200) DELTIM,TSTOP,PRINT

2100 I=0
    MGMR=0
    DO 2150 M=1,MG
        MM = MG*(M)
        DO 2150 N=1,NB
            NN = NB*(N)
            MUSE(N,M)=1

```

```

      IF(I.EQ.NNOUT) GO TO 2130
      DO 2110 J=1,NNOUT
      IF(MM.EQ.MGOUT(J).AND.NN.EQ.NOUT(J)) GO TO 2120
2110  CONTINUE
      GO TO 2130
2120  MUSE(N,M)=0
      I=I+1
      GO TO 2150
2130  MGMB=MGMB+1
2150  CONTINUE
      IF (NSHEAR.EQ.0) GO TO 2500
      I = 0
      DO 2400 M=1,LRBAR
      MM = LRG(M)
      DO 2400 N=1,LSBAR
      NN = LSB(N)
      LUSE(N,M) = 1
      IF (I.EQ.LOUT) GO TO 2400
      DO 2200 J=1,LOUT
      IF (MM.EQ.LROUT(J).AND.NN.EQ.LSOUT(J)) GO TO 2300
2200  CONTINUE
      GO TO 2400
2300  LUSE(N,M) = 0
      I = I + 1
2400  CONTINUE
2500  CONTINUE
      MGMB2=2*MGMB
      XJ=180.0/THETA0
      IF(NPLT.EQ.0) XJ=PI/THETA0
      NBND1 = NBND/10
      NBND2 = NBND - 10*NBND1
      NBUV1 = NBUV/10
      NBUV2 = NBUV - 10*NBUV1
      RETURN

7000  FORMAT(6I12)
7100  FORMAT(6F12.1)
7110  FORMAT (3I12,F12.1)
7120  FORMAT (2I12,F12.1)
7150  FORMAT (9H0NNOUT = I3)
7170  FORMAT(106H1INPUT DATA FOR DEPRCP (MODIFIED TO INCLUDE EXTRA B.C.,
      1 ELASTIC AND TORSIONAL SPRINGS AND IN-PLANE FORCES))
7180  FORMAT (2I4)
7185  FORMAT (7H0NKP = I3)
7200  FORMAT(
      12/10H MBAR      = I2/10H NBAR      = I2/10H LBAR      = I2)
7210  FORMAT (10H0MGMB      = (10I5))
7220  FORMAT (10H0NBND      = (10I5))
7225  FORMAT (10H0NSYMB      = I2/10H NSYMB      = I2/10H0NPLT      = I2/
      2 10H NBUV      = I2/
      3 10H NBND      = I2/
      10H NDERV      = I2)
7230  FORMAT(17H THETA0, IN      = E16.8)
7260  FORMAT(17H THETA0, DEG      = E16.8/17H A, IN      = E16.8)
7280  FORMAT (12H0      FM, IN,4X,21H0HOM, LB=SEC**2/IN**0.4X,
      1 7HEM, PSI/(3E17.8))
7300  FORMAT(17H0T0J      = E16.8/17H SIG0, PSI      = E16.8/17H EP,

```

Reproduced From
Best Available Copy

1 PSI = E16.8/17H EPSIF, IN/IN = E16.8)
7400 FORMAT(6H0FG = /(SE14.6))
7600 FORMAT (10H0NSG = 12/10H NSR = 12/10H KCOUP = 12)
7700 FORMAT (10H0KSG = (10I5))
7800 FORMAT (23H0SIDEG = F4.1/
2 23H ESTRG, LB/IN**2 = E15.6/23H GBARG, LB/IN**2 = E15.6/
3 23H RHOSTG, LB/SEC2/IN4 = E15.6/23H SIGOGT, LB/IN**2 = E15.6/
4 23H SIGOGC, LB/IN**2 = E15.6)
7830 FORMAT (23H0ETSTRG, LB/IN**2 = E15.6/23H EPSG, IN/IN =
1E15.6)
7850 FORMAT (10H NSEGG = 13/10H KSUPG = 13/
1 23H BIGJG, IN**4, = E15.6/22H HOG, IN =E16.6/
2 22H0WEG, IN**2 = E16.6/
2 15X,9H HSTG, IN,21X,8HBSTG, IN)
7900 FORMAT (2(12X,E15.6))
8000 FORMAT (10H0KSH = (10I5))
8050 FORMAT (23H0SIDEB = F4.1/
2 23H ESTRB, LB/IN**2 = E15.6/23H GBARB, LB/IN**2 = E15.6/
3 23H RHOSTB, LB/SEC2/IN4 = E15.6/23H SIGOBT, LB/IN**2 = E15.6/
4 23H SIGORC, LB/IN**2 = E15.6)
8070 FORMAT (23H0ETSTRB, LB/IN**2 = E15.6/23H EPSB, IN/IN =
1E15.6)
8090 FORMAT (10H NSEGB = 13/10H KSUPB = 13/10H NSTB = 13)
8200 FORMAT(15H0ELTIM, SEC = E16.8/15H TSTOP, SEC = E16.8/15H PRINT
1 = E16.8)
8300 FORMAT(9H0STATION 12/5X,15HBIGJR, IN**4 = E15.6/
1 5X,14HHOB, IN = E15.6/5X,14H0ETC, IN = E15.6/
2 5X,14H APEBB, IN**2 E15.6/
2 15X,9H HSTR, IN,21X,8HBSTR, IN)
1600 FORMAT (10H0WL = 12/10H0NSHEAR = 12/
1 10H0NBUC = 12/17H0XLP, IN = E16.8)
1700 FORMAT (6H0LAYER13/27H HM, IN = E16.8/
1 27H RHGM, LB-SEC**2/IN**4 = E16.8/
2 27H EX, PSI = E16.8/
3 27H ET, PSI = E16.8/
4 27H XXND = E16.8/
5 27H THND = E16.8/
6 27H GXT, PSI = E16.8/
7 27H SAT, PSI = E16.8/
8 27H SAC, PSI = E16.8)
1900 FORMAT (11H0EC, PSI = E16.8/11H GC, PSI = E16.8/
1 11H DC, IN = E16.8)
2000 FORMAT (8H0NSPR = 13)
2100 FORMAT (5X,310,E15.6)
2200 FORMAT (37H IDIR NSPG NSPB K (LB/IN))
2300 FORMAT (8H0NTSC = 13)
2400 FORMAT (11X,4HCODE,2X,8HLOCATION,3X,13HC (IN-LB/RAD))
2500 FORMAT (5X,210,E15.6)
2600 FORMAT (8H0NE1 = 4I4)
2700 FORMAT (9H0BOURDARY 13/12H TIMES = SE13.4/(11X,SE13.4))
2800 FORMAT (12H FORCES = SE13.4/(11X,SE13.4))
2900 FORMAT (19H SCALE FACTORS = SE13.4/(18X,SE13.4))
3000 FORMAT (8H0C = E15.6/8H GG = E15.6/8H GB = E15.6)
3100 FORMAT (10H0LSBAK = 12/10H0LSBAK = 12/10H0LOUT = 12)
3200 FORMAT (8H0LRG = (10I5))
3300 FORMAT (8H LSH = (10I5))

3400 FORMAT (16HOLROUT, LSOUT = / (5X,2IS))
 3500 FORMAT(10HOBUCKS = E15.6)

END

H = HM(NL)

F3=RHO/OH3

F1=DM22*A**3/F3

F2=F/F3

F4 = F3/(A*CM11)

F5 = DM11*A**3/F3

F3=F3/(A*CM22)

DT = DELTIM

CALL DTSTEP (F1,F2,F3,F4,F5)

IF (DT.GT.0.0) DELTIM = DT

NELP = 1

NZP = 2

IF (KTYPE.EQ.5) GO TO 2730

NLZ(1) = 1

ZC(1) = -HBAR

NLZ(2) = 1

ZC(2) = ZC(1) + H

IF (KTYPE.LT.3) GO TO 2745

NLZ(2) = 3

ZC(1) = ZC(1) + .5*HM(1)

ZC(2) = ZC(2) - .5*(HM(3) - HM(2))

GO TO 2745

2730 HT = -HBAR

HS = HM(1)

DO 2740 I=1,NL

NLZ(2*I - 1) = 1

NLZ(2*I) = 1

ZC(2*I - 1) = HT

IF (I.GT.1) HS = HM(I) - HM(I-1)

HT = HT + HS

2740 ZC(2*I) = HT

NZP = 2*NL

2745 IF (KDAM.EQ.2) GO TO 2800

DO 2747 I=1,NL

TCRIT(I) = SAT(I)

2747 CCRIT(I) = SAC(I)

2750 CONTINUE

2800 RETURN

3000 KERR = 1

RETURN

END

*DECK DSET3

SUBROUTINE DSET3

*CALL CBLK1

*CALL CBLK2

*CALL CBLK3

*CALL CBLK4

*CALL CBLK5

*CALL CBLK7

*CALL CBLK9

*CALL CBLK10

*CALL CBLK11

Reproduced From
 Best Available Copy

*CALL CBLK13
 *CALL CBLK15
 *CALL CNOVA
 *CALL CBLANK
 *CALL CBLK18

Reproduced From
 Best Available Copy

PRINTOUT DESCRIPTION OF DEPRUP DATA

```

2800 WRITE(6,9300)
      IF(NPLT.EQ.0) WRITE(6,9400)
      IF(NPLT.EQ.1) WRITE(6,9500)
      GO TO (2820,2840,2860,2880,2900), KTYPE
2820 WRITE (6,9600)
      GO TO 2950
2840 WRITE (6,9700)
      GO TO 2950
2860 WRITE (6,9800)
      GO TO 2950
2880 WRITE (6,9820)
      GO TO 2950
2900 WRITE (6,9840)
2950 WRITE (6,13500)
      IF (NBUV1.EQ.1) WRITE (6,13600)
      IF (NBUV1.EQ.3) WRITE (6,13700)
      IF (NBUV1.EQ.5) WRITE (6,13800)
      WRITE (6,13900)
      IF (NBUV2.EQ.1) WRITE (6,13600)
      IF (NBUV2.EQ.3) WRITE (6,13700)
      IF (NBUV2.EQ.5) WRITE (6,13800)
      WRITE (6,14000)
      IF (NBND1.EQ.1) WRITE (6,9900)
      IF (NBND1.EQ.2) WRITE (6,9920)
      IF (NBND1.EQ.3) WRITE (6,9930)
      IF (NBND1.EQ.4) WRITE (6,9940)
      IF (NBND1.EQ.5) WRITE (6,9950)
      IF (NBND1.GT.5) WRITE(6,9955)
      IF (NBND2.EQ.1) WRITE (6,9960)
      IF (NBND2.EQ.2) WRITE (6,9980)
      IF (NBND2.EQ.3) WRITE (6,9990)
      IF (NBND2.EQ.4) WRITE (6,10000)
      IF (NBND2.EQ.5) WRITE (6,10050)
      IF (NBND2.GT.5) WRITE(6,10055)
      IF (NDETV.EQ.1) WRITE(6,10100)
      IF (NDETV.EQ.2) WRITE(6,10200)
      IF (KCOUP.EQ.1) WRITE (6,10250)
      WRITE(6,10800) MG,MB,MBAR,NBAR,LBAR
      WRITE (6,10820)
      DO 2970 N=1,NG
      MM = MGM(M)
      DO 2970 N=1,MB
      NN = MBN(N)
      IF (MUSE(N,M).EQ.0) GO TO 2970
      WRITE (6,10830) MM,NN
2970 CONTINUE
      IF (NSHEAR.EQ.0.AND.(KTYPE+1)/2.EQ.2) WRITE (6,14100)
      IF (NSHEAR.NE.0) WRITE (6,14200)
  
```

Reproduced From
Best Available Copy

```

WRITE (6,10850) XLP
IF(NPLT.EQ.0) WRITE(6,10900) THETA0
IF(NPLT.EQ.1) WRITE(6,11000) THETA0,A
IF (NDERV.EQ.2) GO TO 3500
WRITE (6,12050) HBAR,(I,I=1,NL)
WRITE (6,12100) (HM(I),I=1,NL)
WRITE (6,12200) (KHOM(I),I=1,NL)
WRITE (6,12300) (EX(I),I=1,NL)
WRITE (6,12400) (ET(I),I=1,NL)
WRITE (6,12500) (XXNU(I),I=1,NL)
WRITE (6,12600) (THNU(I),I=1,NL)
WRITE (6,12650) (GXT(I),I=1,NL)
IF (KTYPE.NE.1.AND.KTYPE.NE.3) GO TO 3300
WRITE (6,12900) (SAT(I),I=1,NL)
WRITE (6,13000) (SAC(I),I=1,NL)
GO TO 3400
3300 WRITE (6,12700) (SAT(I),I=1,NL)
WRITE (6,12800) (SAC(I),I=1,NL)
3400 IF (KTYPE.NE.3.AND.KTYPE.NE.4) GO TO 3600
IF (KDM.NE.0) GO TO 3600
WRITE (6,13100) EC,GC,DC
GO TO 3600
3500 IF (KTYPE.EQ.3) WRITE (6,13300) HBAR
WRITE (6,11100) M,RHO,EL,TMU,SIG0,EP,EPSIF
WRITE (6,13400) NSPR,NTSC
3600 WRITE (6,11200) ((FG(N,M),N=1,MR),M=1,MG)
WRITE(6,11300) DELTIM,TSTOP,PRINT
IF (NDERV.EQ.1) GO TO 4020
DO 4000 K=1,LBAR
ZH(K)=GX(K)*H*0.5
ZF(K)=ZH(K)/A
ZG(K)=GX(K)**2
4000 CONTINUE
ZA(1) = ZH(1)/A
ZA(2) = ZR(2)/A
INZ(1) = 1
INZ(2) = LBAR
4020 NNSYMG = 0
NNSYMB = 0
IF (NBND1.GT.3) NNSYMG = 1
IF (NBND2.GT.3) NNSYMB = 1
IF (NBND1.EQ.6) NNSYMG=0
IF (NBND2.EQ.6) NNSYMB=0
IF (NRUV1.GT.3) NNSYMG = 1
IF (NRUV2.GT.3) NNSYMB = 1
IF (NNSYMG.EQ.1.AND.NSYMG.EQ.0) WRITE (6,13200)
IF (NNSYMB.EQ.1.AND.NSYMB.EQ.0) WRITE (6,13200)
NGT = MBAR
NBT = NBAR
NG = NGT
NB = NBT
IF (NSYMG.EQ.1) NG = (NGT+1)/2
IF (NSYMB.EQ.1) NB = (NBT+1)/2
NY2 = 3*NGMB
PIM = PI/FLD(2*(MBAR-1))
PIN = PI/FLD(2*(NBAR-1))

```

Reproduced From
Best Available Copy

```

IF (NSYMG.EQ.1) PIM = 2.*PIM
IF (NSYMB.EQ.1) PIN = 2.*PIN
R=A/H
BUCK = -ABS(BUCKS)
BUCKS=-ABS(BUCKS)/R
XL=XLP/(PI*A)
XL1=1.0/XL
XL2=XL**2
XL3=2.0*XL1
XL4=2.0*XL2
XL5=XL4*R
XL7=1.0/XL2
CN8 = XL**2
IF (KTYPE.EQ.3.AND.NDERV.EQ.2) CN8 = 2.0*CN8
CN9 = CN8/(2.0*R)
IF (NDERV.EQ.1) GO TO 4040
CN10 = 2.0*CN8
CN11 = CN9/(3.0*R)
GO TO 4050
4040 CN10 = 2.*CN8*R
CN11 = CN10
4050 XJ2 = XJ**2
XJ3=XJ*XL1
XJ4=2.0*XJ
XJ5=2.0*XJ3
OPRT1=PRINT*DELTIM
XLP1=XL5
XLP2=2.0*XL*R
IF (NSPR.EQ.0) GO TO 4075
XLP3 = 2.0*XJ/(A*PI*H*XLP)
IF (NSYMG*NSYMB.EQ.1) GO TO 4075
ACCOUNT FOR SYMMETRY.
XLP3 = 4.0*XLP3/ FLOAT((NSYMG+1)*(NSYMB+1))
DO 4060 L=1,NSPR
I = NSPG(L)
J = NSPR(L)
IF (I.EQ.MBAR) BIGK(L) = 0.5*BIGK(L)*FLOAT(NSYMG+1)
IF (J.EQ.MBAR) BIGK(L) = 0.5*BIGK(L)*FLOAT(NSYMB+1)
4060 CONTINUE

4075 IF (NIPF.EQ.0) GO TO 4155
XLP6 = 2.0*(PI*XL)**2*R/(4*THETA0*XLP**3)
IF (NPLT.EQ.1) XLP6 = XLP6*180.0/PI
DO 4152 I=1,4
IF (NFI(1).EQ.0) GO TO 4152
IF (I.LT.3.AND.NSYMB.EQ.0) SFIP(MBAR,I) = 0.5*SFIP(MBAR,I)
IF (I.GT.2.AND.NSYMG.EQ.0) SFIP(MBAR,I) = 0.5*SFIP(MBAR,I)
JLIP(I) = 2
4152 CONTINUE
4155 CONTINUE
SIMPSON S RULE.
MBAR AND NBAR MUST BE ODD NUMBERS FOR FULL PANEL.
DO 4160 I=1,NBAR
F = I-1
GAM(I) = F*PIN
XG(I) = GAM(I)*XLP/PI

```

```

      HJ(I) = 2.0
      PIMA(I) = 2.0*PIM/(3.0*XLP**2)
      IF (NSYMG.EQ.1) PIMA(I) = .5*PIMA(I)
      IF ((I+1)/2.EQ.1/2) HJ(I) = 4.0
4160  CONTINUE
      HJ(1) = 1.0
      IF (NSYMG.EQ.1) HJ(NBAR) = 1.0
      IF (NSYMG.EQ.0) PIMA(NBAR) = PIMA(NBAR)/2.0
      DO 4200 I=1,NBAR
      F = I-1
      BETR(I) = F*PIN
      XB(I) = BETR(I)*THETA0/PI
      HK(I) = 2.0
      PINA(I) = 2.0*PIN/3.0
      IF (NSYMR.EQ.1) PINA(I) = .5*PINA(I)
      IF ((I+1)/2.EQ.1/2) HK(I) = 4.0
      GAMMA(I) = XB(I) - .5*THETA0
      IF (NPLT.EQ.1) GAMMA(I) = GAMMA(I)*NFR*PI/180.
4200  CONTINUE
      IF (NPLT.EQ.1) THETA0 = THETA0*PI/180.
      NMASS = NBAR
      MMASS = NBAR
      HK(1) = 1.0
      IF (NSYMR.EQ.1) HK(NBAR) = 1.0
      IF (NSYMR.EQ.0) PINA(NBAR) = PINA(NBAR)/2.0
      DO 4250 I=1,NBAR
4250  PIMA(I) = PIMA(I)*HJ(I)
      DO 4300 I=1,NBAR
4300  PINA(I) = PINA(I)*HK(I)
      DO 4400 I=1,NBAR
      DO 4400 J=1,NBAR
4400  NUSE(J,I) = 2
      II = 0
      DO 4430 I=1,NGT
      DO 4430 J=1,NBT
      IF (II.EQ.NKP) GO TO 4430
      DO 4410 K=1,NKP
      IF (I.EQ.KPG(K).AND.J.EQ.PPB(K)) GO TO 4420
4410  CONTINUE
      GO TO 4430
4420  NUSE(J,I) = 3
      II = II + 1
4430  CONTINUE

```

CALL STIFF(1)

```

      IF (NTSC.EQ.0) GO TO 4700
      TORSIONAL SPRINGS.
      XLP4=FI**2/(3.*H*FLOAT(NBAR-1)*XLP**3)
      IF (NSYMR.EQ.1) XLP4=2.0*XLP4
      XLP5=(PI*XJ*XL)**2/(3.*H*FLOAT(NBAR-1)*A*THETA0*XLP**2)
      IF (NSYMG.EQ.1) XLP5=2.0*XLP5
      TGI = 0.
      TGP = 0.

```

```

      TB1 = 0.
      TB2 = 0.
      NTSCX = 0
      DO 4085 I=1,NTSC
      J = 1
      K = ISLOC(I)
      IF ((K+1)/2) 4080,4083,4085
4080 J = MHAR
      GO TO 4085
4083 J = NBAR
4085 NTSCX = NTSCX + J
      J = NTSCX + 1
      DO 4096 II = 1,NTSC
      I = NTSC - II + 1
      K = ISLOC(I)
      KK = 1
      IF (K.LT.0) KK = NBAR
      IF (K.LT.-2) KK = MHAR
      IF (K.GT.0) KTSGB(J-1) = KTSGB(I)
      IAK = IAKS(K)
      DO 4094 L=1,KK
      J = J - 1
      LL = KK - L + 1
      ISLOC(J) = IAK
      IF (K.LT.0) KTSGB(J) = LL
      BIGC(J) = BIGC(I)
      IF ((IAK-1)/2) 4094,4090,4088
4088 IF (IAK.EQ.3) TB1 = TB1 + BIGC(J)
      IF (IAK.EQ.4) TB2 = TB2 + BIGC(J)
      IF (KTSGB(J).EQ.MBAR) BIGC(J) = 0.5*BIGC(J)
      GO TO 4092
4090 IF (IAK.EQ.1) TG1 = TG1 + BIGC(J)
      IF (IAK.EQ.2) TG2 = TG2 + BIGC(J)
      IF (KTSGB(J).EQ.MBAR) BIGC(J) = 0.5*BIGC(J)
4092 IF (KTSGB(J).EQ.1) BIGC(J) = 0.5*BIGC(J)
4094 CONTINUE
4096 CONTINUE
      NTSC = NTSCX
      IF (NDERV.EQ.1.OR.KTYPE.EQ.3) GO TO 4100
      DG = EL*A**3/12.
      DB = DG
      GO TO 4110
4100 DG = DM11*A**3
      DB = DM22*A**3
4110 IF (MSG.EQ.0) GO TO 4120
      DO 4135 I=1,MSG
4115 DG = DG + A**3*D11G(I)*PK(KSH(I))/(6.0*FLOAT(NB-1))
4120 IF (NSR.EQ.0) GO TO 4135
      DO 4130 I=1,NSR
      DBX = 0.
      DO 4125 J=1,NBT
4125 DBX = DBX + D22M(J,I)
      DBX = DBX/FLOAT(NBT)
4130 DB = DB + DBX***3*HJ(KSH(I))/(6.0*FLOAT(NB-1))
4135 CONTINUE
      TG1 = TG1*XL*A/(DB*FLOAT(MBAR-1))

```

```

      TG2 = TG2*XL*A/(DG*FLOAT(NBAR-1))
      TB1 = TB1*A/(DB*XJ*FLOAT(MBAR-1))
      TB2 = TB2*A/(DB*XJ*FLOAT(MBAR-1))
      IF(NSYMG.EQ.0) TG2=TB1
      IF(NSYMB.EQ.0) TB2=TB1
      WRITE(6,4600) TB1,TB1, TG2,TB2,DG,DB,XLP4,XLP5
4600  FORMAT(1X,8E15.6)

4700  CALL PLANE
      CALL BOLT

4800  K=0
      OA=1.0/A
      DO 5200 I=1,NGT
      DO 5200 J=1,NBT
      IF(MUSE(J,I).EQ.0) GO TO 5200
      K=K+1
      DW0(K)=0.0
      DWG(K)=0.0
      DWB(K)=0.0
      IF(NSSHEAR.EQ.0) GO TO 5000
      XSXZ(K)=0.
      XSTZ(K)=0.
      PESXZG(K)=0.
      PESTZR(K)=0.
      PESXZR(K)=0.
      PESTZG(K)=0.
5000  CONTINUE
      DO 5100 M=1,NG
      MM=(M-1)*NGT + 1
      DO 5100 N=1,NB
      IF(MUSE(N,M).EQ.0) GO TO 5100
      NN=(N-1)*NBT + J
      FGMN=FG(N,M)*OA
      DW0(K) = FGMN*FP1(MM)*FPS(NN) + DW0(K)
      DWG(K) = FGMN*FP2(MM)*FPS(NN) + DWG(K)
      DWB(K) = FGMN*FP3(MM)*FPS(NN) + DWB(K)
5100  CONTINUE
5200  CONTINUE
      NGNBT = K
      LMAX = LMAX*NGNBT
      NGNB = NG*NBT
      CUR = NPLT
      IF (NSSHEAR.EQ.0) GO TO 5300
      XLP6 = -4.0/(9.0*FLOAT(MBAR-1)*FLOAT(MBAR-1)*C)
      XLP7 = XLP6/GG
      XLP8 = XLP6/GF
      SET UP MODE SHAPES.
      K = 0
      DO 5230 I=1,LMAX
      M = LRG(I)
      XM = M
      DO 5230 J=1,NBAR
      K = K + 1
      X = GAM(J)*XM
      CX = CGS(X)

```

```

      SNX = SIN(X)
      FXZ1(K) = XM*CX
      FXZ2(K) = -SNX*XM**2
      FTZ1(K) = SNX
5230  FTZ2(K) = XM*CX
      K = 0
      DO 5260 I=1,LSHAR
      N = LSH(I)
      XN = 1.
      DO 5260 J=1,NBAR
      K = K + 1
      X = BETR(J)*XN
      CX = COS(X)
      SNX = SIN(X)
      FXZ3(K) = SNX
      FXZ4(K) = XN*CX
      FTZ3(K) = XN*CX
5260  FTZ4(K) = -SNX*XN**2
5300  CONTINUE
      RETURN
9300  FORMAT (1H1,20X,33H0 E P R O P (EXTENDED NOV., 1980)/
1      15H0PANEL ANALYZED)
9400  FORMAT(7H   FLAT)
9500  FORMAT(9H   CURVED)
9600  FORMAT(22H   METAL, SINGLE LAYER)
9700  FORMAT(24H   PLASTIC, SINGLE LAYER)
9800  FORMAT(19H   METAL, HONEYCOMB)
9820  FORMAT(21H   PLASTIC, HONEYCOMB)
9840  FORMAT(22H   PLASTIC, MULTILAYER)
9900  FORMAT(37H   CLAMPED - CLAMPED, GAMMA DIRECTION)
9920  FORMAT(35H   SIMPLE - SIMPLE, GAMMA DIRECTION)
9930  FORMAT(31H   FREE - FREE, GAMMA DIRECTION)
9940  FORMAT(36H   CLAMPED - SIMPLE, GAMMA DIRECTION)
9950  FORMAT(34H   CLAMPED - FREE, GAMMA DIRECTION)
9955  FORMAT(31H   TOR SPRINGS, GAMMA DIRECTION )
9960  FORMAT(36H   CLAMPED - CLAMPED, BETA DIRECTION)
9980  FORMAT(30H   SIMPLE - SIMPLE, BETA DIRECTION)
9990  FORMAT(30H   FREE - FREE, BETA DIRECTION)

0000  FORMAT(35H   CLAMPED - SIMPLE, BETA DIRECTION)
0050  FORMAT(33H   CLAMPED - FREE, BETA DIRECTION)
0055  FORMAT(30H   TOR SPRINGS, BETA DIRECTION )
0100  FORMAT(26H0RESPONSE OPTION = ELASTIC)
0200  FORMAT(34H0RESPONSE OPTION = ELASTIC-PLASTIC)
0250  FORMAT(26H0INERTIA COUPLING INCLUDED)
0800  FORMAT(17H0STRUCTURAL MODEL/
1  47H   NUMBER OF GAMMA MODES (MG) = 13/
2  47H   NUMBER OF BETA MODES (MB) = 13/
3  47H0  NUMBER OF GAMMA INTEGRATION POINTS (MBAR) = 13/
4  47H   NUMBER OF BETA INTEGRATION POINTS (NBAR) = 13/

```

Reproduced From
Best Available Copy

5 47H NUMBER OF Z INTEGRATION POINTS (LBAR) = I3)

0820 FORMAT (24H0MODAL COMBINATIONS USED)

0830 FORMAT (3X,2I4)

0850 FORMAT (35H0 LENGTH OF PANEL, IN (XLP) = E16.8)

0900 FORMAT(35H WIDTH OF PANEL, IN (THETA0) = E16.8)

1000 FORMAT(35H SUBTENDED ANGLE, DEG (THETA0) = E16.8/
2 35H RADIUS, IN (A) = E16.8)

1100 FORMAT(35H THICKNESS, IN = E16.8/
1 35H DENSITY, LB-SEC**2/IN**4 = E16.8/
2 35H ELASTIC MODULUS, PSI = E16.8/
3 35H POISSON(S RATIO = E16.8/
4 35H YIELD STRESS, PSI = E16.8/
5 35H STRAIN HARDENING SLOPE, PSI = E16.8/
6 35H ULTIMATE STRAIN, IN/IN (EPSIF)= E16.8)

1200 FORMAT(26H0INITIAL IMPERFECTIONS, IN/(SE14.6))

1300 FORMAT(17H0TIME INFORMATION/
1 42H INTEGRATION STEP SIZE, SEC (DELTIM) = E16.8/
2 42H STOP TIME, SEC (TSTOP) = E16.8/
3 42H PRINT FREQUENCY (PRINT) = E16.8)

2050 FORMAT (40H0COORDINATE SURFACE POSITION (HBAR), IN E16.8/
1 13H0LAYER NUMBER,22X,4I15/(31X,4I15))

2100 FORMAT (27H CUMULATIVE THICKNESS, IN,13X,6E15.6)

2200 FORMAT (32H MASS DENSITY, LB-SEC**2/IN**4,8X,6E15.6)

2300 FORMAT (33H MODULUS OF ELASTICITY - X, PSI,7X,6E15.6)

2400 FORMAT (40H MODULUS OF ELASTICITY - THETA, PSI 6E15.6)

2500 FORMAT (22H POISSON(S RATIO - X,18X,6E15.6)

2600 FORMAT (26H POISSON(S RATIO - THETA,14X,6E15.6)

2700 FORMAT (31H TENSILE ULTIMATE STRESS, PSI,9X,6E15.6)

2800 FORMAT (35H COMPRESSIVE ULTIMATE STRESS, PSI,5X,6E15.6)

2900 FORMAT (28H TENSILE YIELD STRESS, PSI,12X,6E15.6)

3000 FORMAT (32H COMPRESSIVE YIELD STRESS, PSI,8X,6E15.6)

2650 FORMAT (21H SHEAR MODULUS, PSI,19X,6E15.6)

3100 FORMAT (62H0CORE MODULUS OF ELASTICITY PARALLEL TO CORE DEPTH (EC)
1, PSI = E15.6/
2 63H SHEAR MODULUS OF CORE (GC), PSI =

3 E14.6/
4 62H CORE CELL SIZE (DC), IN
5 E15.6)

3200 FORMAT (41H0** WARNING ** INCONSISTENCY IN SYMMETRY)
3300 FORMAT (42H0 COORDINATE SURFACE POSITION (HBAR), IN E16.8/
3400 FORMAT (3AH0NUMBER OF DISCRETE ELASTIC SPRINGS = 13/
1 52H0NUMBER OF BOUNDARY POINTS WITH TORSIONAL SPRINGS = 13)
3500 FORMAT (37H0 IN-PLANE (U-V) EDGE CONSTRAINTS -)
3600 FORMAT (21H CLAMPED - CLAMPED,)
3700 FORMAT (15H FREE - FREE,)
3800 FORMAT (18H CLAMPED - FREE,)
3900 FORMAT (14+,20X,15HGAMMA DIRECTION)
4000 FORMAT (1H+,20X,14HBETA DIRECTION/
1 33H0 OUT-OF-PLANE (W) CONSTRAINTS -)
4100 FORMAT (36H0SHEAR DEFORMATION OF CORE NEGLECTED)
4200 FORMAT (35H0SHEAR DEFORMATION OF CORE INCLUDED)
END
*DECK SIGMA
SUBROUTINE SIGMA (I,J,M)

THIS S/R DETERMINES THE STRESS-STRAIN RELATIONSHIPS FOR
ELASTIC AND/OR PLASTIC RESPONSE.
SUBROUTINE COMPLETELY REVISED MARCH, 1976.

K - INDEX OF THE INTEGRATION POINT IN THE Z DIRECTION.
I - INDEX OF THE INTEGRATION POINT IN THE BETA DIRECTION.
J - INDEX OF THE INTEGRATION POINT IN THE GAMMA DIRECTION.

*CALL CBLK1
*CALL CBLK3
*CALL CBLK4
*CALL CBLK6
*CALL CBLK7
*CALL CNOVA
*CALL CBLANK
*CALL CBLK15

DATA TOL/5.0E-3/

IF(IFIRST.GT.0) GO TO 300
IFIRST = 1
EPO=SIGO/EL
EPP = 0.0
CM2 = 0.0
SIGO2 = SIGO**2

```

CN1 = (0.5 - TNU)/EL
CN3 = 1.0/EL
TNUSQ = TNU**2
CN4 = (1.0 - TNUSQ)**2
CN12 = (1.0 - TNU + TNUSQ)/CN4
CN13 = (1.0 - 4.0*TNU + TNUSQ)/CN4
CN4 = 0.75/((1.0 + TNU)**2)
CN6 = EL/(1.0 - TNU**2)
CN7 = EL*0.5/(1.0 + TNU)
CN5 = 1.0/CN7
LC = 0
LCMAX = 100
DO 100 L=1,LCMAX
IF (NELP.EQ.1) GO TO 70
ALXX(L) = 0.0
ALTT(L) = 0.0
ALXT(L) = 0.0
BE1(L) = 0.0
BE2(L) = 0.0
BE3(L) = 0.0
TTNU(L) = TNU
70 EPRU(L)=0.0
100 KY(L) = 1

300 KSUM = 0

IJ = LBAR*(4-1)
DO 3050 K=1,LBAR
L = IJ + K
H1 = ZF(K)
DETERMINE APPROPRIATE REGION.
KEY = KY(L)
IF(KEY.GT.3) GO TO 350
GO TO (400,600,700), KEY
350 IF((KEY+1)/2.EQ.KEY/2) GO TO 600
GO TO 700

REGION 1. ELASTIC CURVE.

400 KSUM = KSUM + 1
IF(KSUM.GT.1) GO TO 450
D1 = CN6*(FXX + TNU*ETT)
D2 = CN6*(ETT + TNU*EXX)
D3 = CN7*EXT
D4 = CN6*(XKXX + TNU*XKTT)
D5 = CN6*(XKTT + TNU*XKXX)
D6 = CN7*XKXT
IF(NBUCK .EQ. 0 .OR. NCALL .GT. 0) GO TO 430
IF(D2 .GT. BUCK) GO TO 430
D2 = BUCK*(BUCK/D2)**1.0
430 CONTINUE
S1A(M) = D1
S2A(M) = D2
S3A(M) = D3
S4A(M) = D4
S5A(M) = D5

```

```

      S6A(M) = D6
450  G1 = 01 + H1*04
      G2 = 02 + H1*05
      G3 = 03 + H1*06
      SIG80 = G1*(G1 - G2) + G2**2 + 3.0*G3**2
      IF (NELP.EQ.2) GO TO 470
      EP80(L)=SIG80
      GO TO 3000
470  IF(SIG80.GE.SIG02) GO TO 500
      EP80(L) = SIG80
      GO TO 3000
500  KY(L) = KEY + 1
      LINEARLY INTERPOLATE ON SIGMA BAR TO CORRECT FOR OVERSHOOT.
      SQSIG = SQRT(SIG80)
      B2 = SQRT(EP80(L))
      B1 = (SIG0 - B2)/(SQSIG - B2)
      G1 = SXX(L) + B1*(G1 - SXX(L))
      G2 = STT(L) + B1*(G2 - STT(L))
      G3 = SXT(L) + B1*(G3 - SXT(L))
      SIGXX1(L) = G1
      SIGTT1(L) = G2
      SIGXT1(L) = G3
      T1 = CN3*(G1 - TNU*G2)
      T2 = CN3*(G2 - TNU*G1)
      T3 = CN5*G3
      EXX1(L) = T1
      ETT1(L) = T2
      EXT1(L) = T3
      EP80 = SQRT(CN12*(T1**2 + T2**2) - CN13*T1*T2 + CN4*T3**2)
      EP8(L) = EP80
      EP80(L) = EP80
      IF (JFIRST.EQ.0) JFIRST = 1
      GO TO 3000

```

REGIONS 2 AND 4. PLASTIC LOADING.

```

600  EP8DP = EP8(L)
      H2 = EXX + H1*XXXX - RE1(L)
      H3 = ETT + H1*XTT - RE2(L)
      H4 = EXT + H1*XXXT - RE3(L)
      CN2 = TTNU(L)
      II = 0
610  II = II + 1
      CN22 = CN2**2
      EPR0 = SQRT(((1.0 - CN2 + CN22)*(H2**2 + H3**2) -
1  (1.0 - 4.0*CN2 + CN22)*H2*H3)/(1.0 - CN22)**2 +
2  0.75*H4**2/(1.0 + CN2)**2)
      DELEP = EPR0 - EP80(L)
      EPP = (EP*DELEP + EL*EP80(L))/EP80
      IF (TNU.GT.0.0) CN2 = .5 - EPP*CN1
      IF (ABS(CN2-TTNU(L)).LT.0.0005) GO TO 620
      IF (II.GT.20) GO TO 615
      TTNU(L) = CN2
      GO TO 610
615  WRITE (6,5500) CN2,TTNU(L),TIME
      GO TO 4100

```

```

620 CN2 = TTNU(L)
    IF (EP80.LE.EP80P) GO TO 650
630 EP8(L) = EP80
    IF (EPP.GT.EL.OR.EPP.LT.EP) GO TO 4000
    S1 = EPP/(1.0 - CN2**2)
    S2 = 0.5*EPP/(1.0 + CN2)
    G1 = S1*(H2 + CN2*H3) + ALXX(L)
    G2 = S1*(H3 + CN2*H2) + ALTT(L)
    G3 = S2*H4 + ALXT(L)
    GO TO 3000

```

SECOND TEST FOR UNLOADING IN EITHER REGION 2 OR 4.

```

650 Q1=X1A(M)-EXX1(L) + H1*X4A(M)
    Q2=X2A(M)-ETT1(L) + H1*X5A(M)
    Q3=X3A(M)-EXT1(L) + H1*X6A(M)
    IF(EP.EQ.0.0)GO TO 660
    P1=SXX(L)-SIGXX1(L) + ALXX(L)
    P2=STT(L)-SIGTT1(L) + ALTT(L)
    P3=SXT(L)-SIGXT1(L) + ALXT(L)
    GO TO 670
660 P1=0.0
    P2=0.0
    P3=0.0
670 E1=Q1 - H2
    E2=Q2 - H3
    E3=Q3 - H4
    G1=P1-CN6*(E1+TNU*E2)
    G2=P2-CN6*(E2+TNU*E1)
    G3=P3-CN7*E3
    A1=G1-P1
    A2=G2-P2
    A3=G3-P3
    SIGRD=A1*(A1-A2)+A2**2+3.0*A3**2
    IF (SIGRD.GE.SIG02.AND.DELEP.GE.0.0) GO TO 630

```

```

KY(L)=KEY+1
TTNU(L)=TNU
EP80(L)=SIGRD
BE1(L)=Q1 + BE1(L)
BE2(L)=Q2 + BE2(L)
BE3(L)=Q3 + BE3(L)
IF(EP.EQ.0.1)GO TO 3000
ALXX(L)=P1
ALTT(L)=P2
ALXT(L)=P3
GO TO 3000

```

REGION 3. ELASTIC UNLOADING - RELOADING.

```

700 E1 = BE1(L) - EXX - H1*XXXX
    E2 = BE2(L) - ETT - H1*YKIT
    E3 = BE3(L) - EXT - H1*XXXT
    C1 = ALXX(L)
    C2 = ALTT(L)
    C3 = ALXT(L)
    G1 = C1 - CN6*(E1 + TNU*E2)

```

```

G2 = C2 -
G3 = C3 -
A1 = G1 - C1
A2 = G2 - C2
A3 = G3 - C3
SIG80 = A1*(A1 - A2) + A2**2 + 3.0*A3**2
IF(SIG80.GT.SIG02)GO TO 800
EP80(L)=SIG80
GO TO 3000

LINEARLY INTERPOLATE ON SIGMA BAR TO CORRECT FOR OVERSHOOT.
800 B2 = SQRT(EP80(L))
SQSIG = SQRT(SIG80)
IF(B2.GT.SIG0) GO TO 840
NC = 0
820 B1 = (SQSIG - SIG0)/(SQSIG - B2)
NC = NC + 1
IF(NC.GT.5) GO TO 830
DEL1 = B1*(G1 - SXX(L))
DEL2 = B1*(G2 - SIT(L))
DEL3 = B1*(G3 - SXT(L))
G1 = G1 - DEL1
G2 = G2 - DEL2
G3 = G3 - DEL3
A1 = G1 - ALXX(L)
A2 = G2 - ALTT(L)
A3 = G3 - ALXT(L)
SQSIG = SQRT(A1*(A1-A2) + A2**2 + 3.0*A3**2)
IF(ABS(SQSIG-SIG0)/SIG0.GT.TOL) GO TO 820
GO TO 835
830 WRITE(6,5700) NC,K,I,J,KEY,SQSIG,B1,B2,TIME
LC = LC + 1
IF (LC.GT.LCMAX) GO TO 4100
835 CONTINUE
DEL1 = G1 - SXX(L)
DEL2 = G2 - SIT(L)
DEL3 = G3 - SXT(L)
T1 = X1A(M) + CN3*(DEL1 - TNU*DEL2) + H1*X4A(M)
T2 = X2A(M) + CN3*(DEL2 - TNU*DEL1) + H1*X5A(M)
T3 = X3A(M) + CN5*DEL3 + H1*X6A(M)
GO TO 880
840 WRITE(6,5200) K,I,J,KEY,TIME,B2,SQSIG
T1 = EXX + H1*XXXX
T2 = ETT + H1*AKIT
T3 = EXT + H1*AKXI
LC = LC + 1
IF (LC.GT.LCMAX) GO TO 4100
880 EXX1(L) = T1
ETT1(L) = T2
EXT1(L) = T3
H2 = T1 - BE1(L)
H3 = T2 - BE2(L)
H4 = T3 - BE3(L)
EP80 = SQRT(CN12*(H2**2 + H3**2) - CN13*H2*H3 + CN4*H4**2)
EP80(L) = EP80
EP8(L) = EP80

```

Reproduced From
Best Available Copy

SIGXX1(L) = G1
SIGTT1(L) = G2
SIGXT1(L) = G3
KY(L) = KEY + 1
GO TO 3000

3000 SXX(L) = G1
STT(L) = G2
SXT(L) = G3

3050 CONTINUE
KSUM(M) = KSUM

RETURN

ERROR RETURN.

4000 WRITE (6,5300) EPP,K,I,J,TIME,EPAD,EPBDP,EPBO(L)

4100 WRITE (6,5400)

KERR = 1

RETURN

5200 FORMAT (22H IMMEDIATE RELOADING ,4I3,3E15.6)

5300 FORMAT (28H0EPP IS OUT OF RANGE, EPP = E14.6/

1 3I3,4E15.6)

5400 FORMAT (21H0SOLUTION IS UNSTABLE)

5500 FORMAT (26H VALUE OF NU WONT CONVERGE,2E15.6,15H TIME, SEC =

1 E15.6)

5700 FORMAT (34H CAN NOT TOTALLY CORRECT FOR OVERSHOOT/SIS,4E15.6)

END

*DECK SIGMAB

SUBROUTINE SIGMAB (K1,K2,J,I,M)

THIS PROGRAM COMPUTES INELASTIC STRESSES FOR STIFFENERS.

K1 - GAMMA STIFFENER.

K2 - BETA STIFFENER.

J - BETA POINT NUMBER.

I - GAMMA POINT NUMBER.

M - GRID POINT NUMBER.

ONLY ONE STIFFENER IS ANALYZED PER CALL.

*CALL CBLK1

*CALL CBLK7

*CALL CBLK15

*CALL CBLK16

*CALL CBLANK

IF (NFIRST.GT.0) GO TO 300

NFIRST = 1

MAX = NSMAX*(NSGMB + NSB*NBAR)

DO 100 L=1,MAX

ALX(L) = 0.

BEX(L) = 0.

100 KYX(L) = 1

300 KSUM = 0

IF (K1.EQ.0) GO TO 320

GAMMA DIRECTION.

IJ = (K1-1)*NBAR + I

Reproduced From
Best Available Copy

```

NS = NSEGG(K1)
KKK = K1
ELX = ESTRG(K1)
SIGX = SIGOGT(K1)
EPOX = EPOG(K1)
EPX = ETSTRG(K1)
EX = EXX
XK = XKXX
X1C = X1A(M)
X4C = X4A(M)
GO TO 330
BETA DIRECTION.
320 IJ = NSGMB + (K2-1)*NBAR + J
NS = NSEGB(K2)
KKK=NSG+(K2-1)*NBAR+J
ELX = ESTRB(K2)
SIGX = SIGOBT(K2)
EPOX = EPOB(K2)
EPX = ETSTRB(K2)
EX = ETI
XK = XKTI
X1C = X2A(M)
X4C = X5A(M)
330 LO = NSMAX * (IJ-1)
DO 3050 K=1,NS
L = LO + K
H1 = ZFH(K,KKK)
KEY = KYX(L)
IF (KEY.EQ.1) GO TO 400
IF ((KEY+1)/2.EQ.KEY/2) GO TO 600
GO TO 700

```

REGION 1. ELASTIC REGION.

```

400 KSUM = KSUM + 1
IF (KSUM.GT.1) GO TO 450
D1 = EX*ELX
D4 = XK*ELX
450 G1 = D1 + H1*D4
IF (NELP.EQ.1) GO TO 3000
IF (ABS(G1).LT.SIGX) GO TO 3000
INITIAL YIELDING.
KYX(L) = KEY + 1
G2 = SIGX
IF (G1.LT.0.0) G2 = -SIGX
G1 = G2
SIX1(L) = G1
EX1(L) = G1/ELX
IF (MFIRST.EQ.0) MFIRST = 1
GO TO 3000

```

REGIONS 2 AND 4. INELASTIC REGIONS.

```

600 H2 = EX + H1*XK = HEX(L)
H20 = X1C + H1*X4C = BEX(L)
H3 = ABS(H2)

```

```

      IF (H3.LT.ABS(H20)) GO TO 650
      DELEP = H3 - EPOX
      EPP = (EPX*DELEP + SIGX)/H3
      G1 = EPP*H2 + ALX(L)
      GO TO 3000
      UNLOAD.
650  BEX(L) = 2.0*BEX(L) + H20 - EX1(L)
      ALX(L) = ALX(L) + SX(L) - SIX1(L)
      G1 = (EX + H1*XK - BEX(L))*ELX + ALX(L)
      KYX(L) = KEY + 1
      GO TO 3000

      REGION 3.      ELASTIC.

700  H2 = EX + H1*XK
      A1 = (H2 - BEX(L))*ELX
      G1 = A1 + ALX(L)
      IF (ABS(A1).LE.SIGX) GO TO 3000
      YIELD.
      SXL = SX(L)
      B1 = ABS(SXL - ALX(L))
      B2 = (SIGX - B1)/(ABS(A1) - B1)
      G1 = SXL + B2*(G1 - SXL)
      SIX1(L) = G1
      EX1(L) = X1C + H1*X4C + (G1 - SXL)/ELX
      KYX(L) = KEY + 1

3000  SX(L) = G1
3050  CONTINUE
      KSUMB(IJ) = KSUM
3100  RETURN
      END

```

Reproduced From
Best Available Copy